Recent Progress in **Non-photolithographic** Patterning of

Polymer Thin Films

Mingjun Qiu^{†,Δ,#}, Weiwei Du^{†,Δ,#}, Shangyu Zhou^{†,Δ,#}, Pengzhe Cai^{†,‡}, Yingwu Luo[†],
Xiaoxue Wang^{§,*}, Rong Yang^{◊,*}, Junjie Zhao^{†,Δ,*}

- [†] State Key Laboratory of Chemical Engineering, College of Chemical and Biological Engineering, Zhejiang University, 38 Zheda Rd, Hangzhou, Zhejiang, 310027, China
- ^Δ Institute of Zhejiang University Quzhou, 78 Jiuhua Roulevard North, Quzhou, Zhejiang, 324000, China
- [‡] Department of Polymer Science and Engineering, Zhejiang University, 38 Zheda Rd, Hangzhou 310027, China
- § Department of Chemical and Biomolecular Engineering, The Ohio State University, 151 W. Woodruff Ave, Columbus, OH 43210, U.S.A
- ◊ Robert Frederick Smith School of Chemical & Biomolecular Engineering, Cornell University,
 120 Olin Hall, Ithaca, NY 14853, U.S.A
- # These authors contributed equally.

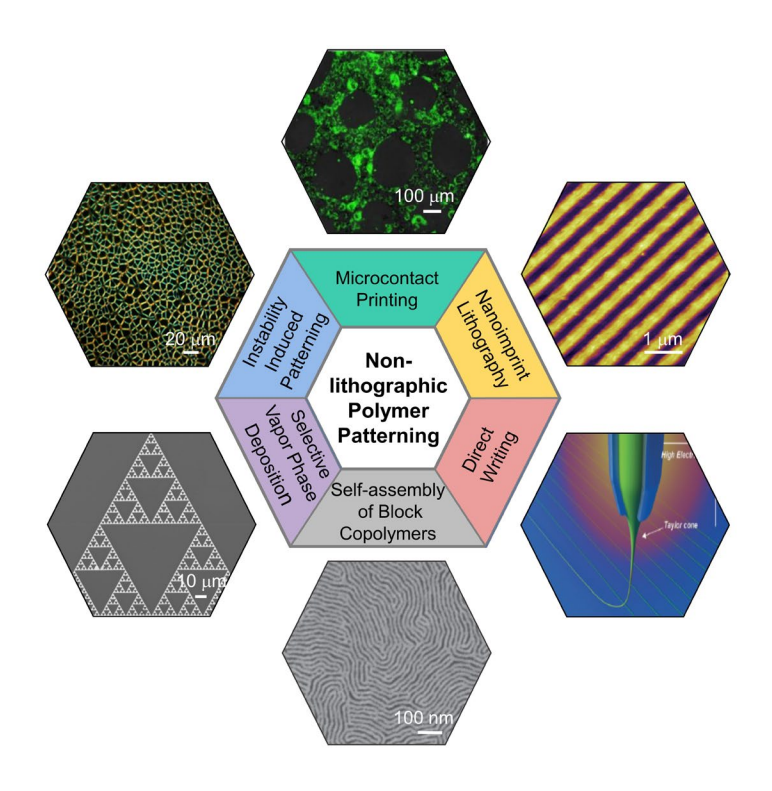
E-mail address: <u>wang.12262@osu.edu</u> (Xiaoxue Wang), <u>ryang@cornell.edu</u> (Rong Yang), <u>junjiezhao@zju.edu.cn</u> (Junjie Zhao)

Abstract

Patterned polymer thin films are essential components in many devices and applications owing to the flexibility, lightweight cost-efficiency. multi-functionality, and Unfortunately, conventional photolithography needs the use of developers and strippers which contain solvents and reagents that may dissolve, swell or degrade the polymer thin film substrates. Alternatively, non-photolithographic strategies provide alternative options and avoid the complicated optical systems, offering versatile routes for fabricating polymeric micro- and nanostructures. In this review, we summarize the recent progress in nonphotolithographic patterning methods including microcontact printing, nanoimprint lithography, direct writing, self-assembly of block copolymers, area-selective vapor phase deposition and instability induced patterning. These patterning approaches have been applied to various applications such as chromic devices, polymer light-emitting diodes, sensors, transistors, and protein and cellular engineering and many other scenarios. Finally, the subsisting challenges and future research directions of non-photolithographic patterning approaches are highlighted from the aspect of resolution, reliability and scalability.

Keywords: Direct writing; Area-selective deposition; Nanoimprint lithography; Soft lithography; Block copolymers; Instability induced patterning

Graphical Abstract



Abbreviations

EBL, electron beam lithography; IBL, ion beam lithography; BCPs, block copolymers; NIL, nanoimprint 1 ithography; SA, self-assembly; LCBCPs, liquid crystal block copolymers; µCP, microcontact printing; CF L, capillary force lithography; PLEDs, polymer light-emitting diodes; PDMS, polydimethylsiloxane; SI-A TRP, surface-initiated atom transfer radical polymerization; ATRP, atom transfer radical polymerization; P AAm, poly(acryl amide); PHEMA, poly(2-hydroxyethylmethacrylate); PGMA, poly(glycidyl methacrylat e); POEGMA, poly(oligo(ethylene glycol)methyl ether methacrylate); ROMP, ring-opening metathesis po lymerization; CAP_{ROMP}, continuous assembly of polymers via ring-opening metathesis polymerization; PD A, polydopamine; MIMIC, micro-molding in capillaries; PU, polyurethane; 3D, three dimensional; MEM S, micro-electromechanical systems; UV, ultraviolet; NOA81, Norland Optical Adhesive 81; POSS, polyh edral oligomeric silsesquioxane; AMONIL MMS4, AMONIL Methyl methanesulfonate; PI, polyimide; P MMA, polymethylmethacrylate; PFO, poly(9,9-dioctylfluroene); Tg, glass transition temperature; P3HT, p oly(3-hexylthiophene-2,5-diyl); AFM, atomic force microscope; SEM, scanning electron microscope; SPL, scanning probe lithography; DPN, dip pen nanolithography; NOA68T, Norland Optical Adhesive 68T; PP L, polymer pen lithography; PS, polystyrene; PEDOT:PSS, poly(3,4-ethylenedioxythiophene)polystyrene sulfonate; EDOT, 3,4-ethylenedioxythiophene; PEDOT, poly(3,4-ethylenedioxythiophene); TADF, therma lly activated delayed fluorescence; EHD, electrohydrodynamic; EFD, electric-field-driven; AJP, aerosol je t printing; NMP, N-Methyl-2-pyrrolidone; APTES, (3-aminopropyl)triethoxysilane; PVP, polyvinylpyrroli done; AS-ALD, area-selective atomic layer deposition; 2D, two dimensional; PS-b-PMMA, polystyrene-b lock-poly(methylmethacrylate); SVA, solvent vapor annealing; PS-b-P2VP, polystyrene-block-poly(2-viny lpyridine); SS-LZA, soft-shear laser zone annealing; LZA, laser zone annealing; DSA, directed self-assem bly; PS-PDMS, polystyrene-polydimethylsiloxane; (P(2VP-co-4VP)-b-PDMS)), (poly(2-vinylpyridine-co -4-vinylpyridne)-b-poly(dimethylsiloxane); PDMSB-b-PS, poly(1,1-dimethyl silacyclobutane)-block-poly styrene; SAMs, self-assembled monolayers; PS-b-PLGA, poly(styrene-block-(lactic acid-alt-glycolic aci d)); iCVD, initiated chemical vapor deposition; PDVB, poly(divinylbenzene); P2VP-b-PS-P2VP, poly(2-v

inylpyridine)-block-polystyrene-block-poly(2-vinylpyridine); PS-r-P2VP, polystyrene-random-poly(2-vin ylpyridine); PS-b-P2VP, polystyrene-block-poly(2-vinylpyridine); PMAA, poly(methyl acrylate acid); PS -b-PMAA, polystyrene-block-poly(methyl acrylate acid); PVD, physical vapor deposition; TEM, transmis sion electron microscopy; MAA, methacrylate acid; oCVD, oxidative chemical vapor deposition; PPy, pol ypyrrole; PT, polythiophene; NiDPP, nickel(II)-5,15-diphenyl porphyrin; AMA, methavrylate; PAMA, pol y(allymethacrylate); AS-MLD, area-selective molecular layer deposition; MLD, molecular layer depositio n; aC, amorphous carbon surface; RIE, reactive ion etching; EDX, energy dispersive X-ray spectroscopy; PNB, polynorbornene; VPP, vapor phase polymerization; CZA, cold zone annealing; IL, ionic liquids; DI A, direct immersion annealing; CD, critical dimension; LER, line edge roughness; LWR, line width rough ness; CDP, condensed droplet polymerization; AuNPs, gold nanoparticles; NLC, nematic liquid crystal; L CPs, liquid crystal polymers; P3BT, poly(3-butylthiophene); P(NDI2OD-T2), poly{[N,N'-bis(2-octyldode cyl)-1,4,5,8-bis(dicarboximide)-2,6-diyl]-alt-5,5'-(2,2'-bithiophene)}; PEC, electrochromic, PANI, polyani line; Tos, tosylate; DMECS, dynamic multicolor electrochromic skin; EFC, electrofluorochromic; DMD, dual-mode displays; PIF8-TAA, polyindenofluoren-8-tryarylamine polymer; NIR, near-infrared; LCEs, liq uid crystal siloxane-based elastomer; LCNs, liquid crystal network; Tch-I, cholesteric-to-isotropic transitio n temperature; Pdots, polymer dots; OLEDs, organic light-emitting diodes; EML, emissive layer; MLA, m icro-lens array; HIL, hole injection layer; PVDF, poly(vinylidene fluoride); EA, emission area; SEP, surfa ce-energy-patterning; AFE, analog front end; PPG, photoplethysmogram; SISC, surfactant-induced solubi lity control; CYTOP, poly(perfluorobutenylvinylether); VOC, volatile organic compound; EGaIn, eutectic gallium-indium metal; TICG, theoretically informed coarse-grain; LC, liquid crystal; IMEC, Interunivers ity Microelectronics Centre; SS, subthreshold swing; gm, transconductance; STEM, scanning transmission electron microscope; ITO, indium-tin-oxide; TU-3, n-type benzobis(thiadiazole);DTBDT-C6, dithieno[2, 3-d;2',3'-d']benzo[1,2-b;4,5-b']dithiophene; DA, donor-accepter; PVDF-HFP, poly(vinylidene fluoride-he xafluoropropylene); HDFB, human dermal fibroblast; SWCNT, single-walled carbon nanotube; CTCs, cir culating tumor cells; PatuT, single human pancreatic tumor cell; BMDMs, bone marrow-derived macroph ages; T-cells, T lymphocytes cells; FN, fibronectin; BMDMs, bone marrow-derived macrophages; PVA, p olyvinyl alcohol; PET, polyethylene terephthalate; IEA, ionic electroactive actuators; CP, conductive poly mer; RI, refractive index; PC, polycarbonate; BREG, bistable reversible electrochemical grating; SMP, sh ape memory polymer; SAXS, small angle X-ray scattering; VPI, vapor phase infiltration

Table of Contents

- 1. Introduction
- 2. Methods for Patterning Polymer Thin Films
 - 2.1 Direct Writing
 - 2.1.1 Scanning Probe Lithography (SPL)
 - 2.1.2 Inkjet Printing
 - 2.2 Area-Selective Vapor Phase Deposition
 - 2.2.1 Physical Masking for Chemical Vapor Deposited Polymers
 - 2.2.2 Pre-Defined Surface for Area-Selective Deposition
 - 2.3 Nanoimprint Lithography (NIL)
 - 2.4 Soft Lithography
 - 2.4.1 Microcontact Printing (μCP)
 - 2.4.2 Micro-molding in Capillaries (MIMIC)
 - 2.4.3 Capillary Force Lithography (CFL)
 - 2.5 Patterning with Block Copolymers (BCPs)
 - 2.5.1 Self-Assembly (SA)
 - 2.5.1.1 Thermal Annealing
 - 2.5.1.2 Solvent Annealing
 - 2.5.2 Directed Self-Assembly (DSA)
 - 2.5.2.1 Topographic Patterning: Graphoepitaxy

- 2.5.2.2 Chemical Patterning: Chemoepitaxy
- 2.5.2.3 Defect Analysis
- 2.6 Instability Induced Patterning
 - 2.6.1 Surface Tension Induced Patterning
 - 2.6.2 Electric Field Induced Patterning
- 2.7 Patterning *via* Polymer Crystallization
- 3. Applications
 - 3.1 Chromic Devices
 - 3.1.1 Electrochromic Devices
 - 3.1.2 Thermochromic Devices
 - 3.2 Polymer Light-Emitting Diodes (PLEDs)
 - 3.3 Sensors
 - 3.4 Transistors
 - 3.5 Protein and Cellular Engineering
 - 3.5.1 Protein Recognition and Cell Sensing
 - 3.5.2 Cell Culture and Tissue Engineering
 - 3.5.3 Cell Therapy
 - 3.6 Other Related Fields
 - 3.6.1 Flexible Energy Harvesters
 - 3.6.2 Soft Actuators
 - 3.6.3 Wetting Control and Self-Cleaning
 - 3.6.4 Optical Applications
- 4. Conclusion & Future Outlook

4.1 Conclusion

4.2 Outlook

1. Introduction

Polymer thin films are widely implemented in virtually every aspect of modern technology and fundamental research owing to their multi-functionality, flexibility, stability and biocompatibility. Patterning of polymer thin films is the backbone of device fabrication. In semiconductor industry, photoresist patterns created in photolithography guide the deposition or etch processes, and has been key to the continuous down-sizing of the transistors. Patterned polymer electrodes and active layers are also indispensable components in many displays such as chromic devices and organic light-emitting diodes (OLEDs)[1,2]. Furthermore, the periodic structures with small feature sizes often endow surfaces with unique optical, mechanical and wetting properties that are not typically accessible with planar polymer films. For instance, the moth-eye patterns with sub-wavelength structures could be potentially used as antireflective coatings[3]. Micro/nano-architectures also provide larger contact area for sensing chemicals and applied stress[4]. Moreover, patterned surfaces with diverse functionalities (e.g. cell-repellent and cell-adhesive polymer brushes) allow specific protein recognition, localized cell adsorption and behavior analysis at single-cell level[5].

Over the past few decades, photolithographic techniques have been widely applied to generate nanoscale patterns. Generally, photolithography uses masks to partially block photosensitive resist films under light exposure. Consequently, the triggered polymerization (negative photoresist) or decomposition reactions (positive photoresist) only take place in the exposed areas. After developing the photoresist film, the pattern can be further transferred to the bottom layer by etching.[6] In addition to photolithography, maskless lithographic techniques such as electron beam lithography (EBL)[7], ion beam lithography (IBL) [8] and direct laser writing[9] have also been investigated for polymer patterning.[10] However, the developers and strippers used in the lithographic techniques are often not compatible with many polymers, leading to the dissolution and thus increased difficulty in patterning polymer films. In order to tackle this

challenge, protective layers, orthogonal lithography and robust polymer semiconductors have all been explored for polymer patterning *via* conventional photolithography.[11–13] Alternatively, Bao's group recently reported a monolithic optical microlithography using light-triggered reactions to form UV-crosslinked patterns of polymeric conductors, semiconductors and dielectrics. This strategy avoids the use of photoresist and does not require protection or pattern transfer processes.[14] While the integration of photolithographic processes with polymer thin films still needs further development, this review only focuses on the advances of polymer patterning using non-photolithographic approaches. Lithographic methods relying on electron beams and ion beams are also not included in this review, because EBL and IBL have become widely available and frequently been integrated in routine fabrication processes. Comprehensive reviews and book chapters on these well-developed methods have already been published [15–17].

Non-photolithographic patterning techniques can be generally classified into three categories based on the flexibility of pattern design. Direct writing methods including scanning probe lithography (SPL) and inkjet printing fall into the Group I with the highest degree of freedom to form arbitrary shapes. Using scanning probes and printing nozzles, direct writing techniques exhibit advantages in directly depositing ink materials onto desired positions, without the need for pre-defined features on the substrates or pattern-transferring mediums such as masks and molds. The second group of methods allow the design of complex pattern geometry, but require the use of pattern-transferring mediums or pre-defined chemical templates. Group II methods include area-selective deposition (ASD), nanoimprint lithography (NIL), microcontact printing (µCP), micro-molding in capillaries (MIMIC) and capillary force lithography (CFL). Typical examples of Group III methods are (directed) self-assembly of block copolymers (BCPs) and instability-induced patterning, which generally produce simple patterns such as stripes and dots. Even with templates, the ability to achieve designable pattern geometry by Group III techniques is limited, compared with Group I and Group II methods.

In this review, we focus on the progress in non-photolithographic patterning of functional polymer thin films in recent five years. Patterning of organic-inorganic hybrid films and biomacromolecules is beyond

the scope of this review. Notice that frequently used terminologies such as "nanopatterning" and "sub-N nm patterning" in research papers often lack explicit description of the critical dimension that the resolution refers to, causing ambiguity for readers. The resolution of patterns discussed in this review only refers to the lateral (in-plane) dimensions. In **Section 2**, we will cover non-photolithographic patterning techniques including SPL, inkjet printing, ASD, NIL, μ CP, MIMIC, CFL, (directed) self-assembly of BCPs, and instability-induced patterning. In **Section 3**, we will discuss the promising applications of patterned polymers thin films in (1) chromic devices, (2) polymer light-emitting diodes (PLEDs), (3) sensors, (4) transistors, (5) protein and cellular engineering, and (6) other related fields. Finally, critical challenges and prospective directions of polymer thin film patterning will be provided for future development.

2. Methods for Patterning Polymer Thin Films

2.1 Direct Writing

Direct writing refers to the process of depositing or dispensing ink materials from a nozzle/tip following a predetermined pattern. Compared with conventional lithographic approaches, direct writing is featured as a maskless technique allowing flexible definition and adjustment of the pattern design. Common direct writing approaches include SPL and printing methods.

2.1.1 Scanning Probe Lithography (SPL)

SPL typically uses a sharp probe to deliver ink for patterning at nm-scale (**Figure 1a**)[18]. As one of the SPL methods, the cantilever-based dip pen nanolithography (DPN) is featured with high resolution (sub-10 nm) and *in-situ* imaging capabilities. Recently, Liu et al. have comprehensively discussed the development and evolution of DPN in their reviews[19,20]. Here we mainly focus on the recent progress of DPN in the past 5 years. DPN can directly pattern a variety of materials, e.g. NOA68T resist[21], PDMS lines[22], and thermo-responsive hydrogels for controllable localized cell growth.[23] In typical DPN processes, the ink is transported through the meniscus that connects the tip and substrate. In order to achieve better control over the ink delivery, efforts have been focused on DPN tip modification, especially with

embedded microchannels[24,25]. Soleymaniha et al. improved the DPN tip by adding a reservoir and a Joule heater on the cantilever (**Figure 1b**)[24]. The thermocapillary stress created by the temperature gradient drives the capillary flow in embedded microfluidic channel of the DPN tip. These modified DPN tips enable 3D printing of nanostructures over areas larger than 1 mm² (**Figure 1c**)[25]. In contrast, conventional DPN has limited process area of several µm².

One of the main challenges for DPN is to improve its process efficiency. Embedding ink reservoir and delivery channels in the tip helps reducing the time for replenishing the ink at the tip. Future optimization is still needed to enlarge the ink storage on the cantilevers, and to provide better control for complex fluids with high viscosity and high content of solid ingredients.

Another strategy to enhance the process throughput is to create multiple tips on a cantilever. However, the fabrication of such cantilever arrays is challenging due to the involvement of complicated photolithography and wet etching processes. In comparison, large number of elastomeric tip arrays can be easily prepared *via* mold replication, enabling high throughput of polymer pen lithography (PPL).[26]-[27] In a typical set up of PPL, the probe array is attached to a holder mounted to the AFM (**Figure 1d-e**).[28] By controlling the contact time and applied pressure, PPL can fabricate features from nanometer-scale to millimeter scale. PPL can be employed to selectively modify existing polymer surface[29], print initiators/catalysts for area-selective growth of polymer brushes[30], and create *in-situ* localized polymerization environment (**Figure 1f-g**)[31]. Besides the abovementioned additive processes, PPL can also be used in subtractive nanomanufacturing. When combined with chemical lift-off lithography, oxygen plasma activated PDMS tip arrays selectively removed hydroxyl terminated alkanethiols in the contact areas.[32] While the deformation of the elastomeric pyramidal pens is used to control the feature size of the pattern in some situations, the deformation of the PPL pens may limit the minimum achievable feature size. Possible solution for this issue is based on the attempts to coat polymer pen arrays with a hard layer (e.g. silica)[33].

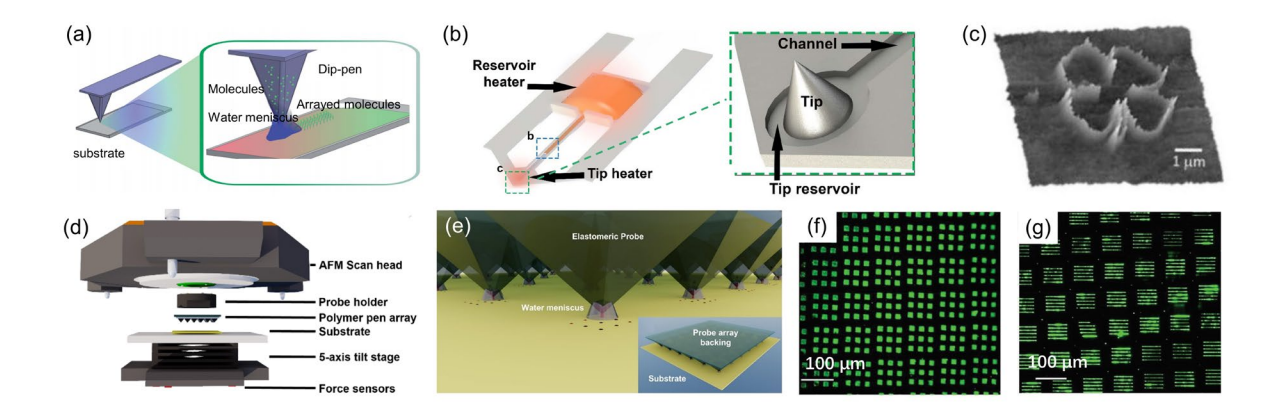


Figure 1. (a) Scheme of a typical DPN process. The inset illustrates the water meniscus formed between the ink-coated tip and the substrate[18]. Copyright 2014. Adapted with permission from the Royal Society of Chemistry. (b) DPN tip modification by integrating a reservoir and a microfluidic channel[24]. Copyright 2016. Adapted with permission from Elsevier Science Ltd. (c) AFM image of the clover pattern fabricated *via* modified DPN tip[25]. Copyright 2018. Adapted with permission from the American Chemical Society. (d) Schematic layout of PPL equipment[28]. (e) Side view and top view (inset) of the polymer pen array used in PPL[28]. Copyright 2018. Adapted with permission from the MyJoVE Corporation. (f-g) Epifluorescence microscopy images for dot and line patterns created *via* PPL[31]. Copyright 2018. Adapted with permission from the Royal Society of Chemistry.

2.1.2 Inkjet Printing

Inkjet printing deposits tiny droplets on the substrate through a nozzle to form a specific pattern. The non-contact nature of inkjet printing and the adoption of binder-less inks can free printed patterns from unwanted residuals and additional rinsing steps. The development of inkjet printing methods have boosted a variety of applications including 3D printing[34–36], heterogeneous catalysis,[37] flexible electronics,[38,39] personalized drug delivery[40], and thin film transistors[41].

Inkjet printing can directly use polymer solution, suspension or emulsion, and has been widely applied for many polymers including vinyl polymers such as polymethylmethacrylate (PMMA) [42], poly(2-vinylpyridine)(P2VP)[43], polystyrene (PS)[44–46] and poly(2-dimethylamino-ethyl methacrylate)[47], organosiloxane polymers[48–50], liquid crystalline polymer[51,52], conjugated polymer[53–56] such as polydiacetylene[57], poly(3-hexylthiophene-2,5-diyl) (P3HT) [58,59] and poly(3,4-ethylenedioxythiophene):poly(styrene sulfonate) (PEDOT:PSS)[60–68], photoresist[69–71] such as SU-8 and NOA81, and copolymers such as poly(lactic-*co*-glycolic acid)[72–75] and poly(vinylidenefluoride-

trifluoroethylene-chlorotrifluoroethylene) terpolymer[76].

Inkjet printers are basically made up of three parts: the motion stage, the vision system and printing nozzle. In the conventional inkjet printing, the ink droplets are pushed out of the thermal or piezoelectric nozzles. Thermal nozzles employ a heater to increase the internal temperature to create a bubble which push the ink droplet out of the nozzle (**Figure 2a**), while the piezoelectric nozzles employ a piezoelectric film. The deformation of the piezoelectric film induces a volumetric change in the reservoir, and the induced abrupt pressure change caused ejection of the droplet. The piezoelectric inkjet printing was used to produce a variety of polymer patterns to fabricate devices, for example, PEDOT:PSS pattern was used as electrode for PLEDs and transistors[77–79], PS for the water-repellent application[80], fluoropolymer AF 1600 for electrofluidic display[81], thermally activated delayed fluorescence (TADF) dendrimer for PLEDs[82,83].

One of the challenges with conventional inkjet printing for polymer patterns is the small range of allowed ink viscosity (5 to 20 cPs) [84]. The high viscosity due to the large molecular weight or high concentration of polymers [84] may affect the ink flow and extrusion, and even lead to polymer agglomeration in the nozzle. Directly using precursor solutions in inkjet printing could avoid the viscosity issue. For example, the plasma-assisted polymerization of the jetted monomers enables the fabrication of PEDOT thin films.[85] For reagents that cannot be mixed in a single flow, separate ink solutions can be cojetted using micro-reactive inkjet printing technique, allowing polymerization reactions to occur only on the desired substrate surface (**Figure 2b**)[86–88].

Another challenge with conventional inkjet printing is the relatively low resolution (no less than 30 µm[89]) due to the limitation of inkjet nozzle. Many methods including electrohydrodynamic (EHD) jet printing are proposed to increase the fineness and reproducibility of patterns. The EHD jet printing employs electrical force between a nozzle and a substrate (**Figure 2c**). A liquid droplet is formed at the outlet of a nozzle as a balance of the surface tension, the gravity force and the electric field force, and the Taylor cone is formed because of the electrostatic charge. When the voltage reaches a critical value, the repulsive electrical force overcomes surface tension, the fluid jet is ejected from the tip of the Taylor cone[35,39]. The diameter of the jet is not limited by the outlet of the nozzle, so EHD jet printing can reach high

resolution (sub-100 nm)[39], besides, the position and morphology can be accurately controlled. Compared with the common ink viscosity range (5 to 20 cPs) for conventional inkjet printing, EHD jet printing allows the use of much wider range of ink viscosity (1 to 100000 cPs)[39]. A variety of parameters, such as surface tension, ink viscosity, conductivity and dielectric constant, were studied to improve the jetting performance[90,91] Li et al. developed a thermally assisted EHD jet printing for patterning biopolymer 3D structures. The applied thermal field raises the temperature only at the jet region, achieving better control of high-molecular weight and high resolution of the pattern (700 nm) (**Figure 2e-f**)[92].

In the case of EHD jet printing, when the height of the printed structures increases, the change of dielectric medium induces the change of intensity and distribution of electric field. This would affect the Taylor cone and ejection behavior negatively. Electric-field-driven (EFD) jet uses a single nozzle electrode to form an electric field (**Figure 2d**)[93], enabling facile fabrication of high-aspect-ratio wall structures.

Aerosol jet printing (AJP) represents a promising extension of inkjet printing. After atomized by ultrasonic or pneumatic atomizer into micro-sized aerosol droplets, inks are carried out by nitrogen gas to focus inside the nozzle for final deposition (**Figure 2i**)[94]. **Figure 2j-k** are printed using AJP[94,95]. Compared with inkjet printing, AJP is capable of patterning larger set of printable materials[96] (including viscous insulators) and easier prototyping of ink formulation with a fine feature of 10 μm[97]. The material versatility of AJP helps researchers to create all AJP printed triboelectric sensors[94] and optoelectronic nose for nitroaromatic vapor sensor[98].

While being generally used as an additive technique, inkjet printing can also be applied as a subtractive process with etchant inks on polymer films[99]. Organic solvents are typically used in inkjet etching. For example, Farjam et al. used N-Methyl-2-pyrrolidone (NMP) as the etchant to dissolve PMMA for creating line patterns[100]. Anisole was also found effective for inkjet etching on PMMA films, enabling the fabrication of lens array films[101]. Similar etching strategy was also adopted for patterning poly(perfluorobutenylvinylether) (CYTOP), an insulation material frequently used in OLED devices[102].

The abovementioned inkjet printing methods can be combined with other processes to generate unique patterns. For example, printed initiator pattern allowed localized surface-initiated atom transfer radical

polymerization (SI-ATRP) for polymer brushes[103], while (3-aminopropyl)triethoxysilane (APTES) patterns were used for grafting as-synthesized polymers[104]. Additive EHD jet printed polyvinylpyrrolidone (PVP) lines (**Figure 2g-h**) and inkjet etched PMMA patterns were both found as effective inhibitors for area-selective atomic layer deposition (AS-ALD) of a range of metal oxides[105]. AJP can be combined with UV direct writing. The UV light was either used to cure the coated PDMS to create two-dimensional (2D) hybrid polymer pattern[95,106], or used to initiate polymerization to fabricate lateral polymeric structures locally[107]. AJP was combined with flexographic to produce polymer optical waveguides. The flexographic method was used to create conditioning lines on a substrate which enabled more straight edges in the later AJP process[108,109].

As a drop-on-demand method, inkjet printing is in general cost-effective and compatible with various substrate materials. However, several issues still need to be addressed to further improve the pattern quality. The non-Newtonian nature of polymer solutions, such as the strain hardening effect, may lead to the difficulty in breaking up the jets and thus uneven distribution of droplet sizes[110]. Surface tension effect may cause the dewetting of ink solutions on the substrate surface, therefore affecting the shape (e.g. the formation of coffee rings) and resolution of the final pattern[111,112]. Nozzle clogging also frequently occurs due to the ink evaporation in the printhead and the use of highly viscous polymer solution.[113] In addition, further exploration of inkjet printing processes for nonplanar substrates is desired for fabricating complex devices structures.

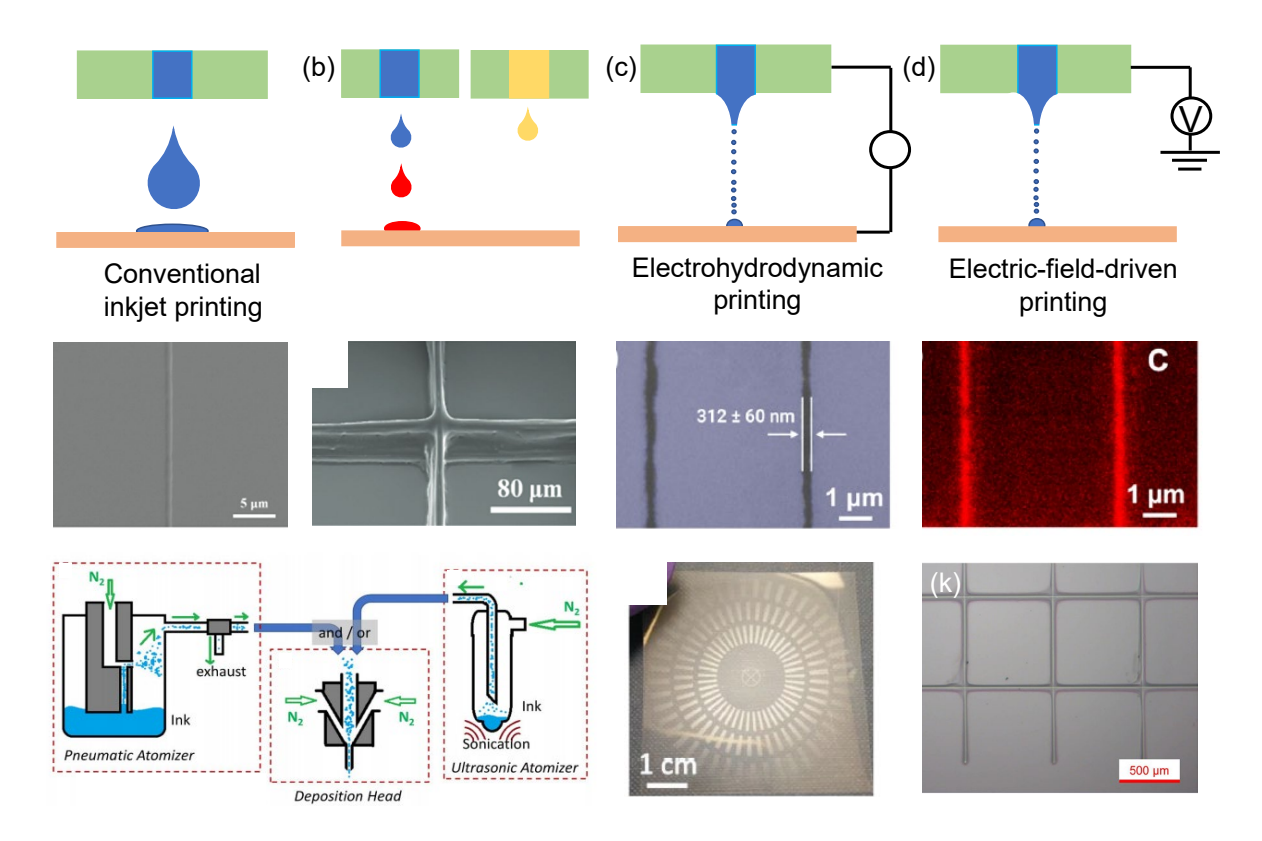


Figure 2. (a-d) Schematic diagram of (a) reactive inkjet printing, (b) conventional inkjet printing, (c) EHD printing and (d) EFD printing. (e-f) SEM image of an inkjet printed line with 700 nm width and a 3D lattice with a 15:1 aspect ratio[92]. Copyright 2018. Adapted with permission from John Wiley & Sons Inc. (g) SEM image and (h) corresponding Auger electron spectroscopy C elemental mapping image of the inkjet printed PVP line patterns as inhibitors for area-selective deposition of Al-doped ZnO[105]. Copyright 2020. Adapted with permission from the American Chemical Society. (i) Schematic layout of an AJP[94]. (j) Photo of AJP pattern on large nylon substrate[94]. Copyright 2018. Adapted with permission from John Wiley & Sons Inc. (k) Optical microscopic image of a PDMS grid pattern fabricated *via* AJP method[95] Copyright 2017. Adapted with permission from AIP publishing.

2.2 Area-Selective Vapor Phase Deposition

Patterning polymer thin films *via* vapor phase deposition processes could be accomplished with physical masking strategy or pre-defined surface chemistry. Physical masks enable the polymer films to shape into desired patterns directly on the exposed substrate surface, while pre-defined surfaces take advantage of intrinsic or modified surface chemistry with the aim of increasing the variation between growth area and nongrowth regions.

2.2.1 Physical Masking for Chemical Vapor Deposited Polymers

Physical masks can be used to generate patterns during chemical vapor deposition of polymers. Common masks include stencils used in physical vapor deposition (PVD), transmission electron microscopy (TEM) grids and lithographically defined pre-patterns. For example, PDMS has been demonstrated as a physical mask in initiated chemical vapor deposition (iCVD) that can be pre-patterned and easily removed from substrate after iCVD of poly(methyl acrylate acid) (PMAA) (Figure 3a). During the deposition, methacrylic acid (MAA) monomer vapor flowed into the reactor chamber was first desublimed onto the pre-patterned surface cooled to temperatures < 0°C, followed with the polymerization of MAA with the aid of tert-butoxy radicals introduced in vapor phase[114]. Figure 3b shows the ability to conformally coating another layer of hydrophobic poly(divinylbenzene) (PDVB) on top of PMAA without damaging the structure. Notice that the phase transition of MAA monomer in this process is not common for typical iCVD methods, because only adsorbed (not condensed or desublimed) monomers are involved in iCVD polymerization in general.

Physical masks applied to oxidative chemical vapor deposition (oCVD) processes enable vapor printing of conjugated polymers such as polypyrrole (PPy), polythiophene (PT), and PEDOT in a single step.[115] As shown in **Figure 3c**, the vapor of monomer(s) and oxidant are simultaneously delivered into the vacuum chamber where the masked substrate is held facing downward on a temperature-controlled plate. The step-growth polymerization of oCVD polymers can proceed directly on a variety of substrates, showing great potential for fabrication of flexible electronic devices. Recently, Boscher et al. reported patterned oCVD polymer of nickel(II) 5,15-diphenyl porphyrin (NiDPP) on paper using a physical mask (**Figure 3d**).[116,117] FeCl₃ was used both as the oxidant and the dopant in this oCVD process. The resulting oCVD poly(NiDPP) pattern exhibits an electrical conductivity of 3.6×10⁻² S cm⁻¹, promising for optoelectronic devices.

In addition to the abovementioned scenarios used during the CVD processes, physical masks can also be applied to chemical vapor deposited photo-active polymers as optical masks for photolithography.[118] Liu et al. synthesized a photoactive polymer *via* iCVD using allyl methacrylate (AMA), an asymmetric divinyl monomer (**Figure 3e**).[119] Poly(allyl methacrylate) (PAMA) film was synthesized *via* iCVD with large amounts of pendant allyl groups due to the lower reactivity of allyl groups than the vinyl groups of AMA. By applying a TEM grid as the photomask on top of the PAMA film, the exposed area can be further crosslinked and transformed into a compact pattern under UV irradiation, leaving the linear PAMA chain in the unexposed area unchanged with high solubility in many organic solvents (**Figure 3f-g**).

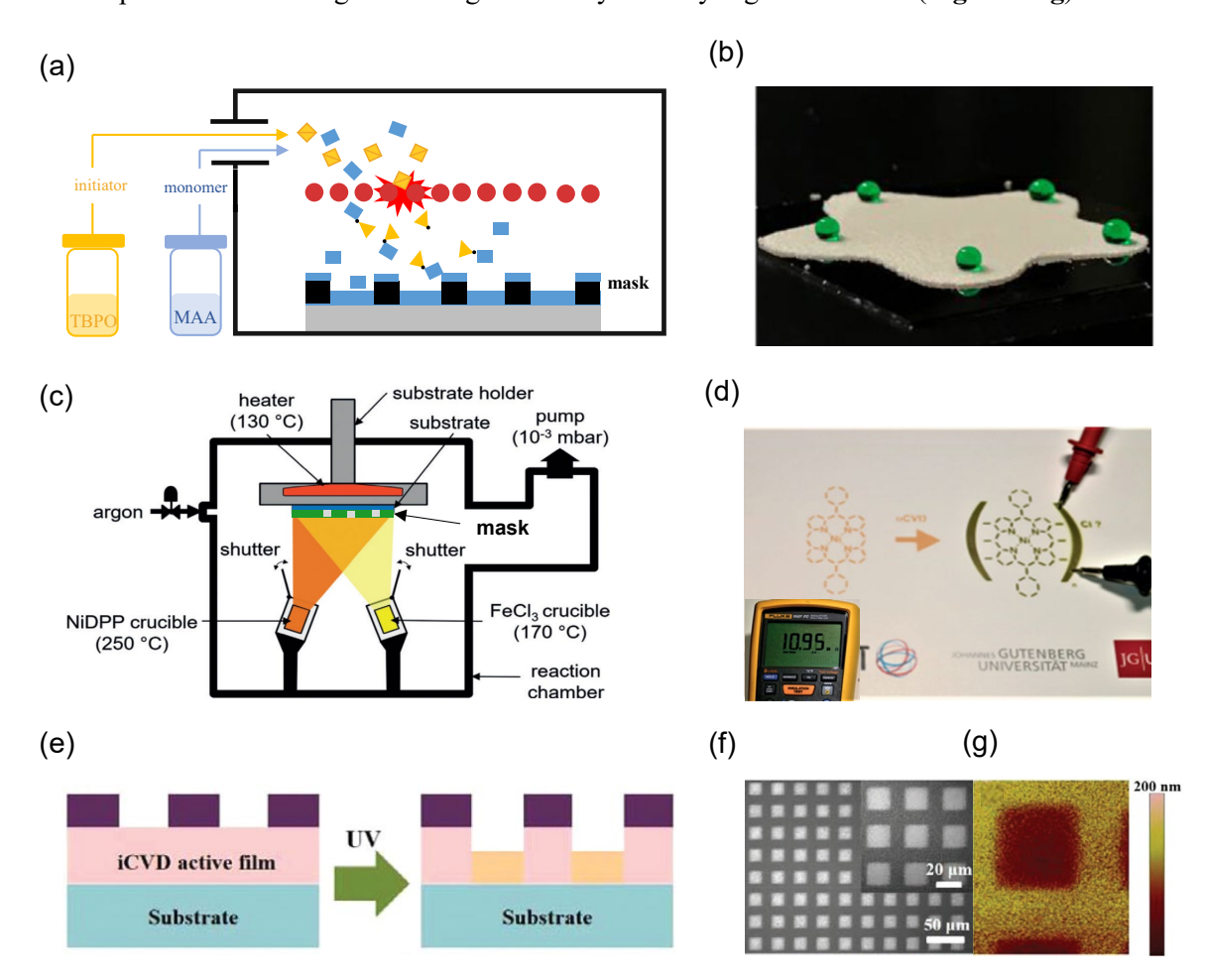


Figure 3. (a) Physical masking strategy for generating patterns in iCVD. (b) PDVB film fabricated through lift-off procedure using PDMS mask.[114] Copyright 2017. Adapted with permission from the Elsevier Science Ltd. (c) Schematic of patterning polymer thin films in oCVD with a mask.[116] (d) Photo of the sublimed NiDPP (orange) and the patterned oCVD NiDPP thin film (green) on paper.[116] Copyright 2019. Adapted with permission from John Wiley & Sons Inc. (e) Process scheme of UV patterning on iCVD PAMA.[119] (f) SEM and (g) AFM of the PAMA pattern after UV exposure for 3 h.[119] Copyright 2019.

Adapted with permission from John Wiley & Sons Inc.

While physical masks are easy to use and cost-effective, the resolution is typically tens of microns due to the limitation of stencil manufacturing and the overspray frequently found when the mask is not in close contact with the substrate. The gap between the mask and the substrate, especially when the substrate has a large surface roughness, may allow thin films to form outside the aperture range of the mask. Consequently, physical masking strategies are not expected to generate sub-micron patterns. However, this patterning method may find suitable applications in solar cells, sensors and LEDs, which have lower resolution requirement than microelectronics.

2.2.2 Pre-Defined Surface for Area-Selective Deposition

Different from the physical constraint created by masks, selective deposition typically takes advantage of the difference in intrinsic or modified surface chemistry on the substrates. Recently, Zhang et al. investigated area-selective molecular layer deposition (AS-MLD) of PI based on the intrinsic difference of Cu (with native CuO_x) and native SiO₂ surface (Figure 4a).[120] The deposition rate of PI films on the Cu substrate was found up to 7.8 Å/cycle at 200°C, while the growth rate on native SiO₂ at the same temperature was close to zero. Accordingly, high area selectivity was achieved on pre-patterned Cu/SiO₂ substrate. As shown in Figure 4b, PI thickness deposited on Cu substrate is around 140 nm, while the film thickness on native SiO₂ is about 10 nm. This area selectivity could be further enhanced with an etchback process, e.g. O₂ plasma etch, to clean up the polymer growth on the nongrowth area of SiO₂ surface. The author proposed a temperature-dependent reaction mechanism that Cu ions catalyzed the preferable formation of crystalline interchain PI at optimal temperature of 200°C, while lower temperature (e.g. at 170 °C) resulted in the predominant slow formation of amorphous ring-closed PI as supported by spectroscopic analysis.

On occasions where intrinsic chemical difference is not sufficient to generate high area selectivity, surface modification on the target area is necessary to enlarge the variation in the interaction between the precursor/monomer and the substrate surface. George et al. has reported a pre-treatment strategy for

selective deposition of nylon-6,2 in MLD recently.[121] The mildly oxidized amorphous carbon surface (aC) by H_2O_2 activates the surface reaction of the growth area with the monomer, while the $-Si(CH_3)_3$ terminated surface on SiO_2 obtained *via* dimethylaminotrimethylsilane modification is unfavorable for nylon-6,2 MLD nucleation. In this way, they achieved > 98% selectivity in the aC growth area even after 100 cycles of nylon-6,2 MLD. This selective deposition process was further demonstrated to compensate aC erosion during reactive ion etching (RIE) through selectively adding nylon on the aC pattern.

Self-assembled monolayers (SAMs) represent another surface modification strategy that is often used in AS-ALD of inorganic materials. Bent et al. extended the similar approach to MLD of PU.[122] They utilized phosphonic acid SAMs as the blocking layers for MLD PU on copper oxide while leaving silicon oxide remain active for surface reaction and nucleation. Combining the AS-MLD method with an acid etching process, the selectivity of PU on Cu/Si pattern was significantly enhanced by 380-fold compared with that without the etchback step.

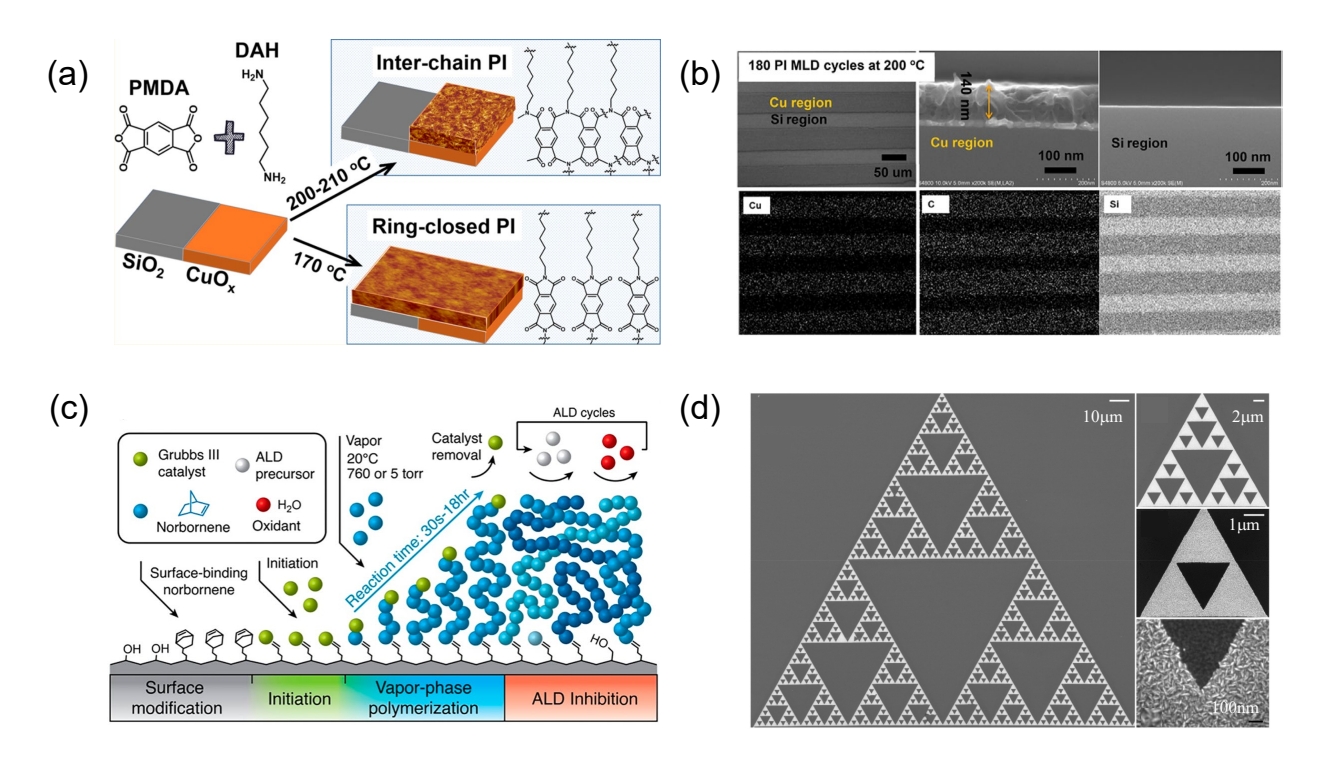


Figure 4. (a) Schematic diagram of AS-MLD of PI on Cu versus native SiO₂[120] (b) SEM and Energy Dispersive X-Ray Spectroscopy (EDX) mapping images for the AS-MLD PI pattern: top-view and cross-sectional SEM images (top row); EDX images to show the distribution of Cu, Si, and C elements (bottom

row).[120] Copyright 2020. Adapted with permission from the American Chemical Society. (c) Illustration of pre-defined catalyst surfaces for area-selective polymerization of PNB *via* ROMP.[123] (d) SEM of Sierpinski's triangle patterns where dark areas represent Cu protected by surface grown polymers while bright areas correspond to AS-ALD of ZnO.[123] Copyright 2020. Adapted with permission from the American Chemical Society.

Aside from the surface pre-treatment to tune the monomer-surface interaction, other strategies to directly pattern catalysts to enable localized surface polymerization have also been reported for vapor phase polymerization (VPP)[124,125] and ring-opening metathesis polymerization (ROMP).[123] Brooke et al. developed a patterning method for conductive PEDOT and PPy film *via* VPP on pre-defined oxidant patterns.[124] The spin-cast oxidant film was exposed to UV irradiation through a photomask to form pre-patterned oxidant film of modified chemical environment. The oxidants in the growth area create more nucleation sites for the polymerization of adsorbed EDOT and pyrrole monomer, leading to high-resolution conjugated polymer patterns. This selective deposition method has been demonstrated capable of fabricating electrochromic devices, which will be further discussed in the application section.

Surface anchored initiators can also provide localized regions for area-selective polymerization. Pattison et al. reported the area-selective polynorbornene (PNB) thin films *via* ROMP initiated by predefined surface-bound Ru-based Grubbs generation III catalyst.[123] With localized polymerization, PNB was selectively deposited on pre-modified 200 nm (SEM scale) Cu line patterns with pitch size of 200 nm. The selectively deposited PNB films was further demonstrated as the inhibiting layers for AS-ALD of ZnO and TiO₂ (**Figure 4c**) *via* preventing metal precursor adsorption on PNB surfaces, e.g. the area selectivity were above 0.99 for 200 cycles of ZnO after the samples underwent a 2 h polymerization. Moreover, the SEM shows that the localized PNB films enable the ASD of ZnO on the complex Sierpinski's triangle pattern, where the sharp corners represent difficulties in keeping the selective growth within the growth area (**Figure 4d**). The work further exploited TiO₂ as an etch mask to protect Si while over-etching Cu into the underlying silicon substrate.

While surface modification is effective in extending the nucleation delay and enlarging the area selectivity for polymer thin film deposition, reactants often unavoidably adsorb and react on the nongrowth

regions, leading to the loss of selectivity after certain period of deposition time. To tackle this challenge, repeating surface functionalization may be adopted for additional nucleation inhibition. Combining etching to remove the film on nongrowth area may also improve the overall selectivity. Another challenge for developing "self-aligning" growth of polymer thin film patterns *via* ASD is to control the unwanted lateral broadening phenomenon (or so-called "mushroom" effect). So far, it is still difficult to generate straight walls that is perpendicular to the sharp pre-defined features, especially when patterned structures with large height-to-width ratios are desired. Future exploration for strategies to inhibit the "mushroom" effect would be key to ASD-enabled "bottom-up" nanomanufacturing.

2.3 Nanoimprint Lithography (NIL)

NIL typically utilizes a stamp to press against a deformable resist layer to make topological patterns on the substrate, demonstrating the scalable production of high-resolution nanostructures (sub-10 nm)[126,127]. In many applications such as microelectronics, a close coupling is required between NIL and etching to achieve the final permanent features.[128] The recent review by Cox et al. has covered the emergent materials and methods of NIL.[129] Here, we mainly focus on the development of NIL methods for polymer patterns in the past five years.

NIL methods can be generally categorized into two types: thermal NIL and ultraviolet (UV) NIL. Thermal NIL, also known as hot embossing lithography, often requires elevated imprint temperature (above the T_g) and high applied pressure (typically on the order of 10⁸-10⁹ Pa) in order to force the polymer to flow into the spaces underneath the stamp[130]. UV NIL requires UV polymerization to crosslink and harden light-sensitive resist materials (e.g. NOA 81[131], POSS resist[132] and AMONIL MMS4 resist[133]) during imprinting, and is often applied for nanoscale grating structures[134]. Both NIL approaches could be potentially integrated into continuous roll-to-roll processes[135].

Figure 5a illustrates a typical process of thermal NIL. Recently, thermal NIL has been used to fabricate micro-/nanoscale pillar structures of polyimide (PI)[136] and PMMA (**Figure 5b)**[137,138]. Li et al. developed a single-step thermal NIL method for poly(9,9-dioctylfluorene) (PFO) patterns, achieving

patterning, molecular chain alignment, and fluorescence enhancement simultenously.[139] By adjusting the initial film thickness, the crystallinity and the orientation of PFO could be tuned to optimize polarizability and light-emitting properties.

The high process temperature of thermal NIL may lead to pattern instability and internal stress, and limit the use for thermosensitive and high-molecular-weight polymers. The large applied pressure may also damage the substrate and molds.[140] Employing shear and solvent provides opportunities for the operation of thermal NIL at relatively low temperature and pressure [141–143]. Performed in a solvent atmosphere, solvent-assisted NIL takes advantage of the plasticization effect that lowers the effective T_g of the polymer.[144] Low operating pressure (up to 4 orders of magnitude smaller than typical NIL)[140] and room-temperature replication of polymer structures are therefore allowed in solvent-assisted NIL.[142,143] Recently, Ding et al. reported a controllable solvent-assisted NIL method to the fabrication of P3HT nanogratings with line width of 80 nm at room temperature (Figure 5c)[142].

The adhesion and friction between the mold and the substrate during NIL typically result in the difficulty in demolding that affects its large-scale implementation[145]. Smoothening the mold surface, optimizing the geometry of stamps, maintaining a suitable draft angle[146], and developing proper mold materials are reported methods to improve the demolding processes. Among these approaches, developing molds with low surface energy is particularly important for generating high-resolution pattern.[147] While common PDMS stamps possess low surface energy, the low modulus of PDMS may lead to mold collapse. To address this issue, Tak et al. developed an isodecyl acrylate and trimethylolpropane triacrylate (IDA/TMPTA) based copolymer mold with adjustable surface energy and mechanical properties, enabling high resolution NIL without surface treatment and additives (Figure 5d).[148]

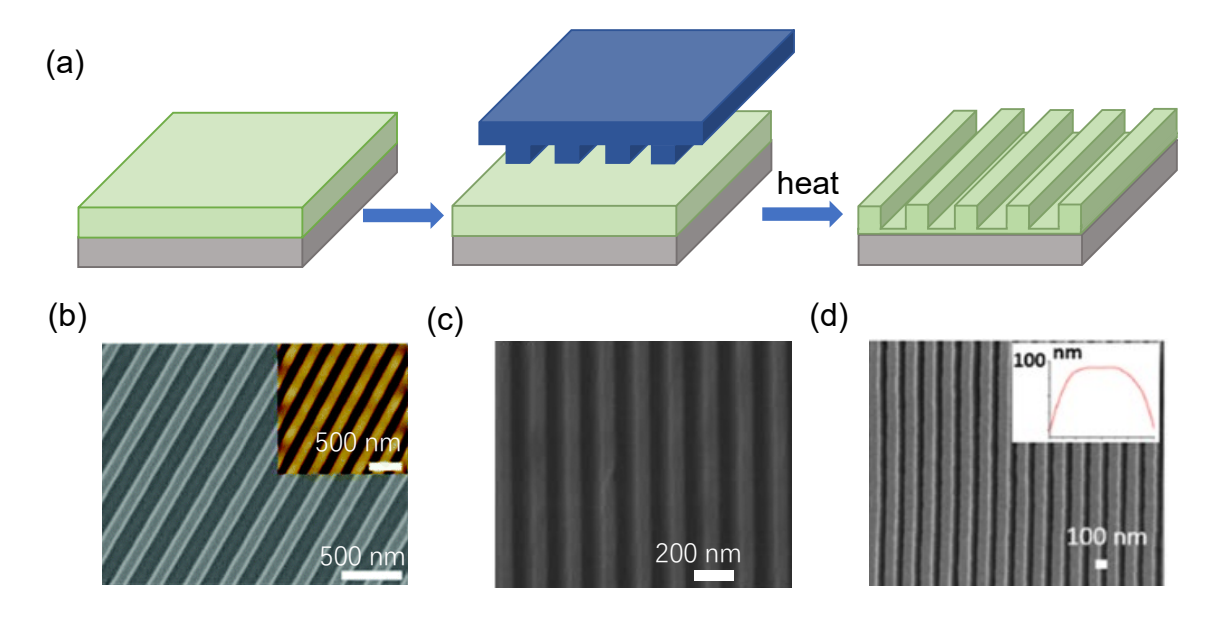


Figure 5. (a) Schematic diagram of the NIL method. (b) Scanning Electron Microscope (SEM) image of the imprinted PMMA line patterns[137]. The inset in (b) is the corresponding AFM image. The scale bars in (b) both represent 500 nm. Copyright 2018. Adapted with permission from the Royal Society of Chemistry. (c) SEM image of the patterned P3HT nanograting film. [142]Copyright 2017. Adapted with permission from the Royal Society of Chemistry. (d) polyurethane acrylate patterns produced by UV-NIL with IDA/TMPTA molds. Inset shows the profile in the pattern. [148]Copyright 2017. Adapted with permission from the IOP Publishing.

2.4 Soft Lithography

One of the characteristics of soft lithography is the use of elastomeric stamps with pre-defined features for pattern formation. Typically, a master with relief structures is fabricated by photolithographic techniques as the mold for preparing the elastomeric stamps (**Figure 6a**). μ CP is one of earliest soft lithography techniques to generate patterned surface using an elastomeric stamp. The process contains fabrication of a poly(dimethylsiloxane) (PDMS) stamp and a subsequent printing step (**Figure 6b**)[149]. μ CP has many advantages including easy replication of the stamps and relatively high printing resolution down to submicon scale.[147] Since Amit Kumar and George Whitesides introduced μ CP in 1993[150], this method has been developed for nearly 30 years and discussed in many excellent reviews[151–153].

2.4.1 Microcontact Printing (μCP)

 μ CP can be used to directly pattern polymers[154–156] as well as to generate monolayer patterns on substrates to initiate, promote or inhibit surface polymerization reactions. For example, μ CP can be

combined with SI-ATRP. Poly(acryl amide) (PAAm) brush micro-patterns were obtained by μCP of ATRP initiators, followed with localized polymerization[5,157]. Similar approach has also been applied to fabricate multicomponent bilayer structures of polymer brushes including poly(2-hydroxyethyl methacrylate) (PHEMA), poly(glycidyl methacrylate) (PGMA) and poly[oligo(ethylene glycol) methyl ether methacrylate] (POEGMA).[158] Moreover, μCP catalyst patterns can be applied to area-selective continuous assembly of polymers *via* ring-opening metathesis polymerization (CAP_{ROMP}). Surface initiated ROMP of norbornene-containing polymer chains enables the formation of patterned crosslinked networks *via* solid-state reactions (**Figure 6e**).[149] In the scenarios when inhibition of polymerization is needed in specific areas, μCP can also be applied to create patterns with passivation surface. For example, regions patterned with octadecyltrichlorosilane exhibit hydrophobic properties to repel undesirable polymer growth during the CAP_{ROMP} process.[149]

Creating hydrophilic patterns on hydrophobic substrate surfaces represents a challenge for μ CP, because the deposited hydrophilic molecules can hardly form covalent bonds to the hydrophobic substrate. Negative μ CP method, however, helps to solve this problem.[159] Plasma-activated PDMS stamp was brought in contact with the polydopamine(PDA)-coated hydrophobic substrate, and then released to remove the PDA from the contact area due to the stronger adhesion between the stamp and the PDA.[159] Consequently, hydrophilic PDA patterns were formed with micrometer resolution on hydrophobic substrate.

2.4.2 Micro-molding in Capillaries (MIMIC)

In μCP processes, insufficient ink may result in uneven pattern distribution. Ink supply to the microchannels formed between the soft stamp and the substrate is therefore desired in certain scenarios. For example, MIMIC uses capillary forces to fill polymer liquids into the channels of the stamp. An elastomeric stamp is typically placed on the substrate surface for polymer liquids to fill. When the stamp lifts off, it leaves polymer patterns on the substrate (**Figure 6c**).[157] For instance, Lilge et al. fabricated polyurethane (PU) microwells by MIMIC and then combined with μCP to construct 3-dimensional (3D) microenvironments for cell culture (**Figure 6f**).[157] Combining MIMIC with microfluidic pervaporation,

Thuau et al. reported a fabrication process for free-standing multilayer microstructures for microelectromechanical systems (MEMS) devices.[160] While MIMIC overcomes the ink insufficiency and enables patterned structures with more complexity in the height direction compared with the μ CP processes, but the slow capillary flow involved in MIMIC is the bottleneck for improving the process throughput for large pattern areas.

2.4.3 Capillary Force Lithography (CFL)

CFL utilizes capillary rise of the polymer to fill the void space of the soft molds when the polymer is heated above T_g (**Figure 6d**). CFL has similar working principle with MIMIC, but is not affected by the slow lateral capillary filling rates. When compared with conventional thermal NIL, CFL generally requires no or small pressure to keep the mold in place, which is one of the main differences between NIL and CFL [161,162].

CFL has been used to pattern a group of polymers and copolymers, such as polycaprolactone[163], polycarbonate[164], Nafion[165], PU[166], PS[167–170], (PS-b-P2VP)[171], poly(latic-co-glycolic acid)[172,173] in the recent 5 years. Thickness of polymer films, molecular weight and processing temperature are important factors influencing the final polymer pattern[170]. CFL can also be used to pattern polymer blends. For example, Liu et al. reported using CFL pattern-directed self-assemble to obtain ordered pattern structures with vertical phase segregation [174]. Due to different affinity of PMMA and PS to the substrates and PDMS molds, annealing the blend in the mold confinement above the T_g of the two polymers enables the formation of the phase-separated pattern (**Figure 6g**), providing opportunities for polymeric nanostructures with both topographic and chemical patterns in one step.

Since Suh et al. first reported CFL in their work[175], this approach has been developed into a versatile, simple method for large-area polymer patterning. However, there are still remaining challenges. Patterning *via* CFL for structures with large height-to-width ratios may be difficult, because of the balance between gravity and capillary forces. The low modulus of PDMS may result in mold collapse, especially when the channel width is much larger than the height[161]. For these applications, stamps with larger modulus need

to be developed while retaining the low surface energy and cheap properties of PDMS. Future studies combining CFL with other patterning techniques may give rise to complex nanostructures. For example, the combination of block copolymer assembly (BCP, detailed introduction in Section 2.5) and CFL may lead to multiscale hierarchical patterns.

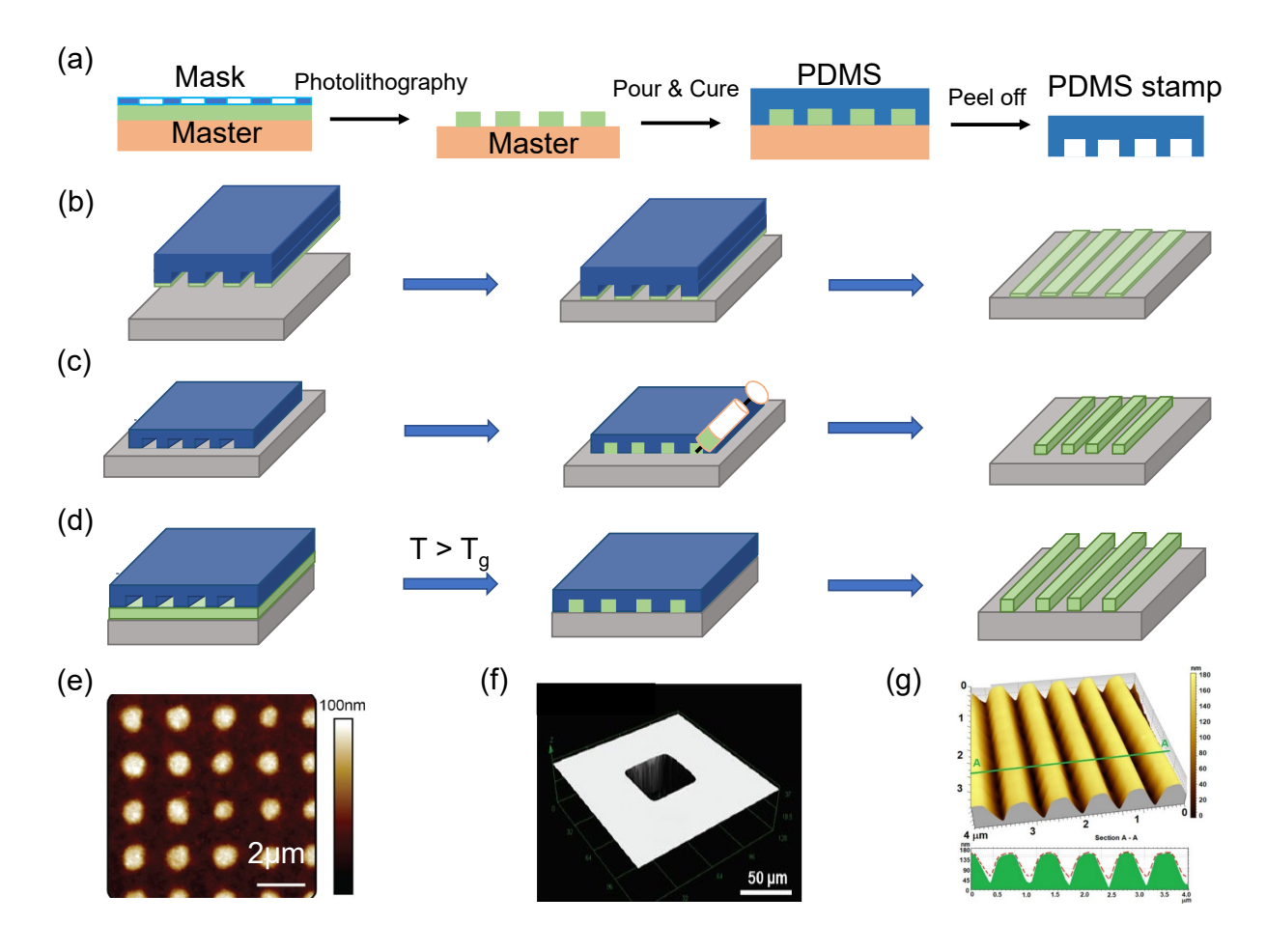


Figure 6. (a) Fabrication of the PDMS stamp for μCP. (b) graphical representation of μCP. (c) Illustration of the MIMIC process. (d) Schematic diagram of the CFL method (e) Atomic Force Microscope (AFM) i mage of the crosslinked norbornene-containing polymer pattern[149]. Copyright 2020. Adapted with perm ission from the American Chemical Society. (f) 3D laser scanning microscopic image of the patterned PU microwells[157]. Copyright 2017. Adapted with permission from the John Wiley & Sons Inc. and (g) AFM image of the patterned PS/PMMA blend film. The cross-sectional profile of the patterned film (continuou s green line) and the profile of the stamp (dashed line)[174]. Copyright 2018. Adapted with permission from the American Chemical Society. Direct link: https://pubs.acs.org/doi/10.1021/acsomega.7b02078. Further permissions related to the material excerpted should be directed to the ACS.

2.5 Patterning with Block Copolymers (BCPs)

2.5.1 Self-Assembly (SA)

Self-assembly enables the microphase segregation in BCPs and thus the formation of ordered periodic nanostructures[176]. The microphase separation of block copolymers (A-B)_n is controlled by the following factors: the degree of polymerization of N, the architectural parameters associated with the number of blocks (n) and the volume fraction (f_A), and the Flory-Huggins interaction parameter χ between A-B segment.[177] The first two factors are related to the translational and configurational entropy, which can be adjusted by changing the stoichiometric ratio of polymerization.[177] The largely enthalpic interaction parameter χ is depended on temperature and can be given as $\chi \approx \alpha/T + \beta$, where α and β are constants specifically defined for n and f_A .[178] Considering the contribution of enthalpy and entropy to Gibbs free energy, χN determines the phase state of BCPs.[177] For BCPs, the f_A controls the geometry of the microphase structure. For a simple classic example of AB diblock copolymer, **Figure 7a** depicts how composition affects the microphase morphology at equilibrium[179]. Spheres (S), cylinders (C), gyroid (G), and lamellae (L) structures can be formed at particular f_A range, given the χN of the diblock copolymer is not too low.[178,180]

2.5.1.1 Thermal Annealing

Thermal annealing has been widely used as a simple process for the self-assembly of BCP thin films. Heating the BCP thin films above the T_g improves the chain mobility, while the process temperature also needs to be controlled below the order–disorder transition temperature. With adequate time, the thermal energy allows the polymer chains to segregate locally and rearrange to a lower energy configuration.[181,182] However, long annealing time, limited pattern resolution, and possible degradation or crystallization of the blocks at high process temperature are common problems in thermal annealing. Cold zone annealing (CZA)[183–186], laser zone annealing (LZA) [187,188] and microwave annealing [189,190] have been reported as alternative thermal annealing approaches for BCP films. In a typical CZA setup, a hot filament placed in between two cold blocks creates a sharp thermal gradient, allowing the BCP

film to flow through and self-assemble below the order—disorder transition temperature [191–193]. LZA represents another method to achieve dynamic thermal gradient, enabling both rapid ordering and controlled orientation[194]. Compared with CZA, LZA usually requires an extra metal layer beneath the BCP film for heat absorption to create temperature gradient, which increases the process complexity and the difficulty in subsequent pattern transfer especially when the self-assembled structures need to serve as the hard mask.

Introducing external shear force is effective for improving the long-range ordering obtained *via* thermal annealing[195]. Karim group reported modified CZA processes with a PDMS pad to generate shear on the BCP films [196–200]. The heating/cooling zones cause the elastomeric PDMS layer to experience alternating expansion and contraction, leading to oscillatory shear to the underlying BCP films during CZA. The shear-enhanced alignment strategy can also be applied to LZA to achieve template-free alignment. Taking advantage of the dramatic difference in the thermal expansion coefficient between a polymer cladding and the rigid substrate, Majewski et al. reported a strategy to generate local shear force using laser-induced thermal expansion of the PDMS cover. This local shear force guides the uniaxial alignment of the self-assembled BCP structures over a large area (Figure 7b)[201]. The ability of shear-enhanced LZA to rapidly achieved long-range ordering lays the foundation for fabricating complex nanostructures. For example, double-layered grids and three-layered hexagonal lattices can both be achieved by repeating the shear-enhanced LZA in different angles (Figure 7c-d). In addition to external force field[202,203], various other methods such as neutral interfacial layers[204–206], magnetic field[207] and electric field[208] have also been reported to improve long-range order by thermal annealing.

Polystyrene-block-poly (methyl methacrylate) (PS-b-PMMA) has been studied as model BCP for a long time, because of the similar surface energy of both blocks with regard to air/vacuum at high temperatures that drives the formation of domains perpendicular to the substrate [209,210]. However, the relatively low χ value of PS-b-PMMA limits the further reduction of the pattern feature size[211]. To solve this problem, various strategies including changing the polarity of either blocks [212–214] and lowering the energy barrier [215,216] have been reported. Adding ionic liquids (IL) [212–214] to PS-b-PMMA improves the effective χ by increasing the polarity of the blocks. For example, a small amount of ionic

liquids with preferential solubility in PMMA homopolymer enhances the polarity of PMMA blocks, and thus reduces the characteristic size of self-assembled PS-*b*-PMMA to sub-10 nm.[212] Adding low-molecular-weight PS and PMMA homopolymers into PS-*b*-PMMA system as "plasticizers" increases the lateral order of the pattern due to the decreased energy barriers. [215,216]

Developing high- χ BCPs is driven by the need for smaller feature size. In high- χ BCPs, the difference of interfacial/surface energies between two blocks induces preferential wetting and leads to parallel structure. Since perpendicular structures are desired in practical applications, designing new BCP structures [209,217–220] and devising neutral layers [221,222] have been investigated to control the orientation of high- χ BCP domains. Yoshimura et al. introduced hydrophobic trifluoroethyl groups to the polymethacrylate blocks that reduces the differences of affinity towards the free surface compared with the PS blocks in the BCPs while maintaining a large incompatibility between the two blocks.[223] Such design of the polymer structure leads to the achievement of perpendicular orientation after thermal annealing. Alternatively, Willson group have found that neutral layers are effective for inducing perpendicular oriented nanostructures in just 1 minute [221]. Common neutral layers require similar affinity with both blocks of the BCP, e.g. random copolymers with similar moieties to the BCP. [221,222] The concept of "neutral layers" has been recently extended to topcoats with grafting to each blocks of the BCPs. For example, Wang et al. investigated vapor-phase deposited topcoats, and found that even though PDVB is generally not considered as "neutral" to PS-b-PMAA, the grafting created between the topcoat and both blocks of the BCP enables the formation of ordered vertical cylinder structures [224].

2.5.1.2 Solvent Annealing

The need for perpendicular orientation of the self-assembled structure, especially for high- χ BCPs, motivates the exploration for alternative annealing methods. Solvent annealing allows solvent molecules to infiltrate and plasticize BCPs, promoting the chain mobility for self-assembly at lower temperature compared with conventional thermal annealing.[181,225,226] During the solvent removal step in solvent annealing, the solvent concentration gradient in the thickness direction contributes to the reorientation of

BCP domains to form perpendicular structures [227,228]. Typical solvent annealing methods include solvent vapor annealing (SVA) and direct immersion annealing (DIA).

In a typical SVA process, solvent vapor is introduced to the chamber which swells the exposed BCP films, followed with a drying step to evaporate the solvent from the film. Changing the annealing temperature[229,230], flow rate[231] and the type of solvents[232,233] in SVA is effective for modulating the morphology of the self-assembled BCP structures[234]. SVA can be widely applied in various BCP systems such as triblock copolymers[234–237], branched BCPs[238,239], carbohydrate-based BCPs[240,241], liquid crystalline block copolymers (LCBCPs)[242,243] and supramolecular BCPs [244]. Notably, introducing LC blocks to BCPs provides additional control over the micro-domain morphology and orientation owing to the duet between BCP phase segregation and LC ordering. For example, Shi et al. showed that the in-plane cylinders obtained *via* SVA of a Si-containing rod-coil LC BCP (**Figure 7e**) can further transform into vertical lamellae structures in a subsequent thermal annealing above the LC transition temperature (**Figure 7f**) [245]. The order-order transition was achieved due to the thermal induced LC ordering to form a hexatic columnar nematic phase.

Employing neutral interfacial layer[224,246,247] and external fields including electric field[248], force field[249–251], microwave[252,253] and combined fields[254,255] is also effective in guiding the macroscopic alignment of BCPs in SVA. Kim et al. achieved defect-free and long-range orientated BCP nanopatterns over centimeter-scale areas using stepwise shear alignment and SVA processes[250]. The mechanical shearing induces macroscopic orientation of PS-*b*-P2VP and the subsequent SVA process promotes chain migration for defect annihilation.

For SVA processes, in-plane structures are frequently found on the top surface of the high- χ BCP films owing to high interfacial energy difference at the air interface. Although RIE can remove the top wetting layer and achieve solely perpendicular structures, developing strategies to inhibit the formation of such skin layer would lead to simplified patterning processes. Besides, the critical role of solvent removal rate in affecting BCP reordering needs further investigation. Past reports have found that varied solvent removal rates may lead to completely different orientation of the micro-domains[256,257]. Although several

mechanisms have been proposed to explain the morphology transformation during the solvent evaporation in SVA including effective neutral surface formation [258], entropy penalty for generating a wetting layer of the block with lower surface tension [259], and ever-changing commensurability during the film deswelling [257].

In order to expedite solvent annealing processes, DIA was developed in 2014.[260] DIA simplified the procedure by changing the solvent exposure from vapor phase to liquid phase, showing potential for integrated roll-to-roll manufacturing.[261–265] However, careful selection for the binary solvent mixture is often required to ensure successful DIA processes. The good solvent accelerates the chain mobility of the BCPs, while the poor solvent needs to inhibit dissolution of the film. Masud et al. achieved rapid vertical ordering of IL-mixed PS-*b*-PMMA films by using a mixture of toluene and heptane.[214] The addition of IL as a plasticizer induces early phase segregation and orientation during the film casting process for PS-*b*-PMMA. The choice of toluene as good solvent and heptane as nonsolvent provides near-neutral solvent environment for both blocks, further promoting the long-range ordering of the perpendicular structures in DIA.

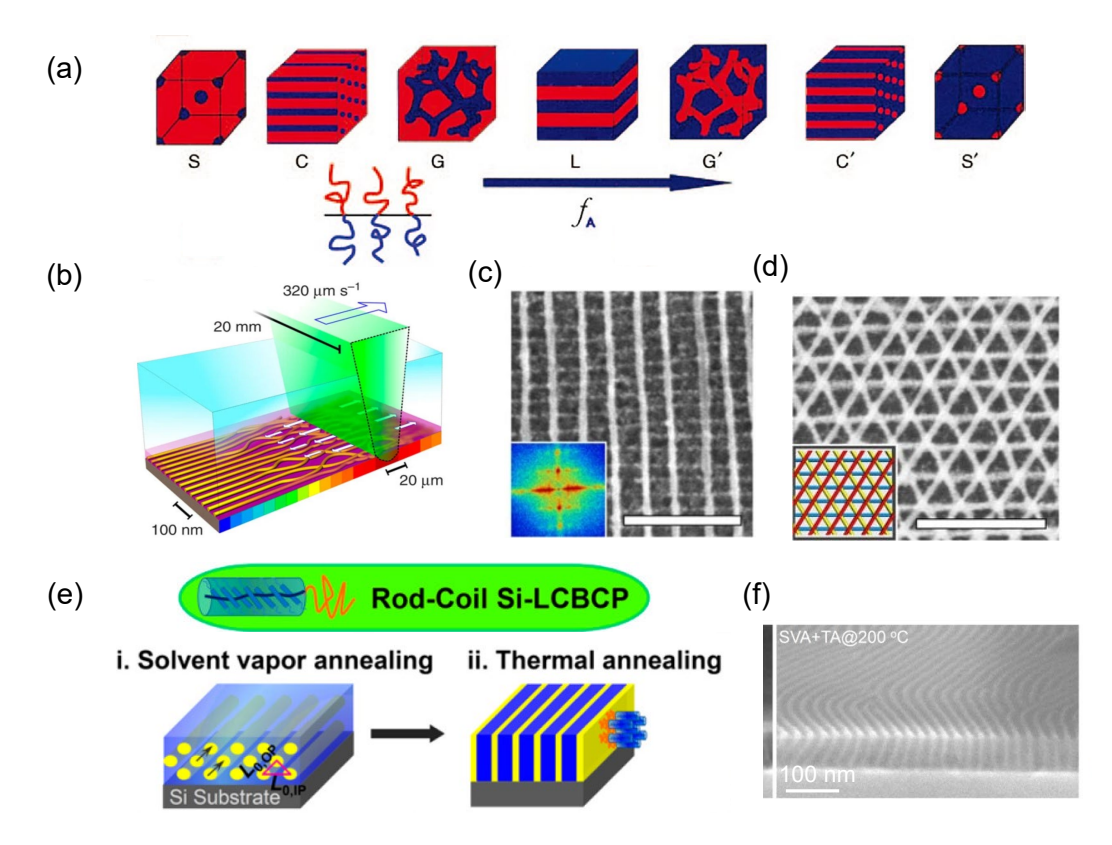


Figure 7. (a) Schematic illustration of the self-assembled nanostructures of BCP including spheres (S), cylinders (C), gyroid (G), and lamellae (L).[179] Copyright 1995. Adapted with permission from the American Chemical Society. (b) Process scheme of Soft-shear laser zone annealing (SS-LZA).[201] (c) SEM of rectangular mesh obtained by two layers of BCP with different molecular weight.[201] (d) SEM of a triangular mesh formed by three continuous rounds of SS-LZA.[201] Copyright 2015. Adapted with permission from the Springer Nature. (e) Schematic drawing of the rod-coil silicon-containing LCBCPs, (i) in-plane cylindrical structures after SVA and (ii) out-of-plane vertical lamellae after thermal annealing.[245] (f) Cross-section SEM images of LCBCPs after SVA and thermal annealing at 200 °C.[245] Copyright 2020. Adapted with permission from the American Chemical Society.

2.5.2 Directed Self-Assembly (DSA)

While self-assembly of BCPs shows high degree of order and fine resolution, controlling specific orientation of microdomains for long-range order while minimizing large-area defects still remains a huge challenge.[84,250] Integrating bottom-up self-assembly with other top-down patterning methods enables the fabrication of highly ordered and defect-free orders in large areas[132]. This strategy, known as DSA, can be categorized into graphoepitaxy and chemoepitaxy categories depending on whether the surface is pre-modified with topographical or chemical patterns[266,267].

2.5.2.1 Topographic Patterning: Graphoepitaxy

With the investigation on topographical patterned substrates with varied geometries, previous works from Ross, Thomas and Berggren et al. have found that BCPs can accommodate different template features and achieve periodic nanostructures in even coarse and imperfect templates [268]. Therefore, DSA on topographically patterned substrates shows enhanced control over the orientation of the assembled structures and reduced defects. Graphoepitaxy uses topographical templates to physically confine the phase separation region of BCPs and direct long-range ordered nanostructures (Figure 8a).[267,269–275] The confined dimensions such as the depth and width [276–280] as well as the surface chemical modification of nanoscale trenches[271,281,282] significantly affect the resulting DSA patterns. For example, Krishnan et al. investigated the DSA of 3-arm star-block copolymer PS–PDMS in pre-defined wells with PS brushes modified sidewalls.[283] The formation of vertical cylinders first occurs near the sidewalls due to lower energy barrier of nucleation, leading to the growth of hexagonally packed cylindrical microdomains toward the center with the increase of annealing time (Figure 8b). Noticeably, even though this method achieved a defect density as low as 3 defects per µm², the number of defects still seems far above the acceptable value for industrial applications[284]. Moreover, the difficulty of removing the topographic templates may affect the device density and limit the further implementation in manufacturing.

Apart from defect density, critical dimension (CD), line edge roughness (LER) and line width roughness (LWR) are also important parameters in assessing the pattern quality. Increasing χ values of BCPs helps to reduce the interfacial width, thus lowering the LER and LWR. Nonetheless, excessively high χ value brings about large kinetic barrier for chain interdiffusion, showing the importance for searching suitable χ . For example, through adjusting the χ value of the (poly(2-vinylpyridine-co-4-vinylpyridne)-b-poly(dimethylsiloxane) (P(2VP-co-4VP)-b-PDMS)), Hur et al. reduced interfacial width of the patterns and shrank the LER and LWR to 1.48 nm and 0.89 nm, respectively (**Figure 8c-d**)[190]. Further exploration is still demanded for searching for the suitable χ value to achieve sub-nm roughness in DSA structures.

Study of the non-equilibrium state provides insights for better understanding the defect formation process of BCP systems. On the occasion of overfilling, metastable state could form as an intermediate

phase before the full conversion to stable state. For example, Aissou et al. found that intermediate structures of "wavy lines and dots" were present as defects in the double gyroid patterns of poly(1,1-dimethyl silacyclobutane)-block-polystyrene (PDMSB-b-PS) (**Figure 8e**) [285]. When the gyroid unit-cell size was larger than the film thickness on the mesas while smaller than that in the trenches, the delayed kinetics of pattern formation resulted in mixed morphologies with metastable structures and the stable state of double gyroids. Full conversion of the intermediate state to the double-gyroid pattern was obtained with extended annealing time.

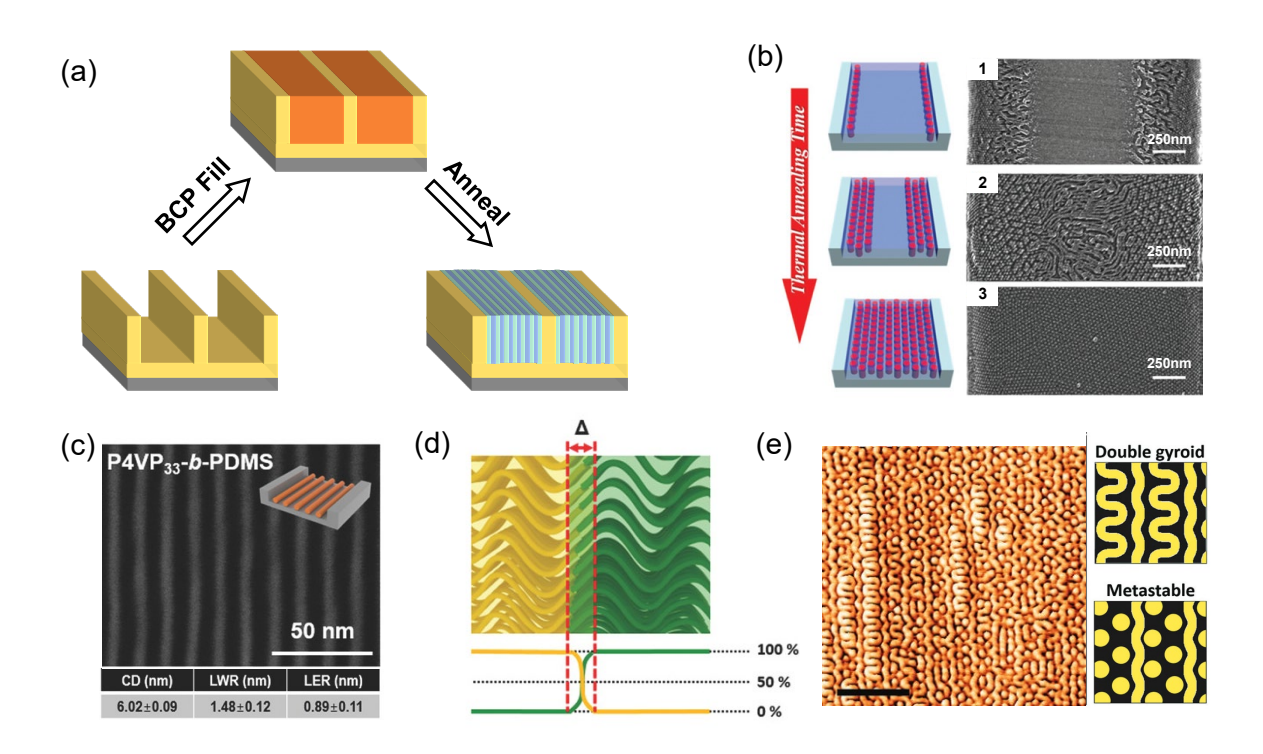


Figure 8. (a) Process scheme of graphoepitaxy. (b) The dynamic process of nucleation and growth during the DSA of 3-arm star-block PS–PDMS through graphoepitaxy. SEM images correspond to annealing time of (1) 30 min, (2) 60 min and (3) 90 min, respectively. [283] Copyright 2018. Adapted with permission from John Wiley & Sons Inc. (c-d) SEM image and theoretical description of the interfacial width of P4VP₃₃-b-PDMS (the weight percentage of 4VP in P(2VP-co-4VP) is 33%). [190] Copyright 2018. Adapted with permission from John Wiley & Sons Inc. (e) AFM image of the double-wave pattern of PDMSB-b-PS film after SVA. Sketches: double gyroid and intermediate structure. Scale bar: 200 nm. [285] Copyright 2017. Adapted with permission from John Wiley & Sons Inc.

2.5.2.2 Chemical Patterning: Chemoepitaxy

Since surface modification was reported effective for controlling the interfacial interactions between

polymer and substrates [286], the pioneering work on DSA of PS-b-PMMA *via* chemoepitaxy was reported by Nealey et al. in early 2000s [287]. Since then, chemoepitaxy has been widely explored for more sophisticated pre-patterns and smaller pattern periods through density multiplication [288,289]. The chemoepitaxy relies on the pre-defined chemical patterns to control the BCP periodicity. Various strategies, such as polymer brush backfill[210,266,290–297], selective SAMs[298], lithographically-defined chemical patterns[299–302], oxygen plasma treatment[303,304] and photoacid-sensitive surface treatment[305] have been investigated to produce chemoepitaxy. These pre-patterning techniques can tune the affinity of the chemically distinct zones with each block of the BCP and thus guide the DSA processes[306]. For example, hydrophilic stripes created on the hydrophobic PS surface *via* O₂ plasma enabled the DSA of poly(styrene-b-(lactic acid-*alt*-glycolic acid)) (PS-b-PLGA)[303]. The more hydrophilic PLGA blocks preferentially wet the oxidized PS strips, while the relatively hydrophobic PS blocks show strong affinity with the untreated regions.

Typically, the period of the pre-defined surface chemical patterns (L_s) is commensurate with the period of the self-assembled BCP structures (L_0)[306,307]. Based on this principle, Ruiz and Nealey et al. first proposed the concept of density multiplication to increase the feature resolution with respect to the pre-patterns[308]. Since then, high density multiplication has been widely reported as a promising option to fabricate structures with sub-10 nm features[266,290–293,295]. For instance, through designing the ratio of width (W) and pitch (L_s) to L_0 , a fourfold density multiplication of self-assembled P2VP-b-PS-b-P2VP was achieved with feature sizes down to 8 nm [210]. (**Figure 9a-b**).

Owing to the ability to provide a neutral interface for each of BCP blocks, introducing thin film topcoats on BCPs is an effective approach to guide the DSA process *via* chemoepitaxy[222,255,309]. Vapor phase deposited topcoat typically grafts to and immobilizes the BCP chains, thus creating equal affinity to each block without the need for proper surface energy of the topcoat relative to the BCP blocks. Suh et al. took advantage of iCVD and grew a ultrathin PDVB topcoat as a neutral interface for the chemoepitaxy of P2VP-*b*-PS-*b*-P2VP.[309] This iCVD topcoat in conjunction with the pre-defined PS-*r*-P2VP strips on the substrate regulate the self-assembly process for the vertical lamellae structures with sub-10 nm line width

(**Figure 9c-d**). Compared to solution-applied topcoats, the insolubility of the highly cross-linked iCVD PDVB topcoat eliminates chemical orthogonality problem, and enables dual-scale patterning *via* photolithography on top of the BCP pattern.

Different from conventional chemoepitaxy, selective chemoepitaxy could achieve multiple assembled structures in a single film of BCP blends. Through varying the spatial parameters of the underlying chemical templates, both homogenous and co-existing phases can be achieved in a blend film with two types of PS-b-PMMA with different PS volume fraction [310] (**Figure 9e**). For example, hexagonal dot arrays dominate when the pitches of the underlying pattern are narrower than 44 nm, while line structures appear for the pitches of the pre-pattern range from ~48 to 54 nm (**Figure 9f**). The competition between interfacial energies and chain distortions was proposed as the governing factor for the co-existing morphologies of BCP blends. Future exploration of this selective DSA method for more sophisticated templates and BCP blends could stimulate more variations of nanoscale BCP patterns.

Chemoepitaxy provides additional control over the long-range order and reduces the feature sizes of the assembled BCP structures. Unfortunately, to achieve sub-10 nm domains by chemoepitaxy generally requires high-resolution chemical pre-patterns with line widths limited in a narrow range (e.g. 0.5 L₀<Width<1.5L₀) [311]. Therefore, the fabrication of pre-patterns often needs advanced lithographic techniques such as electron beam lithography and X-ray interference lithography. Apart from improving the pre-pattern resolution and surface contrast, combining graphoepitaxy could be an alternative approach to increase the guiding strength for further enhancement of the chemoepitaxy quality with less defects and wider process window. [312–314].

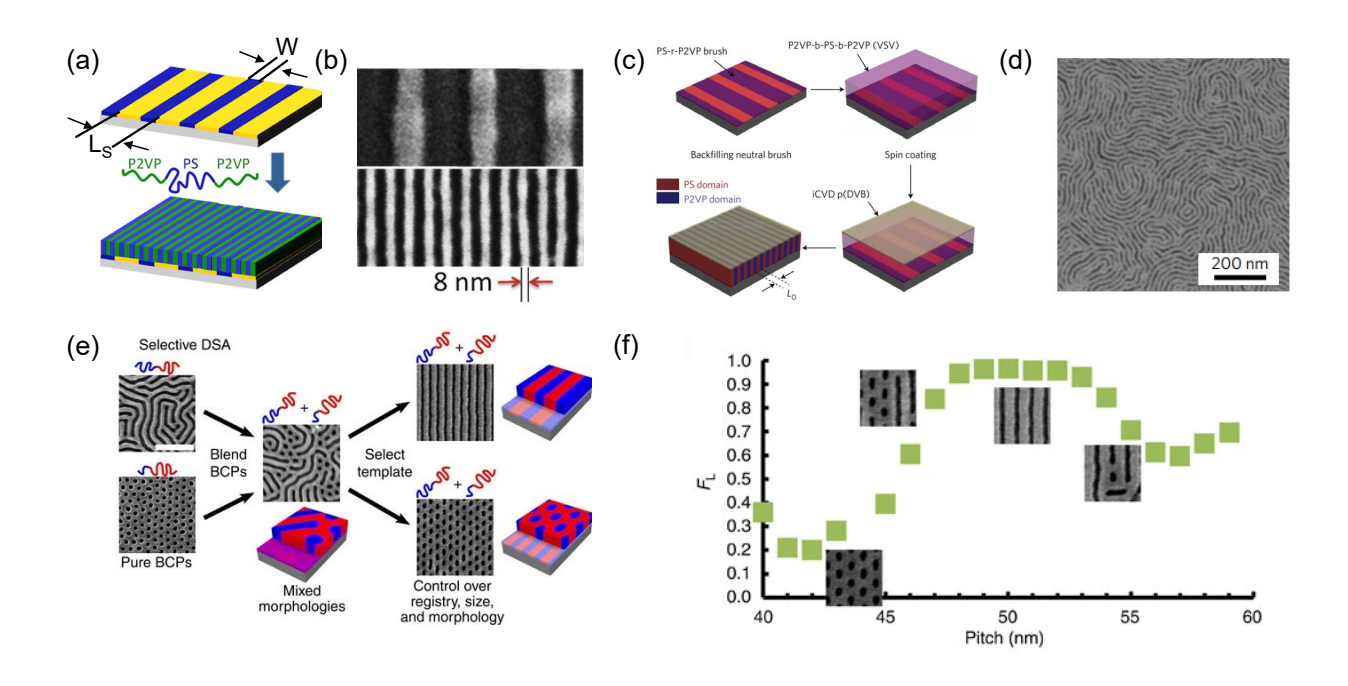


Figure 9. (a) Process scheme of chemoepitaxy for P2VP-*b*-PS-*b*-P2VP triblock copolymer and (b) SEM of the resulting lamellae structure with 4× density multiplication.[210] Copyright 2016. Adapted with permission from the American Chemistry Society. (c) Chemoepitaxy procedure with iCVD topcoat for P2VP-*b*-PS-*b*-P2VP triblock copolymer and (d) SEM of the lamellae pattern obtained after DSA[309] Copyright 2017. Adapted with permission from the Springer Nature. (e) Illustration of the selective DSA methodology where blend BCPs assemble on grating prepatterns. scale bar: 250 nm and (f) Fractional pattern area covered by lines (F_L) versus chemical pattern pitch. F_L=1 denotes a complete lines/spaces pattern. [310] Copyright 2016. Adapted with permission from the Springer Nature.

2.5.2.3 Defect Analysis

Defect control of DSA processes has been the key limiting factor for high-volume manufacturing in industry[292,315–317]. Almost 10 years ago, chemoepitaxy of PS-b-PMMA was successfully demonstrated on the wafer scale of 300 mm at Interuniversity Microelectronics Centre (IMEC).[318] However, achieving both high fidelity and low defectivity of DSA on scalable regions still remains a challenge. Afterwards, IMEC has continued extensive efforts in capturing the defect information at different DSA stages and elucidating the origin of different types of defects, and thus achieved low defectivity over large areas (24 defects cm⁻²) [319]. **Figure 10a** shows the various defect modes after pattern transfer by Si etching process. Typically, dislocations, 1-period bridges, residues and line-wiggling are most common defect features. Even simple defects such as dislocations may have multiple kinetic barriers along the defect

annihilation path, let alone the difficulty in eliminating large and complex defects[317,320]. Further investigation to deepen the understanding of how materials and processes affect the defectivity would help to promote the defect control in DSA processes[284,320–326].

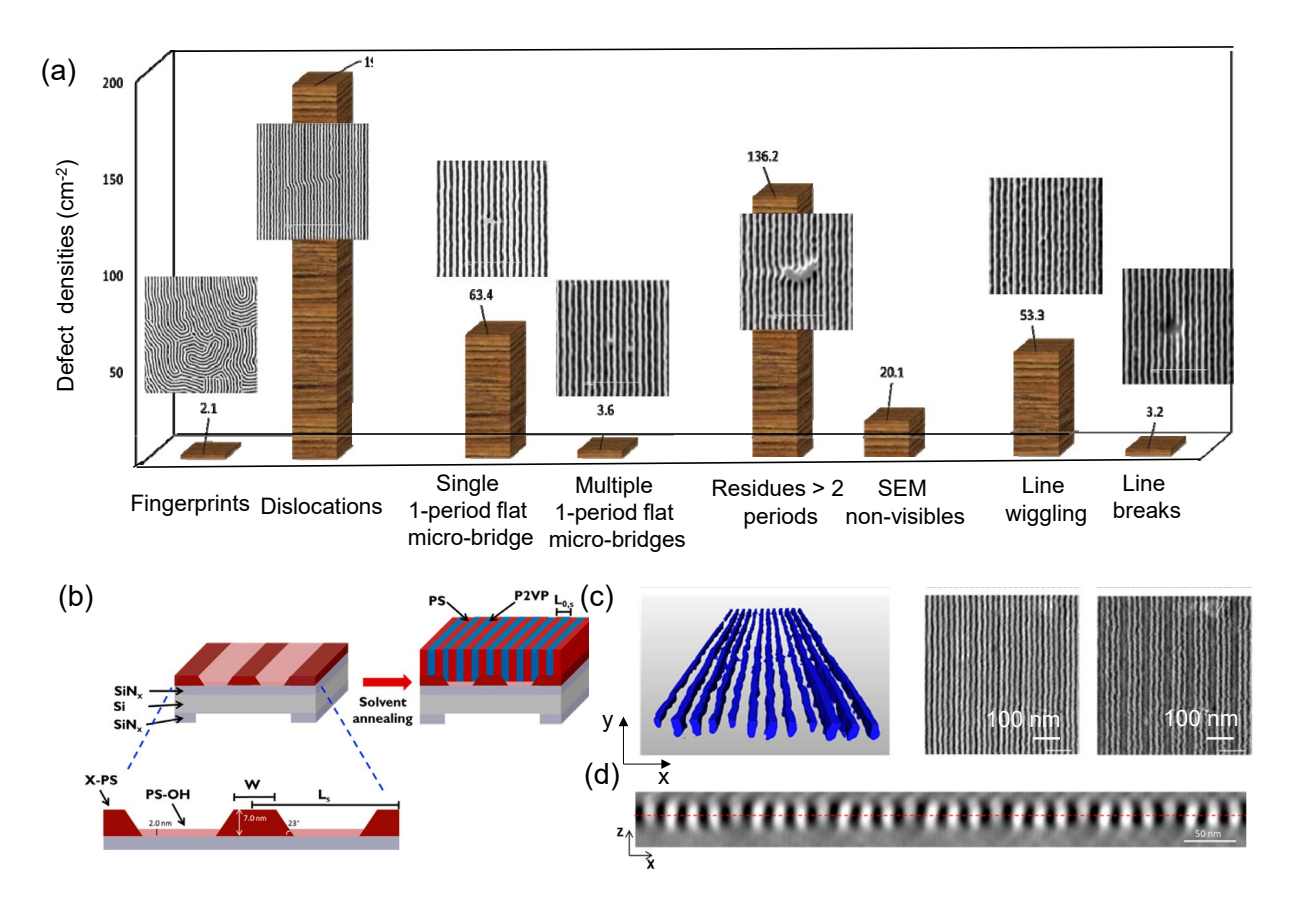


Figure 10. (a) Pareto chart of various defect metrologies after Si etch.[319] Copyright 2015. Adapted with permission from Society of Photo-Optical Instrumentation Engineers (SPIE). (b) Schematic of the hybrid chemical and topographical templates, (c) STEM tomography of P2VP-b-PS-b-P2VP DSA film on hybrid templates with X-PS width equals 1.4 L_0 : 3D visualization of the reconstructed volume (left column), xy slice close to the top layer with $z\approx2$ nm (central column) and xy slice near the bottom film with $z\approx5$ nm (right column) and (d) cross section SEM image of the DSA films on templates with W=1.4 L_0 . The red dash line denotes to the middle of the film (z=13.3 nm).[327] Copyright 2017. Adapted with permission from the American Chemistry Society.

Investigating the through-film morphology and detecting underneath defectivity is critical for developing BCP-related processes. To do this, advanced characterization techniques (e.g. scanning transmission electron microscope (STEM) tomography) is often needed for visualizing the defects embedded in the films. Additionally, simulation tools including theoretically informed coarse-grain (TICG)

provide computational prediction for the geometry and dimensions of the domains [327]. Recently, Segal-Peretz et al. designed and fabricated a topographic template with three kinds of surface chemistry for sidewall-driven DSA of P2VP-b-PS-b-P2VP (Figure 10b)[327]. The top-down probing techniques reveled the variation of P2VP lamellae population in the entire film. For example, Figure 10c shows that the number of P2VP lamellae in a single L_s near the top surface exceeds that close to the bottom of the film. The polymer molecules at the middle of the film are considered less mobile and more constrained compared to the top and bottom surfaces, leading to the minimum positional fluctuation at the middle depth of the film (red dash line in Figure 10d). The work opens up avenues for investigating the relationship between through-film BCP structures and prepatterned templates *via* 3D characterization, providing better illustration for DSA process and guiding better design for directing templates.

2.6 Instability Induced Patterning

Instability induced by gradients of surface tension and charge density can be utilized for polymer thin film patterning. For example, the surface tension gradient resulted from either temperature variation or concentration difference often leads to Bénard–Marangoni convection, enabling pattern formation through dewetting.[328,329] When external electric field[330–332] is applied to polymer layers above the T_g, polarization force present in the dielectric polymer films may also lead to instability, generating topographical structures *via* bottom-up processes.

2.6.1 Surface Tension Induced Patterning

Temperature gradient is often used to generate thermocapillary convection for instability induced patterning. Vertical (Figure 11a) and horizontal (Figure 11b) thermal gradient applied to polymer films can both lead to surface tension gradients that drive convection when the Marangoni dimensionless number exceeds the threshold.[333] Figure 11a illustrates the formation of self-assembly capillary bridges driven by the vertical thermal gradient, while Figure 11b shows the macroscopic motion of polymer films guided by the in-plane thermal gradient.

Apart from the thermal driving force, concentration gradient may also lead to the surface tension difference that causes Marangoni instability. For example, ethanol vapor treatment leads to the spatial concentration gradient in poly(lauryl methacrylate) and allows the pattern formation of a polymer/quantum dot composite film (**Figure 11d**)[334]. Surface tension gradient formed during polymer swelling has also been used for controlled phase separation and instability induced micro-/nanoscale patterning[335].

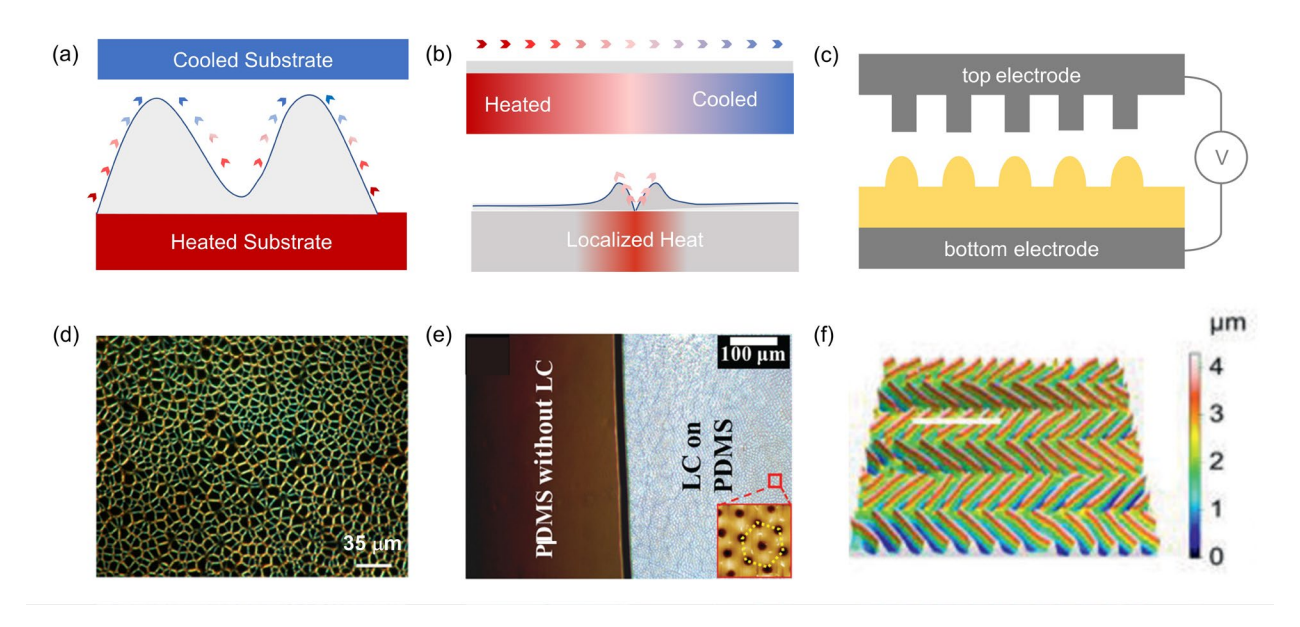


Figure 11. (a-c) Schematic illustration of pattern formation induced by the instability created due to (a) vertical and (b) horizontal thermal gradient as well as (c) electric field. (d) Dark field images of the polymer/quantum dot composite pattern formed from dewetting[334]. Copyright 2017. Adapted with permission from the American Chemical Society. (e) Optical and AFM (inset) images of the NLC microwells fabricated on PDMS substrate[336]. Copyright 2019. Adapted with permission from the Royal Society of Chemistry. (f) 3D image of the LCP films after EHD actuation. The white line indicates the direction that patterns are formed [337]. Copyright 2021. Adapted with permission from John Wiley & Sons Inc.

Dewetting has recently been leveraged during the dropwise condensation of monomer vapor to form discrete dome-shaped patterns on a surface (**Figure 12**)[338]. The monomer drops are solidified *via* a chaingrowth polymerization, initiated by vapor-phase free radicals. The two-step synthesis, namely condensed droplet polymerization (CDP), gives rise to a variety of surface-attached hemispheres with tunable size (from ~100 nm to several μm) while delivering access to a large collection of organic functional moieties.

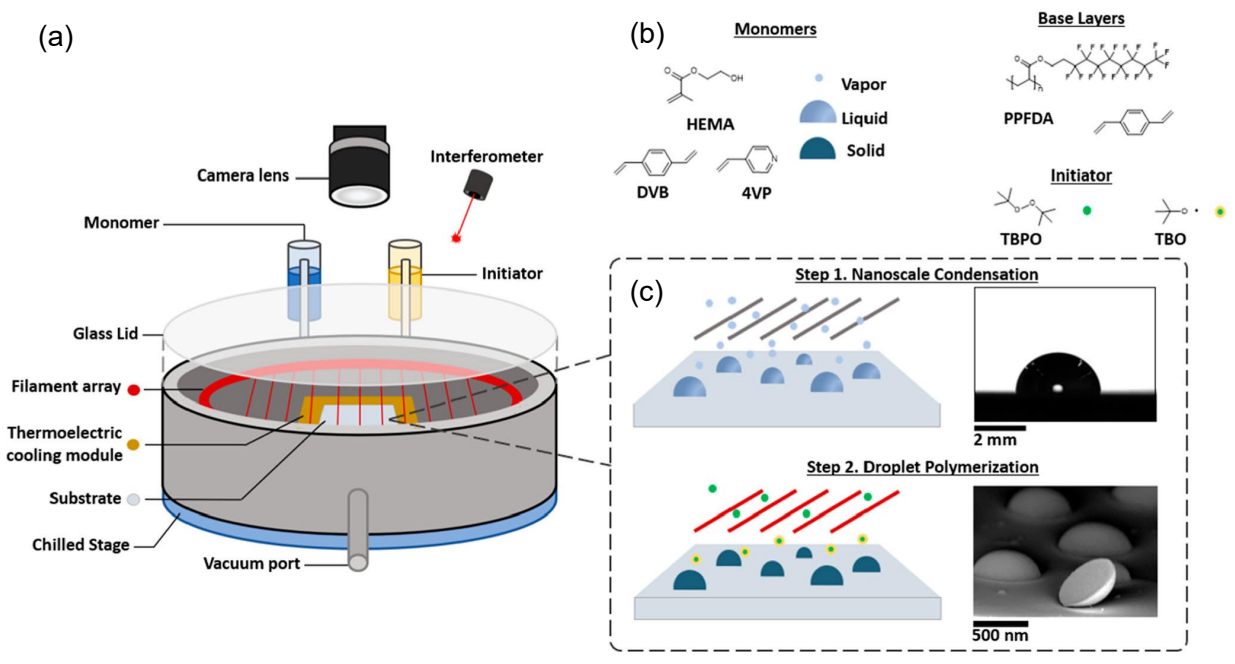


Figure 12. (a) Schematic illustration of the iCVD reactor for CDP. (b) Selected monomers and initiators. (c). two steps depiction of CDP process.[338] Copyright 2022. Adapted with permission from the American Chemical Society.

Random nucleation during the dewetting is difficult to control in instability driven patterning. Introducing nanoparticles as the heterogeneous nucleation sites is effective in dealing with this challenge. Recently, Das et al. deposited gold nanoparticles (AuNPs) underneath the spun-coated PS thin films as the nucleation sites on the PDMS substrates[339]. The surface energy difference between the hydrophobic PDMS surface and hydrophilic AuNPs decreases the size of the dewetted droplets. Compared to pure PDMS surface without nucleation sites, substrates decorated with AuNPs exhibit patterns with 10× smaller feature size.

2.6.2 Electric Field Induced Patterning

Electric field applied across polymer thin films at temperatures above T_g can destabilize the interface between the polymer and air/liquid, thus forming topographical patterns. Changing the structure of patterned electrodes[330] and types of polymers have both been explored to miniaturize the patterns under electric field. Compared to flat electrodes, the 3D electrodes reduce the periodicity of pattern and promote long-range order[84,336](Figure 11c). Various polymer systems including thermoplastic polymers[340], polymer

blends[331], BCPs[332] and liquid crystal polymers[337] have been investigated for obtaining complex micro/nanostructures with small feature size. For example, the alignment and anisotropic properties of liquid
crystalline materials can be utilized for patterning induced by EHD instability. Recently, Roy et al. infused
nematic liquid crystal (NLC) between the PDMS film and the electrode as an orientable soft template for
imprinting microwells on PDMS surface under Maxwell stress (Figure 11e).[336] Taking advantage of the
photo-alignment of liquid crystals, Lv et al. obtained complex 3D structures of liquid crystal polymers (LCPs)
in electric field induced patterning.[337] Figure 11f shows the resulting polarized optical microscopic image of
the LCPs zigzag pattern based on the pre-defined photo-alignment agent.

Surface instability takes advantages of the inherent properties of polymers to generate intriguing patterning. Typically, patterning induced by surface instability tend to evolve towards a more favorable state with minimized surface energy. Therefore, the unstable or metastable polymer films often achieve a variety of morphologies such as pillars, rings and dots, but it is not capable of forming arbitrary micro-/nanoscale shapes as a function of external stimulus.

2.7 Patterning *via* Polymer Crystallization

Thin films provide a confined environment for polymer crystallization, leading to crystalline morphologies that may differs from bulk polymers and thick films[341,342]. During the crystallization in polymer thin films, regular patterns can be generated by localized control over the nuclei formation. For example, by gently brushing the poly(3-butylthiophene) (P3BT) film before solvent annealing, Wei et al. were able to form ordered spherulites along the scratches [343]. The ridges alongside the scratches hinder the diffusion of the polymer chains, thus concentrating P3HT near the scratches for earlier nucleation. In contrast to the random nucleation in the unscratched regions, the spherulites formed preferentially at the stretched areas. Recently, Li et al. developed a seesaw-like pivoting strategy for meniscus-guided deposition, and achieved controllable nucleation at the front of drying during polymer film formation [344]. They built a wedge-shaped setup to confine the P(NDI2OD-T2) solution, and employed sample pivoting to force the polymer solution to flow and thus to redistribute the concentration, narrowing the undercooling region for crystallization. A variety of ordered patterns such as fishbone-like stripes and twined crystalline lines have been generated using this approach.

3. Applications

3.1 Chromic Devices

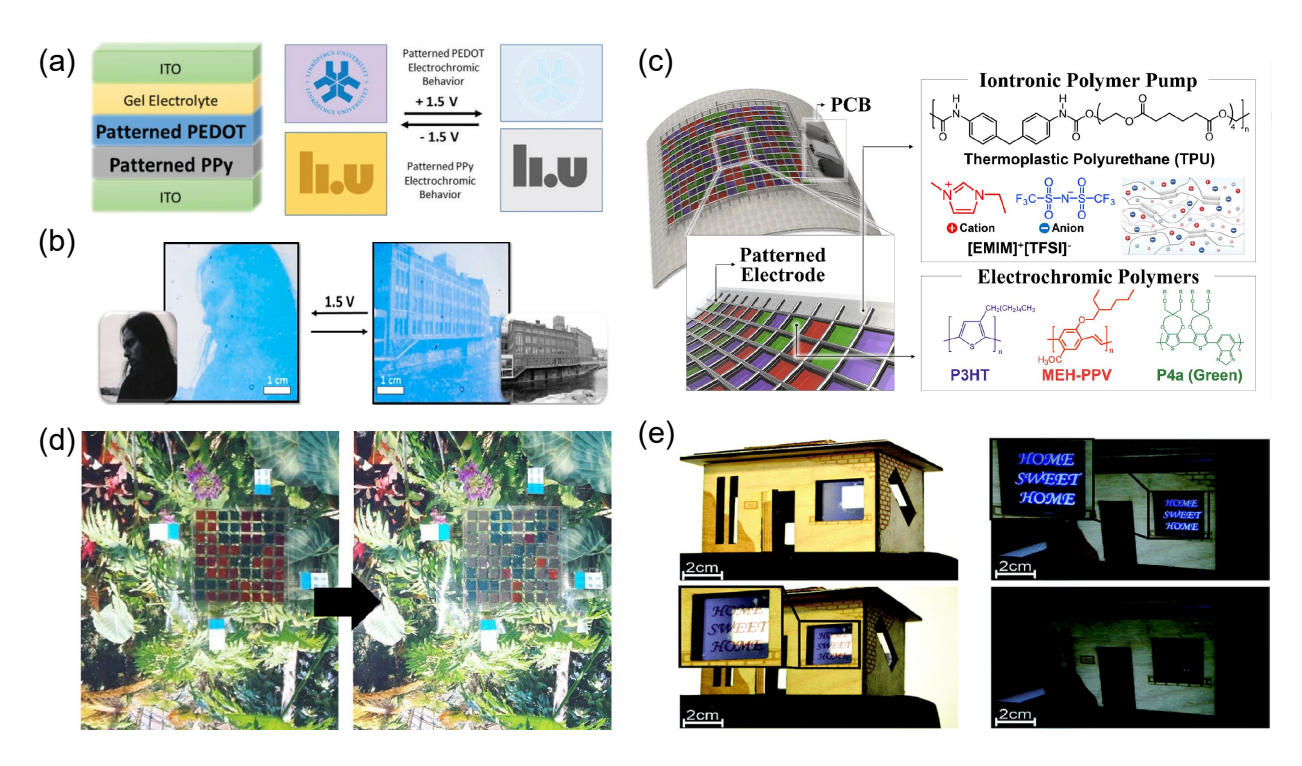


Figure 13. (a) Device architecture of the dual-image electrochromic display with pattern switching under applied voltage bias of ±1.5V.[124] Copyright 2018. Adapted with permission from the Royal Society of Chemistry.(b) Photo of the greyscale electrochromic displays with switchable images (greyscale UV masks inset).[125] Copyright 2019. Adapted with permission from the Multidisciplinary Digital Publishing Institute. (c) Structural design of the DMECS and the polymer materials used in this device.[345] (d) The adaptive camouflage applications of DMECS in outdoor environment.[345] Copyright 2020. Adapted with permission from the Elsevier Science Ltd. (e) The dual-mode displays operated under daylight and dark conditions.[346] Copyright 2019. Adapted with permission from the Royal Society of Chemistry.

3.1.1 Electrochromic Devices

The change of optical properties due to the redox transitions of electroactive materials enables electrochromic (EC) behaviors under applied bias. Common EC materials include metal oxides, metal coordination complexes, and conducting polymers. These materials are promising for many emerging applications such as smart windows, optical switching devices and displays. Compared with inorganic materials, conjugated polymers, such as PEDOT[347–350], P3HT[345,351] and polyaniline

(PANI)[352,353], have advantages of low processing temperature, high optical contrast, fast response time and flexibility. Recent development of novel EC materials include the design of donor-acceptor type conjugated polymers[2] and metallo-supramolecular polymer with variable valence cations[354].

Integrating multiple EC materials in a single device increases the optical contrast in the visible region and enriches the color gamut,[346] further expending the applications ranging from smart window to camouflage device. PEDOT and PPy are two widely studied conjugated polymers that can be operated at complementary states, i.e. PEDOT visible in the reduced state while PPy visible in the oxidized state. Engquist et al. integrated these two polymer patterns between the electrodes for dual-image EC displays.[124] With positive and negative applied biases, the EC device shows two different images (**Figure 13a**). The resolution of the EC patterns could achieve 100 µm *via* the selective VPP method as mentioned in Section 2.5.2. Combining greyscale photomasks, selective VPP processes also allow fabrication of conjugated polymer films with thickness gradient for grayscale displays.[125] **Figure 13b** shows the greyscale EC device based on two layers of pattern PEDOT: tosylate (Tos) films that allow picture-to-picture switching.

Koo et al. demonstrated a dynamic multicolor electrochromic skin (DMECS) *via* integrating the EC material P3HT, poly[2-methoxy-5-(2-ethylhexyl-oxy)-1,4-phenylenevinylene] and P4a on one printed circuit board, showing the purple, orange and green colors respectively (**Figure 13c**)[345]. The multicolor-featured device offers users to selectively switch the coloration and bleaching of patterns through a Bluetooth connection with a mobile color app. In particular, the ionic thermoplastic PU and polyethylene-based material served as flexible electrolyte and electrode in DMECS, respectively. Thus, the technology is able to be used as wearable device to mimic the outside environments and shows adaptive camouflage applications (**Figure 13d**).

Lacking an emissive light source, EC devices typically cannot operate in dark conditions. Adding an electrofluorochromic (EFC) layer to the EC device enables dual display modes, i.e. emissive and reflective, as well as low power consumption. Recently, Pietsch et al. developed a dual-mode displays (DMD) using polyindenofluoren-8-tryarylamine polymer (PIF8-TAA) which possesses both electrochromic and

electrofluorochromic effect[346]. Further introduction of a secondary EC material (e.g. PEDOT and P3HT) enlarges the number of displayable colors. **Figure 13e** shows the DMD in operation under daylight and dark conditions, revealing the potential for smart windows for advertisement.

3.1.2 Thermochromic devices

Thermochromism denotes a phenomenon of color change under thermo-stimuli, exhibiting considerable applications from temperature switches to anti-counterfeiting devices[355]. The thermochromic polymers can be classified into inherent and doped systems.[356] The conjugated (e.g. polydiacetylene, polyacetylene, polythiophenes) and liquid crystalline polymers possess inherent thermochromic properties. The doped thermochromic polymers mostly based on the incorporation of thermochromic pigments[355,357] or interaction with the non-thermochromic additives (e.g. temperature modulate the extent of dye aggregation in polymer matrix).

Recently, Hu et al. synthesized polydiacetylene-based nanosheets *via* self-assembly of the maleic acid-capped monomer molecules and subsequent UV polymerization (**Figure 14a**).[57] The resulting polydiacetylene-based nanosheets exhibit reversible blue-to-red chromism in response to cooling-heating cycles between 25-90°C, which is likely caused by the conformational change of the polydiacetylene backbones. Utilizing the thermochromic effect, the authors inkjet printed patterns of the nanosheets on flexible paper (**Figure 14b**) for displays. It's worth noting that besides direct thermochromism, these polydiacetylene based nanosheets also possess near-infrared (NIR) response due to the heat generation through a photothermal process, demonstrating the possibility of remote control for thermochromic displays. Kragt et al. designed a thermochromic cholesteric coatings composed of a non-cross-linked liquid crystal siloxane-based elastomer (LCEs) that is interpenetrated through an acrylate-based cholesteric liquid crystal network (LCNs).[358] They proposed that above the cholesteric-to-isotropic transition temperature (T_{ch-1}), LCE obtains enough energy to diffuse out of the LCN toward the coating-air interface, leading the winding of the cholesteric pitch and changing the color correspondingly (**Figure 14c**). The process is reversible when cooling the temperature below T_{ch-1} when the LCE diffuses back to LCN under and unwinds the cholesteric pitch. It's possible to fabricate coatings with multicolor images under different processing

conditions *via* controlling the degree of phase separation (**Figure 14d**), providing new revenue as smart windows, optical sensors and so on.

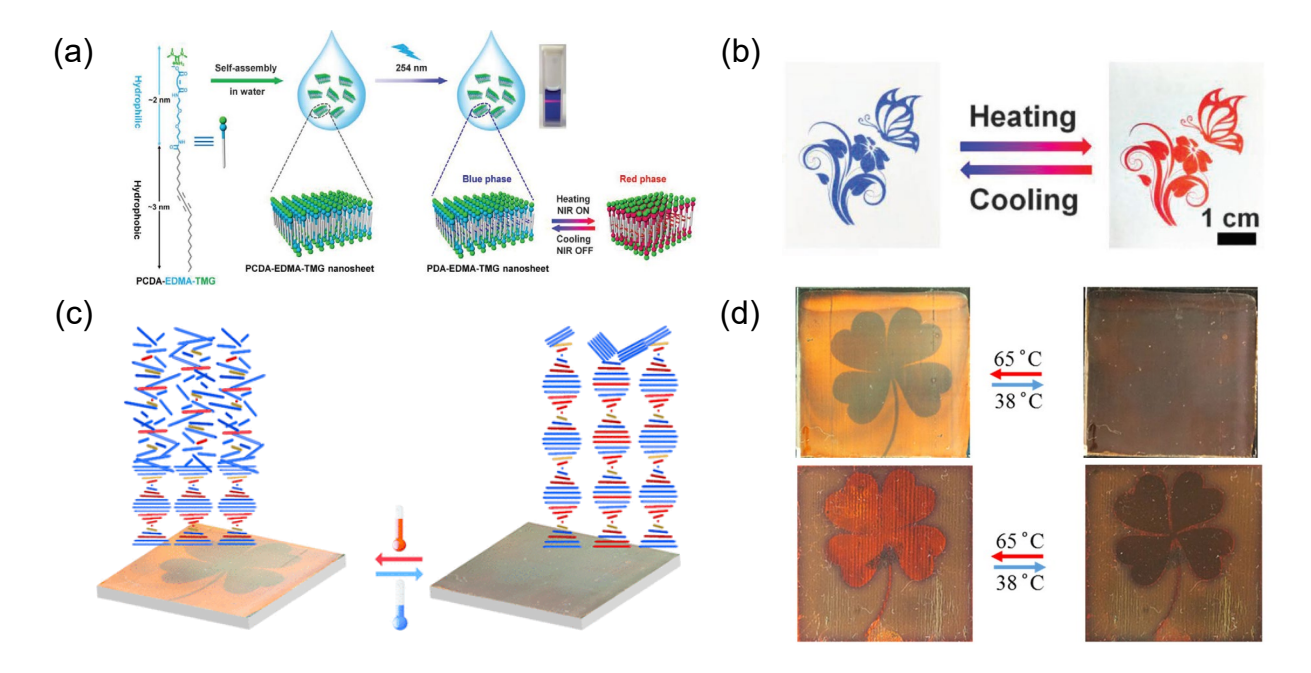


Figure 14. (a) Synthesis procedure for the polydiacetylene-based nanosheets *via* the self-assembly of maleic acid-capped diacetylene monomers followed by UV-induced polymerization.[57] (b) Photos of the thermochromic patterns inkjet-printed on paper during heating and cooling cycles[57]. Copyright 2019. Adapted with permission from John Wiley & Sons Inc. (c) Schematic illustration of the temperature-responsive color-changing mechanism of LCE[358]. (d) Photos of thermochromic multicolor leaf patterns under different UV processing conditions[358]. Copyright 2019. Adapted with permission from the American Chemical Society. Direct link: https://pubs.acs.org/doi/abs/10.1021/acsami.9b08827. Further permissions related to the material excerpted should be directed to the ACS.

As for the doped thermochromic polymers, Yang et al. incorporated thermochromic molecules with multicolor fluorescent polymer dots (Pdots) to fabricate the thermo-stimulating fluorescent ink[357]. The three types of Pdots, PFBTDBT (red), PPE (blue), PFCN (green), enable the ink with full-color emission. The variations of the conformational structure of thermochromic molecules at 25°C and 50°C, determining the fluorescence of PPE and PFCN quenching and recovering respectively. The work printed the personal bank check with numbers by the designed ink, exhibiting the dual-readout abilities since all of the numbers can only be clearly visible at 50°C in UV light. The dual-readout methodology shows the promising prospect in anticounterfeiting fields.

3.2 Polymer Light-Emitting Diodes (PLEDs)

PLEDs have been the emergent technology to fabricate full-color displays and lighting panels owing to the advantages in the facile chemical modification, easy processability, cost-effective and flexibility[359]. Sharing the similar structure with small molecule based OLEDs, PLED devices typically consist of two electrodes, one emissive layer (EML) where electrons and holes recombine, and multiple injection and transport layers for lowering charge transport energy barrier (**Figure 15a**).[360,361] Polymer thin film patterning is widely used in all corners of PLED devices, including (i) micro-lens array (MLA) modified substrates for improved light extraction and enhanced out-coupling power efficiency[362–364], (ii) electrodes [78,365,366], EML [1,83,139,367–371] and hole injection layer (HIL) for patterned illumination[372–375], and (iii) pixel define layer for defining lighting regions[376].

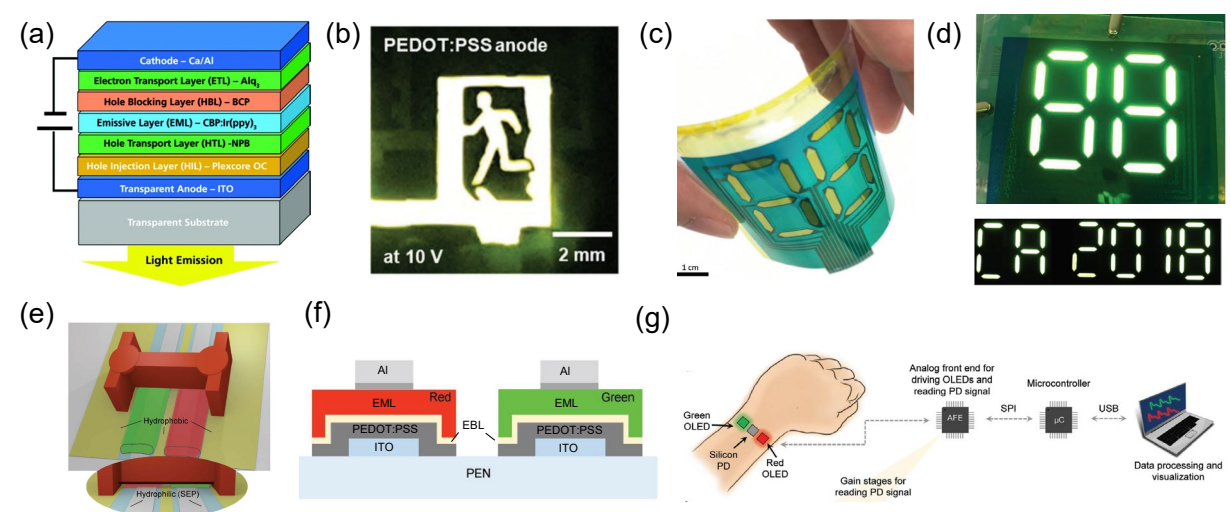


Figure 15. (a) Device architecture of a typical OLED device[360]. Copyright 2017. Adapted with permission from the Royal Society of Chemistry. (b) Photo of a PLED with patterned PEDOT:PSS anode[78]. Copyright 2019. Adapted with permission from John Wiley & Sons Inc. (c-d) Photos of a flexible light-weight display with seven-segment OLEDs displaying "88", "CA", and "2018".[1] Copyright 2018. Adapted with permission from John Wiley & Sons Inc (e) Fabrication procedure of a multicolor PLEDs through SEP technique[369]. (f) Device structure of the multicolor (red and green) PLEDs integrated in a single substrate[369]. (g) Schematic illustration of the oximeter system for acquiring PPG signal from the wrist[369]. Copyright 2017. Adapted with permission from John Wiley & Sons Inc.

Structured polymer electrodes are useful in defining the illumination patterns of soft PLEDs. In order

to avoid solvent damage to bottom organic layers in all-solution processed PLEDs, Hong et al. developed a transfer printing process for PEDOT:PSS transparent conductive electrodes.[78] With the PEDOT:PSS electrodes, the PLEDs showed excellent mechanical flexibility under 1000 bending cycles at a bending radius of 2 mm. Besides, the all-solution processed PLEDs exhibited high current efficiency of 10.4 cd/A. **Figure 15b** presents the glowing logo based on the patterned PEDOT:PSS anode, revealing potential application in emergency lighting.

Light patterns of PLEDs can also be determined by the shape of emissive layers. Han et al. fabricated PLEDs with patterned poly(vinylidene fluoride) (PVDF) emission area (EA) through low-cost spray coating and screen printing.[1] The two methods enabled the OLEDs of luminance 1000 cd m⁻² with similar external quantum efficiency (2.1%) and luminous efficacy (5.5 - 6.3 lm W⁻¹). **Figure 15c** shows the seven-segment flexible display prepared *via* screen printing. The printed Ag traces enable the individual operation of each segment and thus programmable display of letters and digits with a driving board (**Figure 15d**).

In addition to the applications for displays and lighting panel, PLEDs can also be used in healthcare monitoring and wearable sensors. Humphries et al. developed a surface-energy-patterning (SEP) technique to print two emissive polymeric materials on the same flexible substrate for multicolor PLEDs integrated in optoelectronic sensors (**Figure 15e-f**)[369]. The resulting multicolor PLEDs (red and green) were connected to a silicon photodiode and an analog front end (AFE) for data I/O, allowing the measurement of blood oxygenation and photoplethysmogram (PPG) on the wrist simultaneously (**Figure 15g**). The flexibility of polymeric patterned layers allows the optoelectronic sensor to form a close contact with skin for reduced ambient noises.

3.3 Sensors

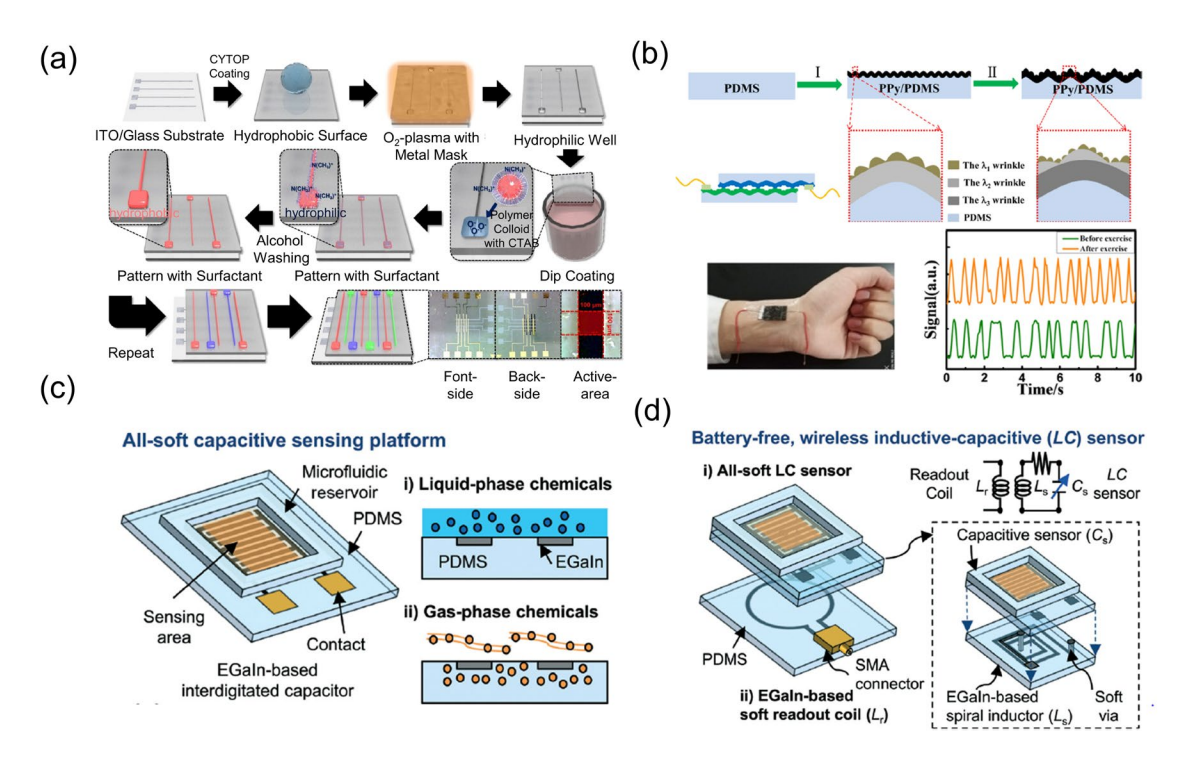


Figure 16. Optical sensors, pressure sensors and chemical sensors based on patterned polymers. (a) surfactant-induced solubility control (SISC) method of water-borne polymeric colloids for the fabrication of optical sensors[377]. Copyright 2020. Adapted with permission from the American Chemical Society. (b) three-scale nested wrinkling PPy films for pressure sensors, the application of pressure sensors as pulse detectors, and the signal recorded by the pulse detectors before and after exercise[4]. Copyright 2018. Adapted with permission from the American Chemical Society. (c-d) all-soft microfluidic chemical sensing platform based on EGaIn patterning and PDMS[378]. Copyright 2017. Adapted with permission from the Royal Society of Chemistry.

Functional polymers play an important role in various sensing applications. For example, they are used in optical sensors as light-sensitive semiconductors[377]; with motion-induced change of conductance, they can be used in strain/pressure sensors[4,379–381]; many polymers provide mechanical or electrical responses after exposure of certain chemicals, contributing to efficient chemical sensors[378,382].

Patterning techniques for polymers play an important role in the fabrication of various polymer-based sensors. The importance of patterning techniques manifests in the following aspects: 1. Specific patterns are essential for implementing various functionalities based on mechanical or chemical mechanisms. For example, in pressure sensors, certain patterns of active materials can enhance the sensitivity for the pressure detection. In chemical sensors, a pattern with high surface-to-volume ratio is generally considered as essential to enhancing the detection sensitivity. 2. Patterning active materials for miniaturized devices is

essential for integrating the sensors into a multifunctional device platform. For example, a modern pointof-care biomedical device usually requires integrated sensors, energy harvesters, signal processing units, signal emitting units and antennas in a single multifunctional flexible platform. To fabricate miniaturized, or even nano-scaled devices for such applications, patterning the active materials is mandatory.

The challenges for polymer patterning in the application of sensing lies in the following aspects: 1. Printable electronics based on polymers relies on water-borne polymer colloids. The size of polymer colloids (>100 nm) causes change of the size of the orifices of the injector during device printing, resulting reliability issues; 2. Fabricating 3D functional structures of polymers for strain/pressure sensing is difficult using traditional patterning methods; 3. Fabricating structures with high surface-to-volume ratio on a well-defined area for chemical sensing is difficult for polymer based materials; Recently researchers have developed various methods to address these challenges. The rest of this section will review some of these efforts.

Sim et al. developed a surfactant-induced solubility control method to address challenge #1 and enabled a water-processed high precision patterning of polymeric semiconductors (**Figure 16a**).[377] After the CYTOP coating, the indium-tin-oxide(ITO)/glass substrate with patterned electrodes is covered with hydrophobic material. After O₂-plama treatment with a metal mask, patterned hydrophilic wells are left to be filled by hydrophilic polymer colloids. Then the surfactant of the colloid miscelles is removed by alcohol washing, leaving the hydrophobic polymer semiconductor in the channels. The same process is repeated for other kinds of semiconducting polymer colloids, until the sensitive semiconducting materials for red, blue and green colors are all patterned on the same substrate. By using this method, the authors demonstrated a full color, color filter-free and all-polymer water-processed image sensor array with 100 μm×100 μm pixel size.

Besides optical sensors, much work has been done on strain and pressure sensors. The main efforts focus on addressing challenge #2 as carefully designed 3D structures are essential for detecting strain and pressure *via* resistive or capacitive change. As shown in **Figure 16b**, Yang et al. reported a pressure sensor based on hierarchically patterned PPy films.[4] The patterned PPy films are formed by oxidative

polymerization growth of PPy film on PDMS substrate in a mixed acidic solution. After that, double-scale nested wrinkles are formed. The following heating/cooling process brings the third surface wrinkling, as a result, a 3-scaling wrinkling surface is formed for piezoresistive pressure sensors. The resulting pressure sensors demonstrate high sensitivity (19.32 kPa⁻¹), low detection limit (1 Pa), short response time (20 ms) and good durability (>1000 circles). This pressure sensor can be used in wearable electronics for pulse detection, voice recognition and microcircuit controlling, as shown in the paper.

To address challenge #3, Kim et al. developed a flexible and stretchable capacitive sensor for volatile organic compound (VOC) based on eutectic gallium-indium liquid metal (EGaIn) filled PDMS mold with high surface-to-volume ratio (**Figure 16c**)[378]. Furthermore, they also fabricated an all-soft inductive-capacitive sensor for battery-free and wireless VOC monitoring (**Figure 16d**). In the case of liquid-phase VOC detection, the measured electrical response agrees well with the theoretical prediction with deviation as low as 3.8%. As for gas-phase VOC sensing, the lightweight (0.5 g) VOC sensor exhibits at least 1.65 folds higher sensitivities than the silicon-based solid-state sensor, promising for wearable sensing devices.

3.4 Transistors

Flexible and stretchable transistors lay the foundation for the logic circuits in "More-than-Moore" wearable electronics. Polymers, including polymer semiconductors, polymer electrolytes, polymer dielectrics, are critical materials for flexible and stretchable transistors. With intrinsic high flexibility, high transparency and low-temperature/low-cost processing, polymers are the ideal material for flexible electronics. In addition, by incorporating elastomers, polymers can be made with same form factor, mechanical properties, and chemical characteristics of human skin[383], thus polymers are essential for stretchable electronics as well. However, patterning polymeric thin film materials, especially polymer semiconductors, *via* photolithography often faces challenges due to the chemical incompatibility with the solutions used for processing photoresists, such as developers or removers[12]. In addition, the diffusion of photoresists, developers or removers will introduce impurities and traps in the polymer films, leading to high subthreshold swing (SS) and low performance[13]. Alternatively, non-photolithographic approaches

offer more flexible patterning options without the limitation of chemical orthogonality. For instance, inkjet printing is one of the most widely used technique for patterning polymer thin films directly. However, inkjet printing method suffers from low resolution (\sim 10-100 μ m) and large feature size (\sim 100-200 μ m)[384]. Therefore, the integrated circuits based on inkjet-printed polymer transistors suffer from low device density with no more than \sim 100 transistors per mm².[384]

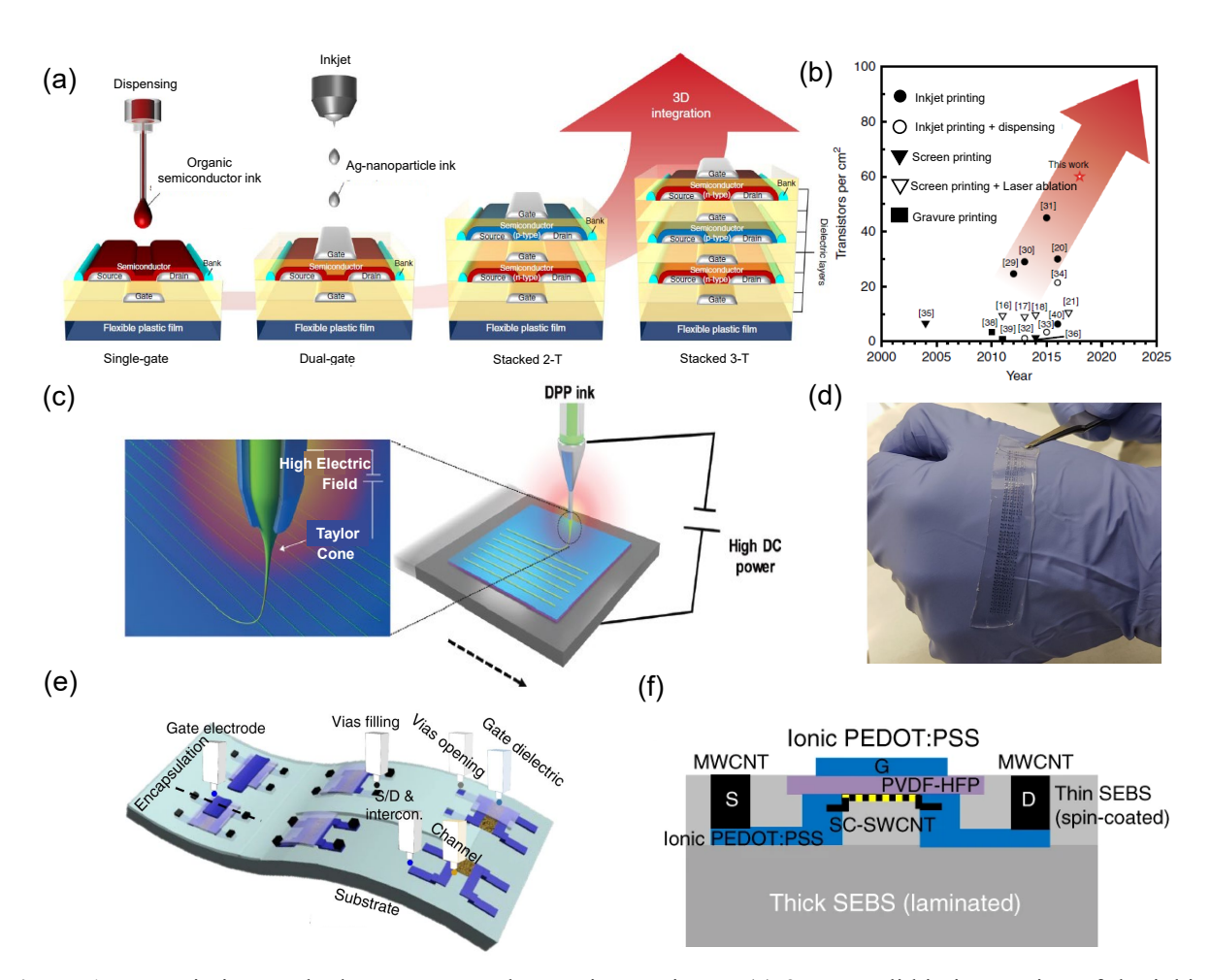


Figure 17. Jet printing methods to pattern polymers in transistors. (a) 3D monolithic integration of the inkjet printed flexible transistors, showing the single-gate architecture, dual-gate architecture, 3D-integrated two (n-/p-type, stacked 2-T) and three (n-/p-/n-type, stacked 3-T) complementary dual-gate organic transistors with shared gate electrodes[384]. (b) The trend of transistor density of printed organic circuits fabricated with various printing techniques.[384] Copyright 2019. Adapted with permission from the Springer Nature. (c) The schematic of the EHD jet printing to pattern the p-conjugated polymers[55]. Copyright 2020. Adapted with permission from the Royal of Society Chemistry. (d) Photograph of a stretchable array of inkjet printed transistors.[383] (e) The schematic showing the fabrication process of the intrinsically stretchable transistor array using inkjet printing. S is source, D is drain, G is gate[383]. (f) The architecture of the intrinsically stretchable transistor fabricated with inkjet printing[383]. Copyright 2019. Adapted with permission from the Springer Nature.

In this section, we will review recent efforts in advancing the integration density of inkjet printed polymeric transistors in flexible integrated circuits. For example, Kwon et al. developed 3D monolithic integration method to enhance the integration density of printed ICs composed of printed polymer transistors. [384] As shown in Figure 17a, they firstly designed a dual gate transistor architecture to fully deplete the polymer semiconductor channel. This design significantly decreases the SS and enhanced the on-off ratio. In addition, the device demonstrates near 0 threshold voltage as a result of the fully depleted channel in operation. With high measured carrier mobility, the transconductance (gm) is also largely enhanced. The channel materials used here are a n-type benzobis(thiadiazole) derivative (TU-3) and a ptype small molecule, dithieno[2,3-d;2',3'-d']benzo[1,2-b;4,5-b']dithiophene (DTBDT-C6) and the dielectric material is Parylene. Furthermore, the researchers built upon the dual gate architecture and stacked the printed transistors vertically to for programmable 3D NAND array (Figure 17a). This universal logic gate array is fundamental for flexible logic circuits, and the authors demonstrated a large-scale flexible logic circuitry implemented by 12×8 3D NAND gate array, which can be extended to ~2700 programmable transistors on the size of a standard credit card. This integration density is much higher than previous reported values (~100 transistors/circuit) (Figure 17b) and is comparable to that of the first commercial 4bit microprocessor.

Donor-accepter (DA) conjugated polymers are a class of polymer semiconductors with high hole or electron mobilities. Patterning this type of high performing polymers is essential for flexible electronics. However, due to the relatively low solubility, patterning DA polymers with jet printing is challenging. As shown in **Figure 17c**, Cheon et al. engineered the backbones and sidechains of DA polymers to achieve balanced EHD jet printing conditions and to allow for intermolecular self-assembly of the polymer chains during the continuous printing.[55] The chemical structures of the patterned DA polymers are shown in **Figure 17c**. High hole mobility of 3.07 cm²V⁻¹s⁻¹ is achieved in their printed large-area polymer transistor arrays.

Researchers have also explored inkjet printing technique for stretchable transistors. As shown in

Figure 17(d-f), Molina-Lopez et al. demonstrated inkjet printed stretchable polymer based transistors.[383] They used single-walled carbon nanotube (SWCNT) to form strain insensitive channels and ionic poly(vinylidene fluoride-hexafluoropropylene) (PVDF-HFP) to form thickness insensitive dielectric layers. With high mobility, high on-off ratio, high transconductance, their devices also demonstrate synaptic behaviors, and thus can be potentially used in brain-machine interface devices and other wearable bioelectronics.

3.5 Protein and Cellular Engineering

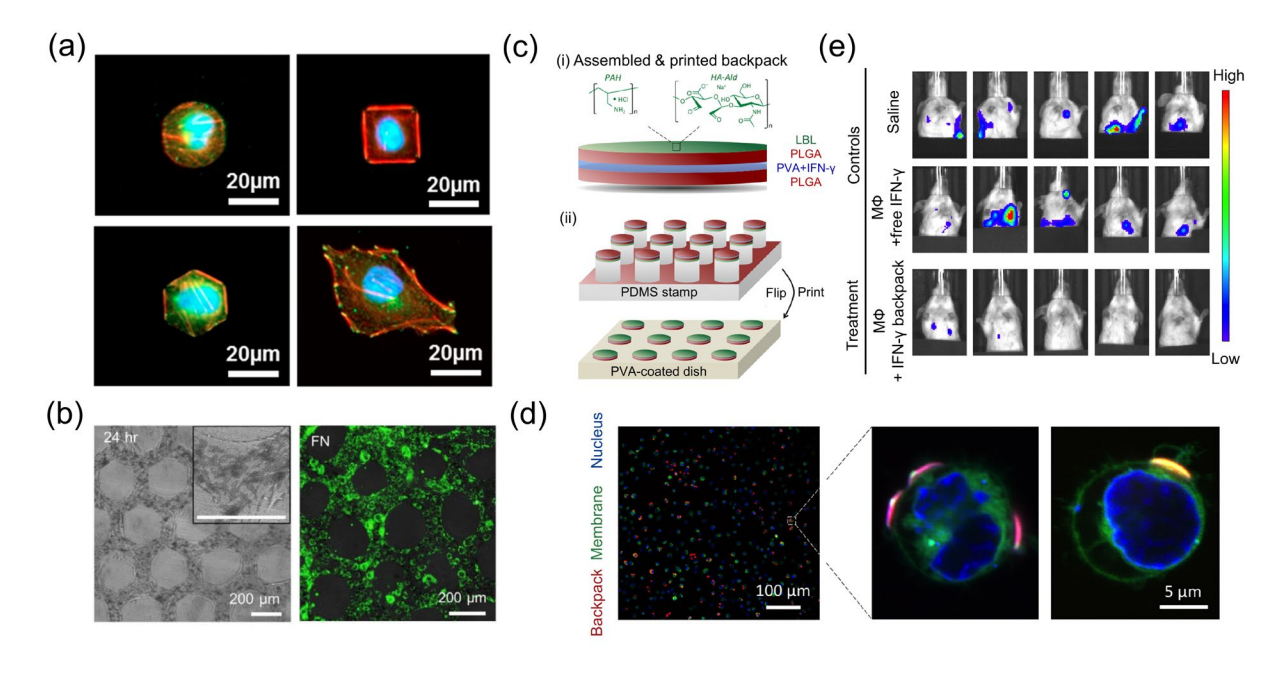


Figure 18. (a)Fluorescence micrographs of PatuT cells on adhesive islands with various geometries (constant area:~ 900 μm²) and on planar substrate after culture for 6 h[5]. Copyright 2016. Adapted with permission from the American Chemical Society. (b) Images of human dermal fibroblast (HDFB) microtissue formation on the honeycomb-patterned hydrogel[156]. Copyright 2021. Adapted with permission from the Elsevier Science Ltd. (c) Schematic illustrations of the structure and preparation of backpacks[385]. (d) Confocal micrography of macrophages (membrane, green; nucleus, blue) displaying backpacks with PLGA discs (red)[385]. (e)Vivo luminescence images of the metastatic colony formation in the mice burdened with breast cancer. The three groups showed mice received silane, unpolarized macrophages with 50 ng of free interferon-γ and backpack-macrophage complex loaded with 50 ng interferon-γ, respectively[385]. Copyright 2020. Adapted with permission from the American Association for the Advancement of Science.

3.5.1 Protein Recognition and Cell Sensing

Polymer coatings, including polymer brushes, play a significant role in controlling biological behaviors[386–388], including protein binding, recognition of biomolecules and promotion of cell attachment [29,389–392]. Patterning of polymer coatings often involves top-down and bottom-up fabrication methods[390,392], providing localized interaction for protein recognition and cell sensing. The top-down techniques include many patterning approaches we have discussed in Section 2, such as μCP[389,391] and PPL[29]. Bog et al. functionalized protein-repellent polymer brushes with localized molecular binding sites *via* PPL, allowing highly specific (99.3%) protein adsorption and reduced biofouling by 92%.[29] Alternatively, Kumar et al. generated binary chemical patterns by bottom-up synthesis of area-selectively grown polymer brushes[392]. Employing CVD and UV photolithography, they pattern SI-ATRP initiator for subsequent growth of polymer brushes, achieving bioactive and bioinert regions with localized protein adsorption.

Taking advantage of the specific binding of proteins, polymer thin film patterns can also be applied to cell separation and recognition. Capture and detection of cells from blood is of great significance in the early diagnosis of cancer. However, the ultra-low concentration of circulating tumor cells (CTCs) leads to the difficulty in insulation and sensing[394]. Creating nanostructures with high surface area and recognition specificity are therefore desired for promoting cellular interaction. For example, Jaiswal et al. used dewetting induced patterning strategy to fabricate PLGA micro-patterned surface with controllable sizes. Through functionalizing the biocompatible PLGA patterns with antigen-specific antibodies, they achieved high CTCs capture yield (92%) [395], demonstrating the enhanced performance for cell recognition compared to planar surfaces.

3.5.2 Cell Culture and Tissue Engineering

Cell culture offers consistent and reproducible model systems, such as organs on a chip models, for biochemical and physiological research, screening and development of drug and biological compounds, and cancer research at the cellular level. For example, culturing stem cells produces specialized cells for replacing and repairing diseased cells, testing the toxicity and effectiveness of drugs, and investigating pathogenesis mechanism.[396,397] Polymer patterns are readily functionalized to resemble the cell microenvironment present *in vivo* and to regulate cell behaviors including survival, proliferation and differentiation, and therefore have been widely applied to the production of high-quality cells and tissues.[5,36,99,141,146–148,359–376]

Compared to cell culture on 2D patterned surface [158], growing cells in 3D patterned structures avoid the planarization of cell nuclei by providing confined spaces that resemble the natural environment [157,400,401]. For example, patterned antifouling polymer brushes inhibit protein adsorption in the nongrowth areas and provide long-term stability for cell differentiation [5]. Lilge et al. used SI-ATRP to grow cell-repellent PAAm brushes and constructed 3D microwells in which the bottom surface was modified with cell-adhesive fibronectin (FN) [5]. The fluorescence microscopy images in Figure 18a show that the PAAm microwells direct the growth of human pancreatic tumor (PatuT) cells within the patterned spaces, while the geometry of the microwells (circular, square and hexagonal) determines the shapes of the cells. The changes of actin fiber structures suggest that the PatuT cells adapt to the local micro-environment during the developmental process. In comparison, cells tend to spread on the planar substrates without the confinement created by microwells. Therefore, the micropatterned 3D structures offer possibility to monitor cell behavior and enable single-cell analysis.

Regulated cell growth on patterns and scaffolds is essential for tissue engineering. Although cell culture in 3D scaffolds is common in tissue engineering[92], the implanted scaffolds may induce foreign body response and inflammation. Growing cell sheets on patterned thermoresponsive polymer surfaces (e.g. PDA[159,405]) is an alternative approach for tissue engineering without 3D scaffold. Shin et al. reported a tissue delivery method using a thermally expandable hydrogel with honeycomb PDA patterns[156]. The honeycomb PDA patterns were designed to mimic the network of blood vessels and nerves. As shown in the SEM and fluorescence microscopy images (**Figure 18b**), the growth of the human dermal fibroblast cells was localized on the FN-functionalized honeycomb pattern, resulting in a honeycomb-shaped tissue

after 24 h of cell culture. The thermal expansion of poly(ethylene oxide)-*b*-poly(propylene oxide) hydrogels enables easy release of the cell sheets for delivery to mouse subcutaneous tissue, where the cell sheets maintained the original structures for over 7 days. With the ability to culture and harvest multiple types of cells, scaffold-free delivery methods are expected to provide opportunities for human tissue reconstruction and bridging the gap between *in-vitro* models and *in-vivo* tests.

3.5.3 Cell Therapy

The mainstream cell therapies rely on the injection and implantation of living T lymphocytes cells (Tcells) to fight diseased cells and accelerate patient recovery. However, T-cell therapies typically require time-consuming preparation of cell population and are only effective on liquid cancers with existing specific antigens. Macrophages are more plastic for engulfing any harmful substances including cancer cells, but tend to shift to protumoral phenotypes after injection. To solve this challenge, Shields et al. integrated bone marrow-derived macrophages (BMDMs) with soft discoidal nanoparticles ("backpacks") via ligandreceptor binding[385]. Loaded with interferon-γ, a cytokine with antitumor activity and proinflammatory stimulated ability, the backpack-macrophage complexes possess the ability to maintain phenotypes deep within the solid tumor. Figure 18c shows the structure and fabrication procedure of the backpacks. Each backpack contains a layer of hydrophilic polyvinyl alcohol (PVA) for incorporation of interferon-y, two layers of PLGA for structural support, and a top cell adhesive layer. Confocal fluorescence microscopy confirms the strong binding between the backpacks and BMDMs (Figure 18d). In vivo experiments using mice burdened with mammary carcinomas reveals that the mice treated with backpack-BMDMs exhibits at least 4.9 times fewer metastaic nodules even in low dose (50 ng), forming a sharp comparison to saline and free interferon-γ group (Figure 18e). The backpacks can be applied to various types of cells without the prior cell modifications[155], showing huge potential for addressing inflammatory diseases facilely.

3.6 Other Related Fields

3.6.1 Flexible Energy Harvesters

Energy harvest is important to deal with the challenge of global warming and depletion of fossil fuel. Flexible energy harvesters have received extensive attention because of its mechanical compliance and potential integration into wearable apparatuses. As one of the energy conversion devices, triboelectric generators utilize the conjunction of frictional electrification and electrostatic induction effects to convert the external mechanical energy into electricity.[415] Triboelectric generators generally consist of two thin films with opposite tribo-polarity that are attached to two electrodes. Creating nanostructures on the surfaces of triboelectric layer helps to improve the contact interface and thus the triboelectrification. For example, polyethylene terephthalate (PET) membrane and microdome-patterned PDMS (Figure 19a) were used to prepare a wearable respiratory energy harvester. The abdominal movement caused the periodic contact and separation of the two triboelectric surfaces, leading to the alternating flow of induced electrons between the electrodes. This device (Figure 19b) is promising for power supply for implanted medical devices[416].

Piezoelectric devices can also act as energy harvesters. Using piezoelectric generators, flexible devices can be self-powered. Han et al. developed a self-powered flexible vision electronic skin composed of a piezoelectric PVDF layer and patterned pixels of photosensitive PPy (**Figure 19c**).[417] This vision skin realized image recognition in exposed to multiple ultraviolet stimuli (**Figure 19d**).

3.6.2 Soft Actuators

Soft actuators deform in response to external stimuli such as electrical signals, chemicals, light and pH[418]. Among all the soft actuators, ionic electroactive actuators (IEA) are attractive due to the ability to achieve large deformation by low voltage.[419] Recently, Khaldi et al. patterned PEDOT electrodes that sandwich an ionic conductive polymer (CP) electrolyte layer for an IEA device (**Figure 19e**).[420] The redox reaction of the PEDOT electrodes cause the migration of the ions in the polyelectrolyte, leading to the volumetric expansion or contraction in response to applied voltage (**Figure 19f**).

3.6.3 Wetting Control and Self-Cleaning

The micro/nano-architectures created by polymer patterning are useful in constructing functional surfaces with different wettability.[421] With increased surface roughness, air can remain trapped between the water drop and the cavities of the surface, forming a Cassie-Baxter state with enhanced effective contact angle and mimicking the lotus-leaf effect to enable self-cleaning characteristics.[422] For example, patterning siloxane functionalized polyurethane-acrylate film with uniform pillars leads to a super-hydrophobic surface with ~140° water contact angle[423]. Additionally, design and fabrication of polymer micro-/nano-structures also enable new applications in liquid transport. Chen et al. prepared PPy microsucker structures *via* electrochemical polymerization, and achieved good control over the orientation and the projected epitaxial length of the microsuckers (**Figure 19g-h**).[424] Consequently, the adhesion to water was easily tuned, unveiling the huge potential for the manipulation and transportation of liquid droplets.

3.6.4 Optical Applications

Optical gratings and anti-reflection coatings are important components in optical and optoelectronic devices[425]. Patterning of polymer thin films is often required in these optical fields. For example, self-assembled BCPs are frequently used templates for transferring patterns deeply into the silicon substrates. Such silicon gratings have been reported with improved sensitivity for refractive index (RI) sensing.[426] Alternatively, Park et al. fabricated dual-mode switchable displays based on PS optical gratings and the gap-filled AgNO₃ as the electrochromic material (**Figure 19i**). Under positive and negative applied potential, the grating device change from transparent state (**Figure 19j**) to metallic mirror based on the redox reaction of Ag⁺.[427]

Reducing Fresnel reflection is important for improving the utilization of incident light. Fabrication of sub-wavelength structures is a commonly used anti-reflection approach. By forming nanostructures with graded RI distribution, high reflection due to sharp RI difference at the interface can be avoided. Recently, Rosenberg et al. developed a solvent-assisted imprint strategy to form moth-eye anti-reflective coating on

curved polycarbonate (PC) substrates (**Figure 19k**)[143]. The resulting sub-wavelength nanostructures reduced the reflectance from ca. 6.5% to ca. 4.5 % in the visible wavelength range, showing effective anti-reflection performance.

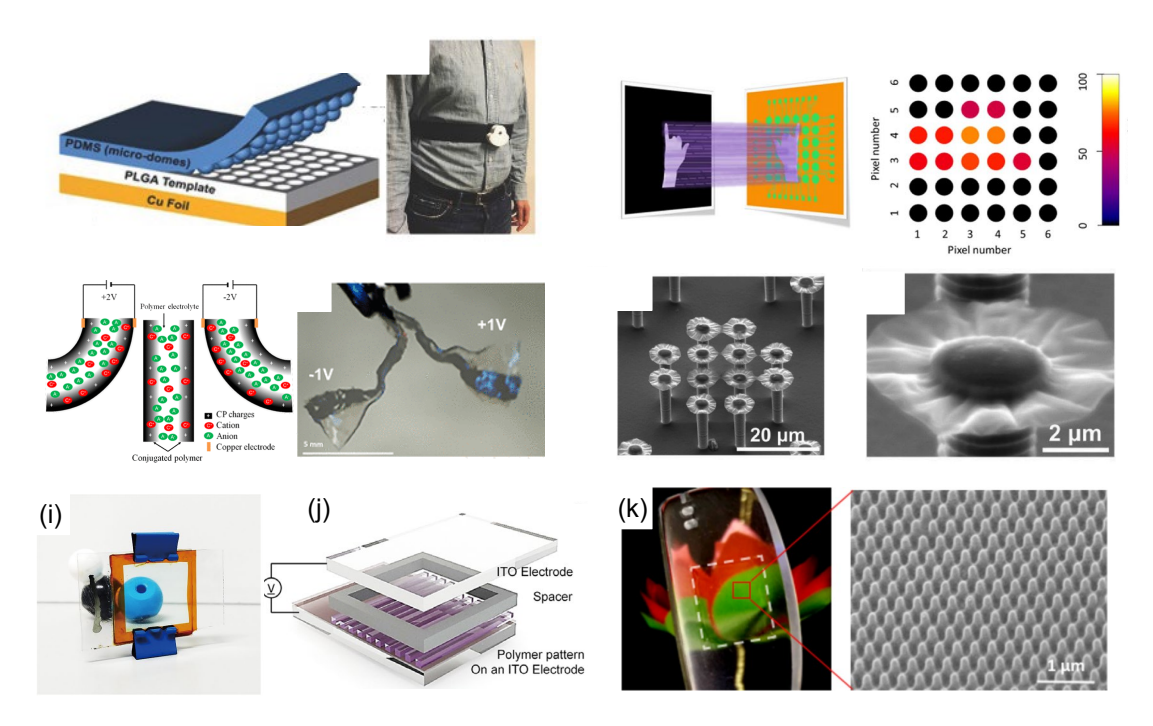


Figure 19: (a) Schematic of the microdome-patterned PDMS film[416]. (b) Photo of the wearable respiratory energy harvester worn around the waist[416]. Copyright 2017. Adapted with permission from John Wiley & Sons Inc. (c) Schematic diagram of the image recognition system[417]. (d) Imaging results of the gesture pattern in (c)[417]. Copyright 2018. Adapted with permission from the IOP Publishing. (e) Three different states of the CP tri-layer actuator: the unbiased (center), the positively biased (left) and the negatively biased states (right). The ionic conductive polymer electrolyte (white region) was sandwiched between the two CP layers (dark regions).[420] (f) Actuation behavior of the tri-layer device under applied voltage bias of ±1 V[420]. Copyright 2018. Adapted with permission from the American Chemical Society. (g-h) SEM images of the PPy microsuckers deposited on the micropillars[424]. Copyright 2018. Adapted with permission from John Wiley & Sons Inc. (i) Photo of the transparent state of the bistable reversible electrochemical grating (BREG).[427] (j) Device structure of the BREG[427]. Copyright 2017. Adapted with permission from the American Chemical Society. (k) Photo of the PC substrate imprinted with the moth-eye antireflective nanostructures. Inset: SEM image of the imprinted PC surface[143]. Copyright 2019. Adapted with permission from the American Chemical Society.

4. Conclusion & Future Outlook

4.1 Conclusion

In summary, we have highlighted the recent advances in non-photolithographic techniques for

patterning of polymer thin films, and discussed the promising applications of the polymer patterns. Compared with photolithography, non-photolithographic methods reported to date offer diverse options for nanofabrication of polymer thin films using more accessible instruments, especially for academic institutes.

As a mask-less method, direct writing opens up opportunities in many diverse applications, owing to the flexibility of patterning design and the ability to form multicomponent patterns. Using sharp scanning probes, SPL allows the precise delivery of various inks at sub-10 nm scale. However, the expensive probes, limited scalability, small number of ink types and spreading of deposited inks all need to be addressed in the future for conventional SPL. Though cantilever-free SPL and external-energy assisted SPL have been developed to enhance the throughput and efficiency [428], tip modification for the precise control over the ink transport in SPL is still worth future investigation. Compared with SPL, inkjet printing is featured with high throughput and low process cost, and has been widely applied in optoelectronics, sensors and transistors. Nevertheless, inkjet printing still faces the challenges of "coffee-ring" effect due to the surface-tension-driven transport of inks.[111,112] Nozzle clogging also frequently occurs due to the ink evaporation in the printhead and the use of highly viscous polymer solution.[113] Solving these problems would further improve the printing resolution and reproducibility.

Area-selective vapor phase deposition of polymer thin films is gaining increasing interest, as it could be applied as hard masks for etching and integrated in device fabrication. The physical masking strategy sacrifices the pattern resolution and manufacturing flexibility. Alternatively, designing pre-defined surface based on the intrinsic or modified surface chemistry can allow the precise control of self-aligned bottom-up patterning. However, the loss of selectivity as the process continues is commonly observed due to the unavoidable nucleation of polymers at the non-growth areas [128,130]. Though multi-step approaches such as combining etching or adding inhibitor replenishing steps have been developed to extend the selectivity window, the prolonged process time as well as additional equipment requirement adds to the complexity for the industrial application. Therefore, future exploration is needed towards high-throughput, selective and single-step vapor-phase deposition.

NIL is a low-cost, high-throughput patterning process capable of fabricating large-are periodic

nanostructures, especially promising for optical devices such as gratings[429]. Nevertheless, thermal NIL still faces difficulty in tackling highly viscous polymers and controlling over polymerization shrinkage during the cooling process. UV NIL can be performed at room temperature, but is limited to photosensitive polymers. In addition, UV NIL has strict requirement of the O₂ level in the ambient environment[145], while the polymer shrinkage during UV curing needs to be addressed [430]. Potential approaches to solve these problems include designing O₂-insensitive photopolymers[431], using precursors with bulky pendants, and adopting ring-opening polymerization[432].

Soft lithography represents a convenient and low-cost surface patterning technique with sub-micrometer features, showing huge potential for area-specific modification especially in biological research fields such as protein recognition and cell engineering. However, the elastomeric stamps used in soft lithography pose three main challenges[151]: (i) the most frequently used PDMS stamp only allows the adsorption of apolar inks and requires non-swelling solvent; (ii) after long-term use, the ink diffusion into the bulk material may affect the pattern transferred from the stamp to substrate in µCP and result in a waste of ink in MIMIC and CFL; (iii) Stamp deformation during the contacting and removing processes may compromise the pattern resolution. Though the first two challenges still need further exploration, using poly(*p*-xylylene) to selectively functionalize the stamp sidewalls has been reported effective for improving the mechanical properties and reducing the deformation[433].

Self-assembly of BCPs has the potential of creating ordered and multifunctional micro- and nanostructures, enabling the potential to be used as hard masks, photonic crystals, and optical waveguides. Furthermore, selectively introducing inorganic materials into patterned BCP films by SIS improves the etch resistance and ultimately helps the pattern transfer. Efforts to further improve the uniformity and control over the defects during the self-assembly across large areas are still desired for practical nanomanufacturing.[434]

Instability induced patterning could be potentially applied to buckling surfaces and stimuli-responsive devices owing to its simplicity, reversibility and scalability[4]. The major obstacles are the formation of arbitrary and small-aspect-ratio structures with varied periodicity[328,435]. To tackle these problems,

patterned electrodes[330], seeded nucleation sites[339] and functional polymers[337] have been investigated. For example, simple spin coating process based on the preferential dewetting on heterogeneous substrates has been developed for self-aligned patterning[121,436]. However, more effort needs to be focused on the experimental and theoretical studies for precisely guiding the morphology during instability induced patterning.

4.2 Outlook

Developing new processes to decrease the feature size is desired for achieving nanoscale highresolution patterns. Graphoepitaxy of cylinder-forming BCPs in hole-guiding templates enables the formation of "hole-in-a-hole" structures for contact hole shrinking [437–439]. However, the control over defects such as BCP overflow and deformed shapes requires further optimization. Alternatively, applying external stimuli (e.g. light and heat) to shrinkable shape memory polymer (SMP) patterns provides another promising route for downscaling the feature size [440–442]. For example, SMP thin films can be first patterned through NIL, µCP, MIMIC, CFL or instability-induced methods, and subsequently exposed to heat to obtain size-contracted nanostructures. Indeed, the synergistic combinations of various patterning technologies are likely low-hanging fruits to achieve smaller features with improved definition. While most past research in additive manufacturing has focused on the optimization of the ink chemistry and properties and/or the printing device, we believe interfacial engineering of the substrate (e.g., by BCPs) could lead to complex morphologies that are currently inaccessible to direct writing technologies. Similarly, additive manufacturing technologies could be leveraged to guide the assembly of BCPs, e.g., by applying shear force using the 3D printing nozzle to induce area-selective annealing of BCP. There are endless possibilities at the intersections of these seemingly orthogonal technologies, the exploration of which will require more indepth collaborations and/or trans-disciplinary expertise.

In-situ characterization for monitoring the patterning processes in real-time is in utmost need to understand how microscopic structures form and to optimize the process parameters. The need for experimental validation of theoretical models [443] also motivates the development of *in-situ*

measurements to obtain time-resolved information during the dynamic structural evolution, especially when non-equilibrium states are involved. The power of *in-situ*, real-time monitoring has recently been demonstrated by the enablement of CDP, during which the growth of nano/microdrops is monitored continuously until the desired size is obtained and polymerization is initiated upon that observation to achieve pattern size control[338]. Currently, *in-situ* synchrotron small angle X-ray scattering (SAXS) has been employed for monitoring the kinetics of BCP microphase separation [444,445]. Such *in-situ* synchrotron characterization is also expected to provide key information about the nucleation delay on nongrowth area in ASD as well as the structure evolution during the instability-induced patterning.

Multi-scale simulation of the patterning processes, especially when *in-situ* characterization techniques are challenging or unavailable, could provide critical guidance to the condition selection and process development. For example, experimental observation is difficult to unveil the microscopic details for the droplet formation, transport and impact/spreading steps on the substrate during the EHD process, owing to the small droplet size and fast droplet speed. In contrast, modeling based on the electrostatic force and surface tension provides the prediction of droplet dimension, spacing and volume [446,447]. Moreover, multi-scale modelling links the simulation of polymer rearrangement at the microscale, phase transition at the mesoscale, deformation at the macro-scale, providing routes to understand the structure development. With future development for coupling computational methods and numerical solvers to cover different scales, multi-scale simulation is expected to offer guidance for establishing process conditions for many of the abovementioned patterning processes especially when external fields and interfacial phenomena are involved.

Introducing the concepts, approaches, and materials from inorganic fabrication processes to the patterning of soft materials can be beneficial. Building upon past research on inorganic nanoparticles (e.g., of Si, ZnO, GaN, and Ge1-xSnx), where solvent-free CVD techniques have been used to gain access to a diversity of pattern/particle morphologies with continuous processing, CVD-based polymer synthesis strategies hold great potential for the scalable production of programmable surface patterns. The exceptional (sub)nanometer-scale feature definition afforded by inorganic CVD techniques could be

transferred to CVD polymerization (e.g., by serving as a substrate with reactive patterns) to improve the quality of soft patterns. Incorporating inorganic materials into polymer thin films could improve the materials properties (e.g. electrical, optical and mechanical performance) and achieve additional functionalities in the resulting hybrid structures. Patterning hybrid films offers new opportunities in photonic circuits, waveguides and non-volatile memory devices. However, the intrinsic incompatibility of inorganic fillers and polymer matrix and the enhancement of interfacial adhesion have been a challenge and subject of intense investigation in recent years [448–450]. Alternatively, vapor phase infiltration (VPI) offers another promising approach to selectively introduce inorganic dopants into as-patterned polymer films. Therefore, the search for new Lewis acid-base interaction between the inorganic VPI precursor and the polymer matrices are expected to enable more synthesis routes for hybrid materials that can be easily integrated into current patterning processes for polymer thin films[451].

Finally, achieving nanoscale resolution in complex topology, such as structures with extreme aspect ratios and irregular 3D geometry, will be crucial for patterning of polymer thin films. Combining different non-photolithographic strategies could lead to advantages that are not achievable by any single patterning process. For example, integrating the NIL or SPL with the self-aligned area-selective vapor-phase deposition could generate a powerful platform for creating complex patterns with sub-10 nm resolution. Additionally, adapting 2D patterning methods into 3D additive manufacturing represents another promising thrust. For instance, 3D polymeric patterns mimic a natural environment for cell culture better than planar 2D surfaces,[5] and can be integrated in MEMS, smart multiplexed displays, shape-memory structures and anti-counterfeiting labels[452]. We anticipate that the continuous development of non-photolithographic patterning techniques would evolve into scalable and reliable fabrication processes enabling many unforeseen application scenarios.

Acknowledgement

We acknowledge the funding from the National Natural Science Foundation of China (22178301, 21938011) and the funding from the Natural Science Foundation of Zhejiang Province (LR21B060003). J. Zhao acknowledges the grant from the Department of Science and Technology of Zhejiang Province (2023C01182), and the grant from Shanxi Institute of Zhejiang University for New Materials and Chemical Industry (2022SZ-TD005). X. Wang would like to thank the startup funding provided by the Ohio State University. This material is based upon work supported by the National Science Foundation Faculty Early Career Development Program under Grant No. CMMI-2144171. Any opinions, findings, and conclusions or recommendations expressed in this material are those of the author(s) and do not necessarily reflect the views of the National Science Foundation.

References

- [1] Han D, Khan Y, Gopalan K, Pierre A, Arias AC. Emission area patterning of organic light-emitting diodes (OLEDs) via printed dielectrics. Adv Funct Mater 2018;28:1802986.
- [2] Neo WT, Li X, Chua S-J, Chong KSL, Xu J. Enhancing the electrochromic performance of conjugated polymers using thermal nanoimprint lithography. RSC Adv 2017;7:49119–24.
- [3] Galeotti F, Trespidi F, Timò G, Pasini M. Broadband and crack-free antireflection coatings by self-assembled moth eye patterns. ACS Appl Mater Interfaces 2014;6:5827–34.
- [4] Yang C, Li L, Zhao J, Wang J, Xie J, Cao Y, Xue M, Lu C. Highly sensitive wearable pressure sensors based on three-scale nested wrinkling microstructures of polypyrrole films. ACS Appl Mater Interfaces 2018;10:25811–8.
- [5] Lilge I, Jiang S, Wesner D, Schönherr H. The effect of size and geometry of poly(acrylamide) brush-based micropatterns on the behavior of cells. ACS Appl Mater Interfaces 2016;8:23591–603.
- [6] Biswas A, Bayer IS, Biris AS, Wang T, Dervishi E, Faupel F. Advances in top–down and bottom–up surface nanofabrication: techniques, applications & future prospects. Adv Colloid Interface Sci 2012;170:2–27.
- [7] Manfrinato VR, Zhang L, Su D, Duan H, Hobbs RG, Stach EA, Berggren KK. Resolution limits of electron-beam lithography toward the atomic scale. Nano Lett 2013;13:1555–8.
- [8] Abbas AN, Liu G, Liu B, Zhang L, Liu H, Ohlberg D, Wu W, Zhou C. Patterning,

- characterization, and chemical sensing applications of graphene nanoribbon arrays down to 5 nm using helium ion beam lithography. ACS Nano 2014;8:1538–46.
- [9] Fischer J, von Freymann G, Wegener M. The materials challenge in diffraction-unlimited direct-laser-writing optical lithography. Adv Mater 2010;22:3578–82.
- [10] Ahn SJ, Kaholek M, Lee W-K, LaMattina B, LaBean TH, Zauscher S. Surface-initiated polymerization on nanopatterns fabricated by electron-beam lithography. Adv Mater 2004;16:2141–5.
- [11] Zhang D, Yin Y, Lv W, Gao F, Pan D, Tu X, Ju S, Su X, Ma X, Sun H, Xu Y, Li S, Shi Y. Sharply increased current in asymmetrically aligned polycrystalline polymer transistors with sub-domain-size channels. IEEE Electron Device Lett 2020;41:589–92.
- [12] Lee EK, Park CH, Lee J, Lee HR, Yang C, Oh JH. Chemically robust ambipolar organic transistor array directly patterned by photolithography. Adv Mater 2017;29:1605282.
- [13] Huang F, Xu Y, Pan Z, Li W, Chu J. Direct patterning on top-gate organic thin-film transistors: improvement of on/off ratio, subthreshold swing, and uniformity. IEEE Electron Device Lett 2020;41:1082–5.
- [14] Zheng Y-Q, Liu Y, Zhong D, Nikzad S, Liu S, Yu Z, Liu D, Wu H-C, Zhu C, Li J, Tran H, Tok JB-H, Bao Z. Monolithic optical microlithography of high-density elastic circuits. Science 2021;373:88–94.
- [15] Sharma E, Rathi R, Misharwal J, Sinhmar B, Kumari S, Dalal J, Kumar A. Evolution in lithography techniques: microlithography to nanolithography. Nanomaterials 2022;12:2754.
- [16] Ito T, Okazaki S. Pushing the limits of lithography. Nature 2000;406:1027–31.
- [17] Cui Z. Nanofabrication by electron beam. In: Cui Z, editor. Nanofabrication: principles, capabilities and limits, Cham: Springer International Publishing; 2017, p. 91–148.
- [18] Romanov V, Davido SN, Gale BK, Brooks BD. A critical comparison of protein microarray fabrication technologies. Crit Rev 2014:24.
- [19] Liu G, Petrosko SH, Zheng Z, Mirkin CA. Evolution of dip-pen nanolithography (DPN): from molecular patterning to materials discovery. Chem Rev 2020;120:6009–47.
- [20] Liu G, Hirtz M, Fuchs H, Zheng Z. Development of dip-pen nanolithography (DPN) and its derivatives. Small 2019;15:1900564.
- [21] Fradkin Z, Roitman M, Bardea A, Avrahamy R, Bery Y, Ohana H, Zohar M. Fabrication of polymeric photonic structures using dip-pen nanolithography. J Micro Nanolithogr MEMS MOEMS 2020;19:1.
- [22] Zohar M, Azulay AR, Bykhovsky D, Fradkin Z, Tapuchi S, Auslender M. PDMS deposition for optical devices by dip-pen nanolithography. Macromol Mater Eng 2017;302:1700053.
- [23] Laing S, Mabbott S, Faulds K, Graham D. Thermoresponsive polymer micropatterns fabricated by dip-pen nanolithography for a highly controllable substrate with potential cellular applications. ACS Appl Mater Interfaces 2016;8:24844.
- [24] Soleymaniha M, Felts JR. Design of a heated micro-cantilever optimized for thermocapillary driven printing of molten polymer nanostructures. Int J Heat Mass Transf 2016;101:166–74.
- [25] Ventrici de Souza J, Liu Y, Wang S, Dörig P, Kuhl TL, Frommer J, Liu G. Three-dimensional

- nanoprinting via direct delivery. J Phys Chem B 2018;122:956-62.
- [26] He Q, Tan C, Zhang H. Recent advances in cantilever-free scanning probe lithography: high-throughput, space-confined synthesis of nanostructures and beyond. ACS Nano 2017;11:4381–6.
- [27] Brown KA, Hedrick JL, Eichelsdoerfer DJ, Mirkin CA. Nanocombinatorics with cantilever-free scanning probe arrays. ACS Nano 2019;13:8–17.
- [28] Lee I-N, Hosford J, Wang S, Hunt JA, Curran JM, Heath WP, Wong LS. Large-area scanning probe nanolithography facilitated by automated alignment and its application to substrate fabrication for cell culture studies. J Vis Exp 2018:56967.
- [29] Bog U, Bruns M, Holmes AE, Rodriguez-Emmenegger C, Fuchs H, Hirtz M. Clickable antifouling polymer brushes for polymer pen lithography. ACS Appl Mater Interfaces 2017;9:12109.
- [30] Ma X, Li F, Xie Z, Xue M, Zheng Z, Zhang X. Size-tunable, highly sensitive microelectrode arrays enabled by polymer pen lithography. Soft Matter 2017;13:3685–9.
- [31] Hosford J, Valles M, Krainer FW, Glieder A, Wong LS. Parallelized biocatalytic scanning probe lithography for the additive fabrication of conjugated polymer structures. Nanoscale 2018;10:7185–93.
- [32] Xu X, Yang Q, Cheung KM, Zhao C, Wattanatorn N, Belling JN, Abendroth JM, Slaughter LS, Mirkin CA, Andrews AM, Weiss PS. Polymer-pen chemical lift-off lithography. Nano Lett 2017;17:3302–11.
- [33] Hedrick JL, Brown KA, Kluender EJ, Cabezas MD, Chen P-C, Mirkin CA. Hard transparent arrays for polymer pen lithography. ACS Nano 2016;10:3144–8.
- [34] Singh S, Ramakrishna S, Berto F. 3D printing of polymer composites: a short review. Mat Design & Process Comms 2020;2.
- [35] Elder B, Neupane R, Tokita E, Ghosh U, Hales S, Kong YL. Nanomaterial patterning in 3D printing. Adv Mater 2020;32:1907142.
- [36] Truby RL, Lewis JA. Printing soft matter in three dimensions. Nature 2016;540:371–8.
- [37] Maleki H, Bertola V. Recent advances and prospects of inkjet printing in heterogeneous catalysis. Catal Sci Technol 2020;10:3140–59.
- [38] Nayak L. A review on inkjet printing of nanoparticle inks for flexible electronics. J Mater Chem C 2019;7:8771–95.
- [39] Ye D, Ding Y, Duan Y, Su J, Yin Z, Huang YA. Large-scale direct-writing of aligned nanofibers for flexible electronics. Small 2018;14:1703521.
- [40] Afsana, Jain V, Haider N, Jain K. 3D printing in personalized drug delivery. Curr Pharm Design 2018;24:5062–71.
- [41] Chung S, Cho K, Lee T. Recent progress in inkjet-printed thin-film transistors. Adv Sci 2019;6:1801445.
- [42] Coppola S, Pagliarulo V, Vespini V, Nasti G, Olivieri F, Grilli S, Ferraro P. Direct fabrication of polymer micro-lens array. Optical Measurement Systems for Industrial Inspection X, vol. 10329, Int J Opt Photonics; 2017, p. 103294Q.
- [43] Roghmans F, Evdochenko E, Stockmeier F, Schneider S, Smailji A, Tiwari R, Mikosch A,

- Karatay E, Kuehne A, Walther A, Mani A, Wessling M. 2D patterned ion-exchange membranes induce electroconvection. Adv Mater Interfaces 2019;6:1801309.
- [44] Solin K, Orelma H, Borghei M, Vuoriluoto M, Koivunen R, Rojas OJ. Two-dimensional antifouling fluidic channels on nanopapers for biosensing. Biomacromolecules 2019;20:1036–44.
- [45] Kwon H, Li X, Hong J, Park CE, Jeong YJ, Moon HC, Kim SH. Non-lithographic direct patterning of carbon nanomaterial electrodes via electrohydrodynamic-printed wettability patterns by polymer brush for fabrication of organic field-effect transistor. Appl Surf Sci 2020;515:145989.
- [46] Han W, Hou P, Sadaf S, Schaefer H, Walder L, Steinhart M. Ordered topographically patterned silicon by insect-inspired capillary submicron stamping. ACS Appl Mater Interfaces 2018;10:7451–8.
- [47] Waynant KV, Koo H-J, Zhang C, Braun PV. Qualitative degradation of the pesticide coumaphos in solution, controlled aerosol, and solid phases on quaternary ammonium fluoride polymer brushes. Polym Adv Technol 2017;28:567–567.
- [48] Mikkonen R, Puistola P, Jönkkäri I, Mäntysalo M. Inkjet printable polydimethylsiloxane for all-inkjet-printed multilayered soft electrical applications. ACS Appl Mater Interfaces 2020;12:11990–7.
- [49] Peng Y, Xiao S, Yang J, Lin J, Yuan W, Gu W, Wu X, Cui Z. The elastic microstructures of inkjet printed polydimethylsiloxane as the patterned dielectric layer for pressure sensors. Appl Phys Lett 2017;110:261904.
- [50] Zhou R, Fang X, Cheng Q, Zhuang L, Li H, Tang B, Zhou G. Inkjet-printed patterned polytitanosiloxane-fluoropolymer composite dielectric layer for micro-optical electrowetting valves. J Phys D: Appl Phys 2020;54:025104.
- [51] Kitamura I, Oishi K, Hara M, Nagano S, Seki T. Photoinitiated marangoni flow morphing in a liquid crystalline polymer film directed by super-inkjet printing patterns. Sci Rep 2019;9:2556.
- [52] Yang J, Zhao W, Yang Z, He W, Wang J, Ikeda T, Jiang L. Printable photonic polymer coating based on a monodomain blue phase liquid crystal network. J Mater Chem C 2019;7:13764–9.
- [53] Kim K, Kim C, Jo Y, Tang X, Lee J-H, Kwon H, Lee J, Kim SH, An TK. Boosting the ambipolar field-effect transistor performance of a DPP-based copolymer via electrohydrodynamic-jet direct writing. J Ind Eng Chem 2019;78:172–7.
- [54] Kim K, Kim SH, Cheon H, Tang X, Oh JH, Jhon H, Jeon J, Kim Y-H, An TK. Electrohydrodynamic-jet (EHD)-printed diketopyrrolopyroole-based copolymer for OFETs and circuit applications. Polymers 2019;11:1759.
- [55] Cheon HJ, Li X, Jeong YJ, Sung MJ, Li Z, Jeon I, Tang X, Girma HG, Kong H, Kwon S-K, An TK, Kim SH, Kim Y-H. A novel design of donor-acceptor polymer semiconductors for printed electronics: application to transistors and gas sensors. J Mater Chem C 2020;8:8410–9
- [56] Kim Y, Bae J, Song HW, An TK, Kim SH, Kim Y-H, Park CE. Directionally aligned

- amorphous polymer chains via electrohydrodynamic-jet printing: analysis of morphology and polymer field-effect transistor characteristics. ACS Appl Mater Interfaces 2017;9:39493–501.
- [57] Hu B, Sun S, Wu B, Wu P. Colloidally stable monolayer nanosheets with colorimetric responses. Small 2019;15:1804975.
- [58] Seiberlich M, Strobel N, Ruiz-Preciado LA, Ruscello M, Lemmer U, Hernandez-Sosa G. Aerosol-jet-printed donor-blocking layer for organic photodiodes. Adv Electron Mater 2021;7:2000811.
- [59] Ciocca M, Giannakou P, Mariani P, Cinà L, Di Carlo A, Tas MO, Asari H, Marcozzi S, Camaioni A, Shkunov M, Brown TM. Colour-sensitive conjugated polymer inkjet-printed pixelated artificial retina model studied via a bio-hybrid photovoltaic device. Sci Rep 2020;10:21457.
- [60] Tang X, Kwon H, Ye H, Kim JY, Lee J, Jeong YJ, Kim SH. Enhanced solvent resistance and electrical performance of electrohydrodynamic jet printed PEDOT:PSS composite patterns: effects of hardeners on the performance of organic thin-film transistors. Phys Chem Chem Phys 2019;21:25690–9.
- [61] Chang J, He J, Lei Q, Li D. Electrohydrodynamic printing of microscale PEDOT:PSS-PEO features with tunable conductive/thermal properties. ACS Appl Mater Interfaces 2018;10:19116–22.
- [62] Park SH, Kim J, Park CE, Lee J, Lee HS, Lim S, Kim SH. Optimization of electrohydrodynamic-printed organic electrodes for bottom-contact organic thin film transistors. Org Electron 2016;38:48–54.
- [63] Jung EM, Lee SW, Kim SH. Printed ion-gel transistor using electrohydrodynamic (EHD) jet printing process. Organic Electronics 2018;52:123–9.
- [64] Maisch P, Eisenhofer LM, Tam KC, Distler A, Voigt MM, Brabec CJ, Egelhaaf H-J. A generic surfactant-free approach to overcome wetting limitations and its application to improve inkjet-printed P3HT:non-fullerene acceptor PV. J Mater Chem A 2019;7:13215–24.
- [65] Tu N, Lee SWR. Inkjet printing PEDOT:PSS without coffee ring effect for QLED applications. 2019 20th International Conference on Electronic Packaging Technology: ICEPT; 2019.
- [66] Mu L, Hu Z, Zhong Z, Jiang C, Wang J, Peng J, Cao Y. Inkjet-printing line film with varied droplet-spacing. Org Electron 2017;51:308–13.
- [67] Ferrari LM, Sudha S, Tarantino S, Esposti R, Bolzoni F, Cavallari P, Cipriani C, Mattoli V, Greco F. Ultraconformable temporary tattoo electrodes for electrophysiology. Adv Sci 2018;5:1700771.
- [68] Gupta AA, Bolduc A, Cloutier SG, Izquierdo R. Aerosol Jet Printing for printed electronics rapid prototyping. IEEE Int. Symp. Circuits Syst 2016, 2016, p. 866–9.
- [69] Di Novo NG, Cantù E, Tonello S, Sardini E, Serpelloni M. Support-material-free microfluidics on an electrochemical sensors platform by aerosol jet printing. Sens 2019;19:1842.
- [70] Cho C-L, Kao H, Chang L-C, Wu Y-H, Chiu H-C. Fully inkjet-printing of metal-polymer-

- metal multilayer on a flexible liquid crystal polymer substrate. Surf Coat Technol 2017;320:568–73.
- [71] Gu Y, Hines DR, Yun V, Antoniak M, Das S. Aerosol-jet printed fillets for well-formed electrical connections between different leveled surfaces. Adv Mater Technol 2017;2:1700178.
- [72] Hwang TH, Kim YJ, Chung H, Ryu W. Motionless electrohydrodynamic (EHD) printing of biodegradable polymer micro patterns. Microelectron Eng 2016;161:43–51.
- [73] Liu T, Huang R, Zhong J, Yang Y, Tan Z, Tan W. Control of cell proliferation in E-jet 3D-printed scaffolds for tissue engineering applications: the influence of the cell alignment angle. J Mat Chem B 2017;5:3728–38.
- [74] Mecozzi L, Gennari O, Coppola S, Olivieri F, Rega R, Mandracchia B, Vespini V, Bramanti A, Ferraro P, Grilli S. Easy printing of high viscous microdots by spontaneous breakup of thin fibers. ACS Appl Mater Interfaces 2018;10:2122–9.
- [75] Coppola S, Nasti G, Vespini V, Grilli S, Russo P, Ferraro P. From electrohydrodynamic instabilities of liquids to the high-resolution ink-jet printing through pyroelectric driving power. J Micro-Nanolithogr MEMS MOEMS 2018;17:031206.
- [76] Liu Q, Le MQ, Richard C, Liang R, Cottinet P-J, Capsal J-F. Enhanced pseudo-piezoelectric dynamic force sensors based on inkjet-printed electrostrictive terpolymer. Org Electron 2019;67:259–71.
- [77] Khan S, Ali S, Khan A, Wang B, Bermak A. Printing sensors on biocompatible substrates for selective detection of glucose. IEEE Sens J 2021;21:4167–75.
- [78] Park J, Yoon H, Kim G, Lee B, Lee S, Jeong S, Kim T, Seo J, Chung S, Hong Y. Highly customizable all solution–processed polymer light emitting diodes with inkjet printed Ag and transfer printed conductive polymer electrodes. Adv Funct Mater 2019;29:1902412.
- [79] Garma LD, Ferrari LM, Scognamiglio P, Greco F, Santoro F. Inkjet-printed PEDOT:PSS multi-electrode arrays for low-cost in vitro electrophysiology. Lab Chip 2019;19:3776–86.
- [80] Yu J, Seipel S, Nierstrasz VA. Digital inkjet functionalization of water-repellent textile for smart textile application. J Mater Sci 2018;53:13216–29.
- [81] Guo Y, Yan J, Shen Z, Jiang H, Tang B, Deng Y, Henzen A, Zhou R, Zhou G. Electrofluidic displays based on inkjet printing and phase change filling. J Micromech Microeng 2020;30:105001.
- [82] C A, Luszczynska B, Szymanski MZ, Ulanski J, Albrecht K, Yamamoto K. Inkjet printing of thermally activated delayed fluorescence (TADF) dendrimer for OLEDs applications. Org Electron 2019;74:218–27.
- [83] Cole CM, Kunz SV, Shaw PE, Thoebes N-P, Baumann T, Blasco E, Blinco JP, Sonar P, Barner-Kowollik C, Yambem SD. A printable thermally activated delayed fluorescence polymer light emitting diode. J Mater Chem C 2020;8:13001–9.
- [84] Nie Z, Kumacheva E. Patterning surfaces with functional polymers. Nat Mater 2008;7:277–90.
- [85] Nitta K, Tsumaki M, Kawano T, Terashima K, Ito T. Printing PEDOT from EDOT via plasma-assisted inkjet printing. J Phys D: Appl Phys 2019;52:315202.

- [86] Teo MY, Stuart L, Aw KC, Stringer J. Micro-reactive inkjet printer for 2D and 3D hydrogel structures. 2018 IEEE/ASME International Conference on Advanced Intelligent Mechatronics (AIM), Auckland: IEEE; 2018, p. 569–73.
- [87] Teo MY, Stuart L, Devaraj H, Liu CY, Aw KC, Stringer J. The *in situ* synthesis of conductive polyaniline patterns using micro-reactive inkjet printing. J Mater Chem C 2019;7:2219–24.
- [88] Teo MY, RaviChandran N, Kim N, Kee S, Stuart L, Aw KC, Stringer J. Direct patterning of highly conductive PEDOT:PSS/ionic liquid hydrogel via microreactive inkjet printing. ACS Appl Mater Interfaces 2019;11:37069–76.
- [89] Derby B. Inkjet printing of functional and structural materials: fluid property requirements, feature stability, and resolution. Annu Rev Mater Res 2010;40:395–414.
- [90] Li W, Wang X, Zheng G, Xu L, Jiang J, Luo Z, Guo S, Sun D. Current characteristics of stable cone–jet in electrohydrodynamic printing process. Appl Phys A 2018;124:711.
- [91] Bae J, Lee J, Kim SH. Effects of polymer properties on jetting performance of electrohydrodynamic printing. J Appl Polym Sci 2017;134:45044.
- [92] Li K, Wang D, Wang Q, Song K, Liang J, Sun Y, Madoua M. Thermally assisted electrohydrodynamic jet high-resolution printing of high-molecular weight biopolymer 3D structures. Macromol Mater Eng 2018;303:1800345.
- [93] Zhang G, Lan H, Qian L, Zhao J, Wang F. A microscale 3D printing based on the electric-field-driven jet. 3D Print Addit Manuf 2020;7:37–44.
- [94] Jing Q, Choi YS, Smith M, Ćatić N, Ou C, Kar-Narayan S. Aerosol-jet printed fine-featured triboelectric sensors for motion sensing. Adv Mater Technol 2019;4:1800328.
- [95] Obata K, Schonewille A, Slobin S, Hohnholz A, Unger C, Koch J, Suttmann O, Overmeyer L. Hybrid 2D patterning using UV laser direct writing and aerosol jet printing of UV curable polydimethylsiloxane. Appl Phys Lett 2017;111:121903.
- [96] Seifert T, Sowade E, Roscher F, Wiemer M, Gessner T, Baumann RR. Additive manufacturing technologies compared: morphology of deposits of silver ink using inkjet and aerosol jet printing. Ind Eng Chem Res 2015;54:769–79.
- [97] Tarabella G, Vurro D, Lai S, D'Angelo P, Ascari L, Iannotta S. Aerosol jet printing of PEDOT:PSS for large area flexible electronics. Flex Print Electron 2020;5:014005.
- [98] Bolse N, Eckstein R, Schend M, Habermehl A, Eschenbaum C, Hernandez-Sosa G, Lemmer U. A digitally printed optoelectronic nose for the selective trace detection of nitroaromatic explosive vapours using fluorescence quenching. Flex Print Electron 2017;2:024001.
- [99] Lee W, Park Y. Inkjet etching of polymers and its applications in organic electronic devices. Polymers 2017;9:441.
- [100] Farjam N, Cho TH, Dasgupta NP, Barton K. Subtractive patterning: high-resolution electrohydrodynamic jet printing with solvents. Appl Phys Lett 2020;117:133702.
- [101] Deferme W, Cramer M, Drijkoningen J, Verboven I. Optimizing the outcoupling efficiency and the radiation pattern of organic light emitting devices by inkjet printing lens arrays films. Proc SPIE, vol. 10687, 2018, p. 1068710–1.
- [102] Wang J, Song C, Zhong Z, Hu Z, Han S, Xu W, Peng J, Ying L, Wang J, Cao Y. In situ patterning of microgrooves via inkjet etching for a solution-processed OLED display. J

- Mater Chem C 2017;5:5005–9.
- [103] Sato T, Urata C. Direct micropatterning of initiator layers for surface-initiated ATRP: spatially-regulated growth of polymer brush and subsequent copper electroless plating. Mol Cryst Liquid Cryst 2019;688:98–104.
- [104] Kopec M, Tas S, Cirelli M, van der Pol R, de Vries I, Vancso GJ, de Beer S. Fluorescent patterns by selective grafting of a telechelic polymer. J Appl Polym Sci 2019;1:136–40.
- [105] Cho TH, Farjam N, Allemang CR, Pannier CP, Kazyak E, Huber C, Rose M, Trejo O, Peterson RL, Barton K, Dasgupta NP. Area-selective atomic layer deposition patterned by electrohydrodynamic jet printing for additive manufacturing of functional materials and devices. ACS Nano 2020;14:17262–72.
- [106] Hohnholz A, Obata K, Nakajima Y, Koch J, Terakawa M, Suttmann O, Overmeyer L. Hybrid UV laser direct writing of UV-curable PDMS thin film using aerosol jet printing. Appl Phys A 2019;125:120.
- [107] Overmeyer L, Hohnholz A, Suttmann O, Kaierle S. Multi-material laser direct writing of aerosol jet layered polymers. CIRP Ann 2019;68:217–20.
- [108] Reitberger T, Hoffmann G-A, Wolfer T, Overmeyer L, Franke J. Printing polymer optical waveguides on conditioned transparent flexible foils by using the aerosol jet technology. Proc SPIE, vol. 9945, 2016, p. 99450G.
- [109] Hoffmann G-A, Wienke A, Reitberger T, Franke J, Kaierle S, Overmeyer L. Thermoforming of planar polymer optical waveguides for integrated optics in smart packaging materials. J Mater Process Technol 2020;285:116763.
- [110] Christanti Y, Walker LM. Surface tension driven jet break up of strain-hardening polymer solutions. J Nonnewton Fluid Mech 2001;100:9–26.
- [111] Tekin E, J. Smith P, S. Schubert U. Inkjet printing as a deposition and patterning tool for polymers and inorganic particles. Soft Matter 2008;4:703–13.
- [112] Singh M, Haverinen HM, Dhagat P, Jabbour GE. Inkjet printing—process and its applications. Adv Mater 2010;22:673–85.
- [113] Sumaiya S, Kardel K, El-Shahat A. Organic solar cell by inkjet printing—an overview. Technologies 2017;5:53.
- [114] Dianat G, Gupta M. Sequential deposition of patterned porous polymers using poly(dimethylsiloxane) masks. Polymer 2017;126:463–9.
- [115] Liu Z, Liu S, Dong R, Yang S, Lu H, Narita A, Feng X, Müllen K. High power in-plane micro-supercapacitors based on mesoporous polyaniline patterned graphene. Small 2017;13:1603388.
- [116] Bengasi G, Baba K, Frache G, Desport J, Gratia P, Heinze K, Boscher ND. Conductive fused porphyrin tapes on sensitive substrates by a chemical vapor deposition approach. Angew Chem Int Ed 2019;58:2103–8.
- [117] Bengasi G, Baba K, Back O, Frache G, Heinze K, Boscher ND. Reactivity of nickel(II) porphyrins in oCVD processes-polymerisation, intramolecular cyclisation and chlorination. Chem Eur J 2019;25:8313–20.
- [118] Petruczok CD, Gleason KK. Initiated chemical vapor deposition-based method for

- patterning polymer and metal microstructures on curved substrates. Adv Mater 2012;24:6445–50.
- [119] Yang H, Wang H, Feng J, Ye Y, Liu W. Solventless synthesis and patterning of UV-responsive poly(allyl methacrylate) film. Macromol Chem Phys 2019;220:1900299.
- [120] Zhang C, Vehkamäki M, Pietikäinen M, Leskelä M, Ritala M. Area-selective molecular layer deposition of polyimide on Cu through Cu-catalyzed formation of a crystalline interchain polyimide. Chem Mater 2020;32:5073–83.
- [121] Junige M, George SM. Area-selective molecular layer deposition of nylon 6,2 polyamide: Growth on carbon and inhibition on silica. J Vac Sci Technol, A 2021;39:023204.
- [122] Closser RG, Bergsman DS, Ruelas L, Hashemi FSM, Bent SF. Correcting defects in area selective molecular layer deposition. J Vac Sci Technol, A 2017;35:031509.
- [123] Pattison TG, Hess AE, Arellano N, Lanzillo N, Nguyen S, Bui H, Rettner C, Truong H, Friz A, Topuria T, Fong A, Hughes B, Tek AT, DeSilva A, Miller RD, Qiao GG, Wojtecki RJ. Surface initiated polymer thin films for the area selective deposition and etching of metal oxides. ACS Nano 2020;14:4276–88.
- [124] Brooke R, Edberg J, Iandolo D, Berggren M, Crispin X, Engquist I. Controlling the electrochromic properties of conductive polymers using UV-light. J Mater Chem C 2018;6:4663–70.
- [125] Brooke R, Edberg J, Crispin X, Berggren M, Engquist I, Jonsson MP. Greyscale and paper electrochromic polymer displays by UV patterning. Polymers 2019;11:267.
- [126] Hua F, Sun Y, Gaur A, Meitl MA, Bilhaut L, Rotkina L, Wang J, Geil P, Shim M, Rogers JA, Shim A. Polymer imprint lithography with molecular-scale resolution. Nano Lett 2004;4:2467–71.
- [127] Krauss PR, Chou SY. Nano-compact disks with 400 Gbit/in2 storage density fabricated using nanoimprint lithography and read with proximal probe. Appl Phys Lett 1997;71:3174—6.
- [128] Posseme N, editor. Front matter. Plasma etching processes for CMOS devices realization, Elsevier; 2017, p. i–iii.
- [129] Cox LM, Martinez AM, Blevins AK, Sowan N, Ding Y, Bowman CN. Nanoimprint lithography: emergent materials and methods of actuation. Nano Today 2020;31:100838.
- [130] Sun H. Recent progress in low temperature nanoimprint lithography. Microsyst Technol 2015;21:1–7.
- [131] Mohapatra S, Kumari S, Moirangthem RS. Fabrication of a cost-effective polymer nanograting as a disposable plasmonic biosensor using nanoimprint lithography. Mater Res Express 2017;4:076202.
- [132] Borah D, Cummins C, Rasappa S, Senthamaraikannan R, Salaun M, Zelsmann M, Liontos G, Ntetsikas K, Avgeropoulos A, Morris MA. Nanopatterning via self-assembly of a lamellar-forming polystyrene-block-poly(dimethylsiloxane) diblock copolymer on topographical substrates fabricated by nanoimprint lithography. Nanomater 2018;8:32.
- [133] Hamouda F, Aassime A, Bertin H, Gogol P, Bartenlian B, Dagens B. Tunable diffraction grating in flexible substrate by UV-nanoimprint lithography. J Micromech Microeng

- 2017;27:025017.
- [134] Chen Y, Wang Z, Kulkarni MM, Wang X, Al-Enizi AM, Elzatahry AA, Douglas JF, Dobrynin AV, Karim A. Hierarchically patterned elastomeric and thermoplastic polymer films through nanoimprinting and ultraviolet light exposure. ACS Omega 2018;3:15426–34.
- [135] Lee JH, Na M, Kim J, Yoo K, Park J, Kim JD, Oh DK, Lee S, Youn H, Kwak MK, Ok JG. Rapid and conformal coating of polymer resins by airbrushing for continuous and high-speed roll-to-roll nanopatterning: parametric quality controls and extended applications. Nano Converg 2017;4:11.
- [136] Jun J, Lee J-H, Choi H-J, Moon S, Kim I-D, Lee H. Fabrication of optically-functionalized colorless polyimide patterns with high durability. Appl Surf Sci 2017;423:881–6.
- [137] Li Y, Choi J, Sun Z, Russell TP, Carter KR. Fabrication of sub-20 nm patterns using dopamine chemistry in self-aligned double patterning. Nanoscale 2018;10:20779–84.
- [138] Gee A, Jaafar AH, Kemp NT. Nanoscale junctions for single molecule electronics fabricated using bilayer nanoimprint lithography combined with feedback controlled electromigration. Nanotechnology 2020;31:155203.
- [139] Li XH, Shen XZ, Gao X, Weng YY. Enhancement of light-emitting properties by simultaneously patterning and controlling molecular alignment in polyfluorene thin films. Rsc Advances 2017;7:55885–90.
- [140] Voicu NE, Ludwigs S, Crossland EJW, Andrew P, Steiner U. Solvent-vapor-assisted imprint lithography. Adv Mater 2007;19:757–61.
- [141] Brazil O, Usov V, Pethica JB, Cross GLW. Large area thermal nanoimprint below the glass transition temperature via small amplitude oscillatory shear forming. Microelectron Eng 2017;182:35–41.
- [142] Ding G, Wang K, Li X, Wang C, Hu Z, Liu J. Nanoimprinting-induced molecular orientation in poly(3-hexylthiophene) nanogratings and its extraordinary retention after thermal annealing. Polym Chem 2017;8:2666–74.
- [143] Rosenberg M, Schvartzman M. Direct resistless soft nanopatterning of freeform surfaces. ACS Appl Mater Interfaces 2019;11:43494–9.
- [144] Schift H. Nanoimprint lithography: an old story in modern times? a review. J Vac Sci Technol B 2008;26:458–80.
- [145] Li M, Chen Y, Luo W, Cheng X. Interfacial interactions during demolding in nanoimprint lithography. Micromachines (Basel) 2021;12:349.
- [146] Schift H. Nanoimprint lithography: 2D or not 2D? a review. Appl Phys A 2015;121:415–35.
- [147] Bhagoria P, Mathew Sebastian E, Kumar Jain S, Purohit J, Purohit R. Nanolithography and its alternate techniques. Mater Today: Proc 2020;26:3048–53.
- [148] Tak H, Tahk D, Jeong C, Lee S, Kim T. Surface energy-tunable iso decyl acrylate based molds for low pressure-nanoimprint lithography. Nanotechnology 2017;28:405301.
- [149] Pattison TG, Spanu A, Friz AM, Fu Q, Miller RD, Qiao GG. Growing patterned, cross-linked nanoscale polymer films from organic and inorganic surfaces using ring-opening metathesis polymerization. ACS Appl Mater Interfaces 2020;12:4041.
- [150] Kumar A, Whitesides GM. Features of gold having micrometer to centimeter dimensions

- can be formed through a combination of stamping with an elastomeric stamp and an alkanethiol "ink" followed by chemical etching. Appl Phys Lett 1993;63:2002–4.
- [151] Perl A, Reinhoudt DN, Huskens J. Microcontact printing: limitations and achievements. Adv Mater 2009;21:2257–68.
- [152] Alom Ruiz S, Chen CS. Microcontact printing: a tool to pattern. Soft Matter 2007;3:168–77.
- [153] Kaufmann T, Jan Ravoo B. Stamps, inks and substrates: polymers in microcontact printing. Polym Chem 2010;1:371–87.
- [154] Widyaya VT, Riga EK, Müller C, Lienkamp K. Submicrometer-sized, 3D surface-attached polymer networks by microcontact printing: using UV-cross-linking efficiency to tune structure height. Macromolecules 2018;51:1409–17.
- [155] Miao Y, Liu H, Cheng W, Liu Y, Kim S, Yuan X, Kusi-Appiah A, Lenhert S, Ma T, Ren Y, Chung H, Guan J. Conjugating micropatches to living cells through membrane intercalation. ACS Appl Mater Interfaces 2020;12:29110.
- [156] Kim S, Lee S, Kim C, Shin H. One-step harvest and delivery of micropatterned cell sheets mimicking the multi-cellular microenvironment of vascularized tissue. Acta Biomater 2021:176–87.
- [157] Lilge I, Jiang S, Schönherr H. Long-term stable poly(acrylamide) brush modified transparent microwells for cell attachment studies in 3D. Macromol Biosci 2017;17:1600451.
- [158] Chen L, Li P, Lu X, Wang S, Zheng Z. Binary polymer brush patterns from facile initiator stickiness for cell culturing. Faraday Discuss 2019;219:189–202.
- [159] Wu H, Wu L, Zhou X, Liu B, Zheng B. Patterning hydrophobic surfaces by negative microcontact printing and its applications. Small 2018;14:1802128.
- [160] Thuau D. Engineering polymer MEMS using combined microfluidic pervaporation and micro-molding. Microsyst Nanoeng 2018;4:15.
- [161] Ho D, Zou J, Zdyrko B, Iyer KS, Luzinov I. Capillary force lithography: the versatility of this facile approach in developing nanoscale applications. Nanoscale 2014;7:401–14.
- [162] Suh K y., Lee H h. Capillary force lithography: large-area patterning, self-organization, and anisotropic dewetting. Adv Funct Mater 2002;12:405–13.
- [163] Gwon Y, Park S, Kim W, Han T, Kim H, Kim J. Radially patterned transplantable biodegradable scaffolds as topographically defined contact guidance platforms for accelerating bone regeneration. J Biol Eng 2021;15:12.
- [164] Xing W, Zhang D, Zhang L, Zhang S, Huang Y, Li J, Guo A, Li W, Zhao F. Stamping of a replica with resolution doubling that of the master via capillary force lithography. Opt Mater 2021;120:111467.
- [165] Choi JS, Tsui JH, Xu F, Lee SH, Sung S-K, Lee HJ, Wang C, Kim HJ, Kim D-H. Fabrication of micro- and nanopatterned nafion thin films with tunable mechanical and electrical properties using thermal evaporation-induced capillary force lithography. Adv Mater Interfaces 2021;8:2002005.
- [166] Han CM, Lee B-K. Effect of hydrophilicity of polydimethylsiloxane stamp in capillary force

- lithography process of thermoplastic polyurethane. Microelectron Eng 2018;190:38–43.
- [167] Li B, Agarwal V, Ho D, Vede J-P, Iyer KS. Systematic assessment of surface functionality on nanoscale patterns for topographic contact guidance of cells. New J Chem 2018;42:7237–40.
- [168] Saurakhiya N, Sachan P, Kumar R, Sharma A. Micropatterned arrays of functional materials by self-organized dewetting of ultrathin polymer films combined with electrodeposition. RSC Adv 2016;6:73176–85.
- [169] Florence SS, Can N, Sachan P, Gupta RK, Arockiasamy L, Adam H, Umadevi M. Large scale ZnTe nanostructures on polymer micro patterns via capillary force photolithography, Rhodes, Greece: 2016, p. 020001.
- [170] Pendyala P, Grewal HS, Kim HN, Cho I-J, Yoon E-S. Individual role of the physicochemical characteristics of nanopatterns on tribological surfaces. ACS Appl Mater Interfaces 2016;8:30590–600.
- [171] Guo L, Philippi M, Steinhart M. Substrate patterning using regular macroporous block copolymer monoliths as sacrificial templates and as capillary microstamps. Small 2018;14:1801452.
- [172] Jiang W, Zhang C, Tran L, Wang SG, Hakim AD, Liu H. Engineering nano-to-micron-patterned polymer coatings on bioresorbable magnesium for controlling human endothelial cell adhesion and morphology. ACS Biomater Sci Eng 2020;6:3878–98.
- [173] Lee MS, La W-G, Park E, Yang HS. Synergetic effect of 3,4-dihydroxy-1-phenylalanine-modified poly(lactic-co-glycolic acid) nanopatterned patch with fibroblast growth factor-2 for skin wound regeneration. J Biomed Mater Res B Appl Biomater 2017;105:594–604.
- [174] Liu X, Bhandaru N, Banik M, Wang X, Al-Enizi AM, Karim A, Mukherjee R. Capillary force lithography pattern-directed self-assembly (CFL-PDSA) of phase-separating polymer blend thin films. ACS Omega 2018;3:2161–8.
- [175] Suh KY, Kim YS, Lee HH. Capillary force lithography. Adv Mater 2001;13:1386–9.
- [176] Orilall MC, Wiesner U. Block copolymer based composition and morphology control in nanostructured hybrid materials for energy conversion and storage: solar cells, batteries, and fuel cells. Chem Soc Rev 2011;40:520–35.
- [177] Bates FS, Fredrickson GH. Block copolymer thermodynamics: theory and experiment. Annu Rev Phys Chem 1990;41:525–57.
- [178] Lo T-Y, Krishnan MR, Lu K-Y, Ho R-M. Silicon-containing block copolymers for lithographic applications. Prog Polym Sci 2018;77:19–68.
- [179] Khandpur AK, Foerster S, Bates FS, Hamley IW, Ryan AJ, Bras W, Almdal K, Mortensen K. Polyisoprene-polystyrene diblock copolymer phase diagram near the order-disorder transition. Macromolecules 1995;28:8796–806.
- [180] Park C, Yoon J, Thomas EL. Enabling nanotechnology with self assembled block copolymer patterns. Polymer 2003;44:6725–60.
- [181] Jin C, Olsen BC, Luber EJ, Buriak JM. Nanopatterning via solvent vapor annealing of block copolymer thin films. Chem Mater 2017;29:176–88.
- [182] Nowak SR, Yager KG. Photothermally directed assembly of block copolymers. Adv Mater

- Interfaces 2020;7:1901679.
- [183] Merekalov AS, Derikov YI, Ezhov AA, Govorun EN, Kudryavtsev YV. Evolution of microstructure in block copolymer thin films during zone annealing. Polym Sci Ser A 2018;60:723–33.
- [184] Singh M, Wu W, Basutkar MN, Strzalka J, Al-Enizi AM, Douglas JF, Karim A. Ultra-fast vertical ordering of lamellar block copolymer films on unmodified substrates. Macromolecules 2021;54:1564–73.
- [185] Luo Y, Wang X, Zhang R, Singh M, Ammar A, Cousins D, K. Hassan M, Ponnamma D, Adham S, Ali Al-Maadeed MA, Karim A. Vertically oriented nanoporous block copolymer membranes for oil/water separation and filtration. Soft Matter 2020;16:9648–54.
- [186] Singh M, Basutkar M, Samant S, Singh G, Karim A. Directed self-assembly of block copolymers with dynamic thermal gradients. Soft Matter and Biomaterials on the Nanoscale, World Scientific; 2020, p. 373–409.
- [187] Jiang J, Jacobs AG, Wenning B, Liedel C, Thompson MO, Ober CK. Ultrafast self-assembly of sub-10 nm block copolymer nanostructures by solvent-free high-temperature laser annealing. ACS Appl Mater Interfaces 2017;9:31317–24.
- [188] Leniart AA, Pula P, Sitkiewicz A, Majewski PW. Macroscopic alignment of block copolymers on silicon substrates by laser annealing. ACS Nano 2020;14:4805–15.
- [189] Liao Y, Liu K, Chen W-C, Wei B, Borsali R. Robust sub-10 nm pattern of standing sugar cylinders via rapid "microwave cooking." Macromolecules 2019;52:8751–8.
- [190] Hur YH, Song SW, Kim JM, Park WI, Kim KH, Kim Y, Jung YS. Thermodynamic and kinetic tuning of block copolymer based on random copolymerization for high-quality sub-6 nm pattern formation. Adv Funct Mater 2018;28:1800765.
- [191] Basutkar MN, Samant S, Strzalka J, Yager KG, Singh G, Karim A. Through-thickness vertically ordered lamellar block copolymer thin films on unmodified quartz with cold zone annealing. Nano Lett 2017;17:7814–23.
- [192] Singh G, Yager KG, Smilgies D-M, Kulkarni MM, Bucknall DG, Karim A. Tuning molecular relaxation for vertical orientation in cylindrical block copolymer films via sharp dynamic zone annealing. Macromolecules 2012;45:7107–17.
- [193] Berry BC, Bosse AW, Douglas JF, Jones RL, Karim A. Orientational order in block copolymer films zone annealed below the order—disorder transition temperature. Nano Lett 2007;7:2789–94.
- [194] Majewski PW, Yager KG. Millisecond ordering of block copolymer films via photothermal gradients. ACS Nano 2015;9:3896–906.
- [195] Angelescu DE, Waller JH, Adamson DH, Deshpande P, Chou SY, Register RA, Chaikin PM. Macroscopic orientation of block copolymer cylinders in single-layer films by shearing. Adv Mater 2004;16:1736–40.
- [196] Singh M, Agrawal A, Wu W, Masud A, Armijo E, Gonzalez D, Zhou S, Terlier T, Zhu C, Strzalka J, Matyjaszewski K, Bockstaller M, Douglas JF, Karim A. Soft-shear-aligned vertically oriented lamellar block copolymers for template-free sub-10 nm patterning and hybrid nanostructures. ACS Appl Mater Interfaces 2022;14:12824–35.

- [197] Singh G, Yager KG, Berry B, Kim H-C, Karim A. Dynamic thermal field-induced gradient soft-shear for highly oriented block copolymer thin films. ACS Nano 2012;6:10335–42.
- [198] Zhang R, Singh G, Dang A, Dai L, Bockstaller MR, Akgun B, Satija S, Karim A. Nanoparticle-driven orientation transition and soft-shear alignment in diblock copolymer films via dynamic thermal gradient field. Macromol Rapid Commun 2013;34:1642–7.
- [199] Samant S, Hailu S, Singh M, Pradhan N, Yager K, Al-Enizi AM, Raghavan D, Karim A. Alignment frustration in block copolymer films with block copolymer grafted TiO₂ nanoparticles under soft-shear cold zone annealing. Polym Adv Technol 2021;32:2052–60.
- [200] Zhang R, Lee B, Bockstaller MR, Al-Enizi AM, Elzatahry A, Berry BC, Karim A. Soft-shear induced phase-separated nanoparticle string-structures in polymer thin films. Faraday Discuss 2016;186:31–43.
- [201] Majewski PW, Rahman A, Black CT, Yager KG. Arbitrary lattice symmetries via block copolymer nanomeshes. Nat Commun 2015;6:7448.
- [202] Choo Y, Majewski PW, Fukuto M, Osuji CO, Yager KG. Pathway-engineering for highly-aligned block copolymer arrays. Nanoscale 2018;10:416–27.
- [203] Basutkar MN, Majewski PW, Doerk GS, Toth K, Osuji CO, Karim A, Yager KG. Aligned morphologies in near-edge regions of block copolymer thin films. Macromolecules 2019;52:7224–33.
- [204] Liu K, Yang C-M, Yang B-M, Zhang L, Huang W-C, Ouyang X-P, Qi F-G, Zhao N, Bian F-G. Directed self-assembly of vertical PS-b-PMMA nanodomains grown on multilayered polyelectrolyte films. Chin J Polym Sci 2020;38:92–9.
- [205] Yang W-C, Hong J-W, Chang J-H, Chen Y-F, Nelson A, Wang Y-M, Chiang Y-W, Wu C-M, Sun Y-S. Dispersity effects on phase behavior and structural evolution in ultrathin films of a deuterated polystyrene-block-poly(methyl methacrylate) diblock copolymer. Polymer 2020;210:123027.
- [206] Someya Y, Mizuochi R, Wakayama H, Tadokoro S, Kozawa M, Sakamoto R. Orientation control of silicon containing block-co-polymer with resolution beyond 10nm. Advances in Patterning Materials and Processes XXXIV, vol. 10146, 2017, p. 101461Y.
- [207] Yue B, Jin X, Zhao P, Zhu M, Zhu L. Directed self-assembly of templatable block copolymers by easily accessible magnetic control. Small 2019;15:1804572.
- [208] Han KH, Kang H, Lee GY, Lee HJ, Jin HM, Cha SK, Yun T, Kim JH, Yang GG, Choi HJ, Ko YK, Jung H-T, Kim SO. Highly aligned carbon nanowire array by e-field directed assembly of PAN-containing block copolymers. ACS Appl Mater Interfaces 2020;12:58113–21.
- [209] Nakatani R, Takano H, Chandra A, Yoshimura Y, Wang L, Suzuki Y, Tanaka Y, Maeda R, Kihara N, Minegishi S, Miyagi K, Kasahara Y, Sato H, Seino Y, Azuma T, Yokoyama H, Ober CK, Hayakawa T. Perpendicular orientation control without interfacial treatment of raft-synthesized high-χ block copolymer thin films with sub-10 nm features prepared via thermal annealing. ACS Appl Mater Interfaces 2017;9:31266–78.
- [210] Xiong S, Wan L, Ishida Y, Chapuis Y-A, Craig GSW, Ruiz R, Nealey PF. Directed self-assembly of triblock copolymer on chemical patterns for sub-10-nm nanofabrication via

- solvent annealing. ACS Nano 2016;10:7855–65.
- [211] Sunday DF, Chen X, Albrecht TR, Nowak D, Rincon Delgadillo P, Dazai T, Miyagi K, Maehashi T, Yamazaki A, Nealey PF, Kline RJ. Influence of additives on the interfacial width and line edge roughness in block copolymer lithography. Chem Mater 2020;32:2399–407.
- [212] Chen X, Zhou C, Chen S-J, Craig GSW, Rincon-Delgadillo P, Dazai T, Miyagi K, Maehashi T, Yamazaki A, Gronheid R, Stoykovich MP, Nealey PF. Ionic liquids as additives to polystyrene-block-poly(methyl methacrylate) enabling directed self-assembly of patterns with sub-10 nm features. ACS Appl Mater Interfaces 2018;10:16747–59.
- [213] Chen X, Seo T, Rincon-Delgadillo P, Matsumiya T, Kawaue A, Maehashi T, Gronheid R, Nealey PF. Directed self-assembly of PS-b-PMMA with ionic liquid addition. Advances in Patterning Materials and Processes XXXIII, vol. 9779, Int J Opt Photonics; 2016, p. 97790S.
- [214] Masud A, Wu W, Singh M, Tonny W, Ammar A, Sharma K, Strzalka JW, Terlier T, Douglas JF, Karim A. Solvent processing and ionic liquid-enabled long-range vertical ordering in block copolymer films with enhanced film stability. Macromolecules 2021;54:8512–25.
- [215] Doerk GS, Yager KG. Rapid ordering in "wet brush" block copolymer/homopolymer ternary blends. ACS Nano 2017;11:12326–36.
- [216] Doerk GS, Li R, Fukuto M, Yager KG. Wet brush homopolymers as "smart solvents" for rapid, large period block copolymer thin film self-assembly. Macromolecules 2020;53:1098–113.
- [217] Li Y, Xu Y, Cao S, Zhao Y, Qu T, Iyoda T, Chen A. Nanoporous films with sub-10 nm in pore size from acid-cleavable block copolymers. Macromol Rapid Commun 2017;38:1600662.
- [218] Qu T, Guan S, Zheng X, Chen A. Perpendicularly aligned nanodomains on versatile substrates via rapid thermal annealing assisted by liquid crystalline ordering in block copolymer films. Nanoscale Adv 2020;2:1523–30.
- [219] Shi L-Y, Lee S, Cheng L-C, Huang H, Liao F, Ran R, Yager KG, Ross CA. Thin film self-assembly of a silicon-containing rod-coil liquid crystalline block copolymer. Macromolecules 2019;52:679–89.
- [220] Chambers LC, Huang Y, Jack KS, Blakey I. Spatial control of the topography of photosensitive block copolymer thin films. Polym Chem 2019;10:3135–45.
- [221] Bates CM, Seshimo T, Maher MJ, Durand WJ, Cushen JD, Dean LM, Blachut G, Ellison CJ, Willson CG. Polarity-switching top coats enable orientation of sub–10-nm block copolymer domains. Science 2012;338:775–9.
- [222] Kim DH, Kim SY. Universal interfacial control through polymeric nanomosaic coating for block copolymer nanopatterning. ACS Nano 2020:12.
- [223] Yoshimura Y, Chandra A, Nabae Y, Hayakawa T. Chemically tailored high-χ block copolymers for perpendicular lamellae via thermal annealing. Soft Matter 2019;15:3497–506.
- [224] Wang HS, Oh S, Choi J, Jang W, Kim KH, Arellano CL, Huh J, Bang J, Im SG. High-fidelity, sub-5 nm patterns from high-χ block copolymer films with vapor-deposited ultrathin, cross-

- linked surface-modification layers. Macromol Rapid Commun 2020;41:1900514.
- [225] Cummins C, Alvarez-Fernandez A, Bentaleb A, Hadziioannou G, Ponsinet V, Fleury G. Strategy for enhancing ultrahigh-molecular-weight block copolymer chain mobility to access large period sizes (>100 nm). Langmuir 2020;36:13872–80.
- [226] Shi L-Y, Liao F, Cheng L-C, Lee S, Ran R, Shen Z, Ross CA. Core–shell and zigzag nanostructures from a thin film silicon-containing conformationally asymmetric triblock terpolymer. ACS Macro Lett 2019;8:852–8.
- [227] Son JG, Gotrik KW, Ross CA. High-aspect-ratio perpendicular orientation of PS-b-PDMS thin films under solvent annealing. ACS Macro Lett 2012;1:1279–84.
- [228] Chavis MA, Smilgies D-M, Wiesner UB, Ober CK. Widely tunable morphologies in block copolymer thin films through solvent vapor annealing using mixtures of selective solvents. Adv Funct Mater 2015;25:3057–65.
- [229] Kim K, Park S, Kim Y, Bang J, Park C, Ryu DY. Optimized solvent vapor annealing for long-range perpendicular lamellae in PS-b-PMMA films. Macromolecules 2016;49:1722–30.
- [230] Hulkkonen H, Salminen T, Niemi T. Automated solvent vapor annealing with nanometer scale control of film swelling for block copolymer thin films. Soft Matter 2019;15:7909–17.
- [231] Gotrik KW, Hannon AF, Son JG, Keller B, Alexander-Katz A, Ross CA. Morphology control in block copolymer films using mixed solvent vapors. ACS Nano 2012;6:8052–9.
- [232] Rasappa S, Schulte L, Borah D, Hulkkonen H, Ndoni S, Salminen T, Senthamaraikanan R, Morris MA, Niemi T. Morphology evolution of PS-b-PDMS block copolymer and its hierarchical directed self-assembly on block copolymer templates. Microelectron Eng 2018;192:1–7.
- [233] Leniart AA, Pula P, Tsai EHR, Majewski PW. Large-grained cylindrical block copolymer morphologies by one-step room-temperature casting. Macromolecules 2020;53:11178–89.
- [234] Lee S, Cheng L-C, Gadelrab KR, Ntetsikas K, Moschovas D, Yager KG, Avgeropoulos A, Alexander-Katz A, Ross CA. Double-layer morphologies from a silicon-containing ABA triblock copolymer. ACS Nano 2018;12:6193–202.
- [235] Cetintas M, Kamperman M. Self-assembly of PS-b-PNIPAM-b-PS block copolymer thin films via selective solvent annealing. Polymer 2016;107:387–97.
- [236] Xiong S, Li D, Hur S-M, Craig GSW, Arges CG, Qu X-P, Nealey PF. The solvent distribution effect on the self-assembly of symmetric triblock copolymers during solvent vapor annealing. Macromolecules 2018;51:7145–51.
- [237] Zhang W, Sun Z, Jiang Y, Liu X, Gupta R, Russell TP, Coughlin EB. Tuning microdomain spacing with light using ortho-nitrobenzyl-linked triblock copolymers. J Polym Sci Pt B-Polym Phys 2018;56:355–61.
- [238] Kim H, Kang B-G, Choi J, Sun Z, Yu DM, Mays J, Russell TP. Morphological behavior of A₂B block copolymers in thin films. Macromolecules 2018;51:1181–8.
- [239] Antoine S, Aissou K, Mumtaz M, Pecastaings G, Buffeteau T, Fleury G, Hadziioannou G. Nanoscale archimedean tilings formed by 3-miktoarm star terpolymer thin films. Macromol Rapid Commun 2019;40:1800860.

- [240] Gestranius M, Otsuka I, Halila S, Hermida-Merino D, Solano E, Borsali R, Tammelin T. High-resolution patterned biobased thin films via self-assembled carbohydrate block copolymers and nanocellulose. Adv Mater Interfaces 2020;7:1901737.
- [241] Liao Y, Goujon LJ, Reynaud E, Halila S, Gibaud A, Wei B, Borsali R. Self-assembly of copper-free maltoheptaose-block-polystyrene nanostructured thin films in real and reciprocal space. Carbohydr Polym 2019;212:222–8.
- [242] Shi L-Y, Yin C, Zhou B, Xia W, Weng L, Ross CA. Annealing process dependence of the self-assembly of rod-coil block copolymer thin films. Macromolecules 2021;54:1657–64.
- [243] Byun I-J, Lee J-H, Jeong K-U, Han Y-K. Synthesis of high X block copolymers with LC moieties and PMMA segments using RAFT polymerization, and their nanostructure morphologies. Polymer 2018;145:184–93.
- [244] Evans K, Xu T. Self-assembly of supramolecular thin films: role of small molecule and solvent vapor annealing. Macromolecules 2019;52:639–48.
- [245] Shi L-Y, Lan J, Lee S, Cheng L-C, Yager KG, Ross CA. Vertical lamellae formed by two-step annealing of a rod-coil liquid crystalline block copolymer thin film. ACS Nano 2020;14:4289–97.
- [246] Park WI, Choi YJ, Yuk JM, Seo HK, Kim KH. Enhanced self-assembly of block copolymers by surface modification of a guiding template. Polym J 2018;50:221–9.
- [247] Borah D, Cummins C, Rasappa S, Watson SMD, Pike AR, Horrocks BR, Fulton DA, Houlton A, Liontos G, Ntetsikas K, Avgeropoulos A, Morris MA. Nanoscale silicon substrate patterns from self-assembly of cylinder forming poly(styrene)-block-poly(dimethylsiloxane) block copolymer on silane functionalized surfaces. Nanotechnology 2016;28:044001.
- [248] Kathrein CC, Bai W, Nunns A, Gwyther J, Manners I, Böker A, Tsarkova L, Ross CA. Electric field manipulated nanopatterns in thin films of metalorganic 3-miktoarm star terpolymers. Soft Matter 2016;12:4866–74.
- [249] Sung SH, Farnham WB, Burch HE, Brun Y, Qi K, Epps TH. Directional self-assembly of fluorinated star block polymer thin films using mixed solvent vapor annealing. J Polym Sci B Polym Phys 2019;57:1663–72.
- [250] Kim YC, Shin TJ, Hur S-M, Kwon SJ, Kim SY. Shear-solvo defect annihilation of diblock copolymer thin films over a large area. Sci Adv 2019;5:eaaw3974.
- [251] Kang H, Kim K, Sohn B-H. Shearing with solvent vapor annealing on block copolymer thin films for templates with macroscopically aligned nanodomains. Nanotechnology 2020;31:455302.
- [252] Liao Y, Chen W-C, Borsali R. Carbohydrate-based block copolymer thin films: ultrafast nano-organization with 7 nm resolution using microwave energy. Adv Mater 2017;29:1701645.
- [253] Han J, Kim J-S, Shin JM, Yun H, Kim Y, Park H, Kim BJ. Rapid solvo-microwave annealing for optimizing ordered nanostructures and crystallization of regionegular polythiophene-based block copolymers. Polym Chem 2019;10:4962–72.
- [254] Jo S, Jeon S, Kim H, Ryu CY, Lee S, Ryu DY. Balanced interfacial interactions for

- fluoroacrylic block copolymer films and fast electric field directed assembly. Chem Mater 2020;32:9633–41.
- [255] Oh J, Suh HS, Ko Y, Nah Y, Lee J-C, Yeom B, Char K, Ross CA, Son JG. Universal perpendicular orientation of block copolymer microdomains using a filtered plasma. Nat Commun 2019;10:2912.
- [256] Kim G, Libera M. Morphological development in solvent-cast polystyrene—polybutadiene—polystyrene (SBS) triblock copolymer thin films. Macromolecules 1998;31:2569–77.
- [257] Albert JNL, Young W-S, Lewis RL, Bogart TD, Smith JR, Epps TH. Systematic study on the effect of solvent removal rate on the morphology of solvent vapor annealed aba triblock copolymer thin films. ACS Nano 2012;6:459–66.
- [258] Albert JNL, Epps TH. Self-assembly of block copolymer thin films. Mater Today 2010;13:24–33.
- [259] Khanna V, Cochran EW, Hexemer A, Stein GE, Fredrickson GH, Kramer EJ, Li X, Wang J, Hahn SF. Effect of chain architecture and surface energies on the ordering behavior of lamellar and cylinder forming block copolymers. Macromolecules 2006;39:9346–56.
- [260] Park WI, Tong S, Liu Y, Jung IW, Roelofs A, Hong S. Tunable and rapid self-assembly of block copolymers using mixed solvent vapors. Nanoscale 2014;6:15216–21.
- [261] Kim MJ, Park WI, Choi YJ, Jung YK, Kim KH. Ultra-rapid pattern formation of block copolymers with a high-χ parameter in immersion annealing induced by a homopolymer. RSC Adv 2016;6:21105–10.
- [262] Longanecker M, Modi A, Dobrynin A, Kim S, Yuan G, Jones R, Satija S, Bang J, Karim A. Reduced domain size and interfacial width in fast ordering nanofilled block copolymer films by direct immersion annealing. Macromolecules 2016;49:8563–71.
- [263] Modi A, Bhaway SM, Vogt BD, Douglas JF, Al-Enizi A, Elzatahry A, Sharma A, Karim A. Direct immersion annealing of thin block copolymer films. ACS Appl Mater Interfaces 2015;7:21639–45.
- [264] Wu W, Singh M, Masud A, Wang X, Nallapaneni A, Xiao Z, Zhai Y, Wang Z, Terlier T, Bleuel M, Yuan G, Satija SK, Douglas JF, Matyjaszewski K, Bockstaller MR, Karim A. Control of phase morphology of binary polymer grafted nanoparticle blend films via direct immersion annealing. ACS Nano 2021;15:12042–56.
- [265] Park WI, Kim JM, Jeong JW, Jung YS. Deep-nanoscale pattern engineering by immersion-induced self-assembly. ACS Nano 2014;8:10009–18.
- [266] Wan L, Ruiz R, Gao H, Albrecht TR. Self-registered self-assembly of block copolymers. ACS Nano 2017;11:7666–73.
- [267] Cha SK, Yong D, Yang GG, Jin HM, Kim JH, Han KH, Kim JU, Jeong S-J, Kim SO. Nanopatterns with a square symmetry from an orthogonal lamellar assembly of block copolymers. ACS Appl Mater Interfaces 2019;11:20265–71.
- [268] Bita I, Yang JKW, Jung YS, Ross CA, Thomas EL, Berggren KK. Graphoepitaxy of self-assembled block copolymers on two-dimensional periodic patterned templates. Science 2008;321:939–43.

- [269] Choi J, Li Y, Kim PY, Liu F, Kim H, Yu DM, Huh J, Carter KR, Russell TP. Orthogonally aligned block copolymer line patterns on minimal topographic patterns. ACS Appl Mater Interfaces 2018;10:8324–32.
- [270] Brassat K, Kool D, Nallet CGA, Lindner JKN. Understanding film thickness-dependent block copolymer self-assembly by controlled polymer dewetting on prepatterned surfaces. Adv Mater Interfaces 2020;7:1901605.
- [271] Borah D, Rasappa S, Senthamaraikannan R, Holmes JD, Morris MA. Graphoepitaxial directed self-assembly of polystyrene-block-polydimethylsiloxane block copolymer on substrates functionalized with hexamethyldisilazane to fabricate nanoscale silicon patterns. Adv Mater Interfaces 2014;1:1300102.
- [272] Lee Y-AL, Pryamitsyn V, Rhee D, de la Cruz MO, Odom TW. Strain-dependent nanowrinkle confinement of block copolymers. Nano Lett 2020;20:1433–9.
- [273] Sungjune Park. Manipulating the sequences of block copolymer patterns on corrugated substrates. Polymer 2019;180:121726.
- [274] Legrain A, Fleury G, Mumtaz M, Navarro C, Arias-Zapata J, Chevalier X, Cayrefourcq I, Zelsmann M. Straightforward integration flow of a silicon-containing block copolymer for line–space patterning. ACS Appl Mater Interfaces 2017;9:43043–50.
- [275] Choi YJ, Byun MH, Park TW, Choi S, Bang J, Jung H, Cho J-H, Kwon S-H, Kim KH, Park WI. Rapid and cyclable morphology transition of high-χ block copolymers via solvent vapor-immersion annealing for nanoscale lithography. ACS Appl Nano Mater 2019;2:1294–301.
- [276] Cheng L-C, Gadelrab KR, Kawamoto K, Yager KG, Johnson JA, Alexander-Katz A, Ross CA. Templated self-assembly of a PS-branch-PDMS bottlebrush copolymer. Nano Lett 2018;18:4360–9.
- [277] Choi J, Huh J, Carter KR, Russell TP. Directed self-assembly of block copolymer thin films using minimal topographic patterns. ACS Nano 2016;10:7915–25.
- [278] Gangnaik AS, Ghoshal T, Georgiev YM, Morris MA, Holmes JD. Fabrication of Si and Ge nanoarrays through graphoepitaxial directed hardmask block copolymer self-assembly. J Colloid Interface Sci 2018;531:533–43.
- [279] Choi J, Gunkel I, Li Y, Sun Z, Liu F, Kim H, Carter KR, Russell TP. Macroscopically ordered hexagonal arrays by directed self-assembly of block copolymers with minimal topographic patterns. Nanoscale 2017;9:14888–96.
- [280] Choi JW, Li Z, Black CT, Sweat DP, Wang X, Gopalan P. Patterning at the 10 nanometer length scale using a strongly segregating block copolymer thin film and vapor phase infiltration of inorganic precursors. Nanoscale 2016;8:11595–601.
- [281] Lee D-E, Ryu J, Hong D, Park S, Lee DH, Russell TP. Directed Self-Assembly of Asymmetric Block Copolymers in Thin Films Driven by Uniaxially Aligned Topographic Patterns. ACS Nano 2018;12:1642–9.
- [282] Koh H-D, Kim M-J. Directed self-assembly on photo-crosslinked polystyrene sub-layers: nanopattern uniformity and orientation. Materials 2016;9:648.
- [283] Krishnan MR, Lu K-Y, Chiu W-Y, Chen I-C, Lin J-W, Lo T-Y, Georgopanos P, Avgeropoulos

- A, Lee M-C, Ho R-M. Directed self-assembly of star-block copolymers by topographic nanopatterns through nucleation and growth mechanism. Small 2018:11.
- [284] Delgadillo PR, Suri M, Durant S, Cross AJ, Nagaswami VR, Heuvel DV den, Gronheid R, Nealey PF. Defect source analysis of directed self-assembly process. J Micro Nanolithogr MEMS MOEMS J MICRO-NANOLITH MEM 2013;12:031112.
- [285] Aissou K, Mumtaz M, Portale G, Brochon C, Cloutet E, Fleury G, Hadziioannou G. Templated sub-100-nm-thick double-gyroid structure from si-containing block copolymer thin films. Small 2017;13:1603777.
- [286] Mansky P, Liu Y, Huang E, Russell TP, Hawker C. Controlling polymer-surface interactions with random copolymer brushes. Science 1997;275:1458–60.
- [287] Ouk Kim S, Solak HH, Stoykovich MP, Ferrier NJ, de Pablo JJ, Nealey PF. Epitaxial self-assembly of block copolymers on lithographically defined nanopatterned substrates. Nature 2003;424:411–4.
- [288] Edwards EW, Montague MF, Solak HH, Hawker CJ, Nealey PF. Precise control over molecular dimensions of block-copolymer domains using the interfacial energy of chemically nanopatterned substrates. Adv Mater 2004;16:1315–9.
- [289] Stoykovich MP, Müller M, Kim SO, Solak HH, Edwards EW, de Pablo JJ, Nealey PF. Directed assembly of block copolymer blends into nonregular device-oriented structures. Science 2005;308:1442–6.
- [290] Sunday DF, Ren J, Liman CD, Williamson LD, Gronheid R, Nealey PF, Kline RJ. Characterizing patterned block copolymer thin films with soft X-rays. ACS Appl Mater Interfaces 2017;9:31325–34.
- [291] Pang Y, Wan L, Huang G, Zhang X, Jin X, Xu P, Liu Y, Han M, Wu G-P, Ji S. Controlling block copolymer–substrate interactions by homopolymer brushes/mats. Macromolecules 2017;50:6733–41.
- [292] Chen X, Delgadillo PR, Jiang Z, Craig GSW, Gronheid R, Nealey PF. Defect annihilation in the directed self-assembly of block copolymers in films with increasing thickness. Macromolecules 2019;52:7798–805.
- [293] Yang G-W, Wu G-P, Chen X, Xiong S, Arges CG, Ji S, Nealey PF, Lu X-B, Darensbourg DJ, Xu Z-K. Directed self-assembly of polystyrene-b-poly(propylene carbonate) on chemical patterns via thermal annealing for next generation lithography. Nano Lett 2017;17:1233–9.
- [294] Wan L, Ji S, Liu C-C, Craig GSW, Nealey PF. Directed self-assembly of solvent-vapor-induced non-bulk block copolymer morphologies on nanopatterned substrates. Soft Matter 2016;12:2914–22.
- [295] Pang Y, Jin X, Huang G, Wan L, Ji S. Directed self-assembly of styrene-methyl acrylate block copolymers with sub-7 nm features via thermal annealing. Macromolecules 2019;52:2987–94.
- [296] Giammaria T, Gharbi A, Paquet A, Nealey P, Tiron R. Resist-free directed self-assembly chemo-epitaxy approach for line/space patterning. Nanomaterials 2020;10:2443.
- [297] Williamson LD, Seidel RN, Chen X, Suh HS, Rincon Delgadillo P, Gronheid R, Nealey PF.

- Three-tone chemical patterns for block copolymer directed self-assembly. ACS Appl Mater Interfaces 2016;8:2704–12.
- [298] Leuschel B, Gwiazda A, Heni W, Diot F, Yu S-Y, Bidaud C, Vonna L, Ponche A, Haidara H, Soppera O. Deep-UV photoinduced chemical patterning at the micro- and nanoscale for directed self-assembly. Sci Rep 2018;8:10444.
- [299] Chang T-H, Xiong S, Jacobberger RM, Mikael S, Suh HS, Liu C-C, Geng D, Wang X, Arnold MS, Ma Z, Nealey PF. Directed self-assembly of block copolymer films on atomically-thin graphene chemical patterns. Sci Rep 2016;6:31407.
- [300] Liu G, Nealey PF. Improved block copolymer domain dispersity on chemical patterns via homopolymer-blending and molecular transfer printing. Polymer 2017;116:99–104.
- [301] Chang T-H, Xiong S, Liu C-C, Liu D, Nealey PF, Ma Z. The one-pot directed assembly of cylinder-forming block copolymer on adjacent chemical patterns for bimodal patterning. Macromol Rapid Commun 2017;38:1700285.
- [302] Gottlieb S, Lorenzoni M, Evangelio L, Fernández-Regúlez M, Ryu YK, Rawlings C, Spieser M, Knoll AW, Perez-Murano F. Thermal scanning probe lithography for the directed self-assembly of block copolymers. Nanotechnology 2017;28:175301.
- [303] Zhang X, He Q, Chen Q, Nealey PF, Ji S. Directed self-assembly of high χ poly(styrene-b-(lactic acid-alt-glycolic acid)) block copolymers on chemical patterns via thermal annealing. ACS Macro Lett 2018;7:751–6.
- [304] Evangelio L, Gramazio F, Lorenzoni M, Gorgoi M, Espinosa FM, García R, Pérez-Murano F, Fraxedas J. Identifying the nature of surface chemical modification for directed self-assembly of block copolymers. Beilstein J Nanotechnol 2017;8:1972–81.
- [305] Lane AP, Maher MJ, Willson CG, Ellison CJ. Photopatterning of block copolymer thin films. ACS Macro Lett 2016;5:460–5.
- [306] Liu C-C, Ramírez-Hernández A, Han E, Craig GSW, Tada Y, Yoshida H, Kang H, Ji S, Gopalan P, de Pablo JJ, Nealey PF. Chemical patterns for directed self-assembly of lamellae-forming block copolymers with density multiplication of features. Macromolecules 2013;46:1415–24.
- [307] Jeong S-J, Kim JY, Kim BH, Moon H-S, Kim SO. Directed self-assembly of block copolymers for next generation nanolithography. Mater Today 2013;16:468–76.
- [308] Ruiz R, Kang H, Detcheverry FA, Dobisz E, Kercher DS, Albrecht TR, de Pablo JJ, Nealey PF. Density multiplication and improved lithography by directed block copolymer assembly. Science 2008;321:936–9.
- [309] Suh HS, Kim DH, Moni P, Xiong S, Ocola LE, Zaluzec NJ, Gleason KK, Nealey PF. Sub-10-nm patterning via directed self-assembly of block copolymer films with a vapour-phase deposited topcoat. Nat Nanotechnol 2017;12:575–81.
- [310] Stein A, Wright G, Yager KG, Doerk GS, Black CT. Selective directed self-assembly of coexisting morphologies using block copolymer blends. Nat Commun 2016;7:12366.
- [311] Jacobberger RM, Thapar V, Wu G-P, Chang T-H, Saraswat V, Way AJ, Jinkins KR, Ma Z, Nealey PF, Hur S-M, Xiong S, Arnold MS. Boundary-directed epitaxy of block copolymers. Nat Commun 2020;11:4151.

- [312] Blachut G, Sirard SM, Maher MJ, Asano Y, Someya Y, Lane AP, Durand WJ, Bates CM, Dinhobl AM, Gronheid R, Hymes D, Ellison CJ, Willson CG. A hybrid chemo-/grapho-epitaxial alignment strategy for defect reduction in sub-10 nm directed self-assembly of silicon-containing block copolymers. Chem Mater 2016;28:8951–61.
- [313] Shi L-Y, Lee S, Du Q, Zhou B, Weng L, Liu R, Ross CA. Bending behavior and directed self-assembly of rod-coil block copolymers. ACS Appl Mater Interfaces 2021;13:10437–45.
- [314] Huang H, Liu R, Ross CA, Alexander-Katz A. Self-directed self-assembly of 3D tailored block copolymer nanostructures. ACS Nano 2020;14:15182–92.
- [315] Doise J, Koh JH, Kim JY, Zhu Q, Kinoshita N, Suh HS, Delgadillo PR, Vandenberghe G, Willson CG, Ellison CJ. Strategies for increasing the rate of defect annihilation in the directed self-assembly of high-χ block copolymers. ACS Appl Mater Interfaces 2019;11:48419–27.
- [316] Li J, Rincon-Delgadillo PA, Suh HS, Mannaert G, Nealey PF. Understanding kinetics of defect annihilation in chemoepitaxy-directed self-assembly. ACS Appl Mater Interfaces 2021;13:25357–64.
- [317] Ren J, Zhou C, Chen X, Dolejsi M, Craig GSW, Rincon Delgadillo PA, Segal-Peretz T, Nealey PF. Engineering the kinetics of directed self-assembly of block copolymers toward fast and defect-free assembly. ACS Appl Mater Interfaces 2018;10:23414–23.
- [318] Delgadillo PAR, Thode CJ, Nealey PF, Gronheid R, Wu H, Cao Y, Neisser M, Somervell MH, Nafus K. Implementation of a chemo-epitaxy flow for directed self-assembly on 300-mm wafer processing equipment. J Micro Nanolithogr MEMS MOEMS J MICRO-NANOLITH MEM 2012;11:031302.
- [319] Pathangi H, Chan BT, Bayana H, Vandenbroeck N, Heuvel DVD, Look LV, Rincon-Delgadillo P, Cao Y, Kim J, Lin G, Parnell D, Nafus K, Harukawa R, Chikashi I, Nagaswami V, D'Urzo L, Gronheid R, Nealey P. Defect mitigation and root cause studies in IMEC's 14nm half-pitch chemo-epitaxy DSA flow. Alternative Lithographic Technologies VII, vol. 9423, SPIE; 2015, p. 106–20.
- [320] Li J, Rincon-Delgadillo PA, Suh HS, Mannaert G, Nealey PF. Kinetic approach to defect reduction in directed self-assembly. J Micro Nanolithogr MEMS MOEMS 2019;18:043502.
- [321] Somervell M, Yamauchi T, Okada S, Tomita T, Nishi T, Iijima E, Nakano T, Ishiguro T, Nagahara S, Iwaki H, Dojun M, Ozawa M, Yatsuda K, Tobana T, Negreira AR, Parnell D, Kawakami S, Muramatsu M, Rathsack B et al. High-volume manufacturing equipment and processing for directed self-assembly applications. Advances in Patterning Materials and Processes XXXI, vol. 9051, SPIE; 2014, p. 125–35.
- [322] Rathsack B, Somervell M, Hooge J, Muramatsu M, Tanouchi K, Kitano T, Nishimura E, Yatsuda K, Nagahara S, Hiroyuki I, Akai K, Hayakawa T. Pattern scaling with directed self assembly through lithography and etch process integration. Alternative Lithographic Technologies IV, vol. 8323, SPIE; 2012, p. 52–65.
- [323] Ito C, Durant S, Lange S, Harukawa R, Miyagi T, Nagaswami V, Delgadillo PR, Gronheid R, Nealey P. Inspection of directed self-assembly defects. Alternative Lithographic

- Technologies VI, vol. 9049, SPIE; 2014, p. 512-9.
- [324] Pathangi H, Vaid V, Chan BT, Vandenbroeck N, Li J, Hong SE, Cao Y, Durairaj B, Lin G, Somervell M, Kitano T, Harukawa R, Sah K, Cross A, Bayana H, D'Urzo L, Gronheid R. DSA materials contributions to the defectivity performance of 14nm half-pitch LiNe flow at IMEC. Alternative Lithographic Technologies VIII, vol. 9777, SPIE; 2016, p. 84–9.
- [325] Pathangi H, Heuvel DVD, Bayana H, Bouckou L, Brown J, Parisi P, Gosain R. The use of eDR-71xx for DSA defect review and automated classification. Metrology, Inspection, and Process Control for Microlithography XXIX, vol. 9424, SPIE; 2015, p. 779–86.
- [326] Cao Y, Her Y, Delgadillo PR, Vandenbroeck N, Gronheid R, Chan T, Hashimoto Y, Romo A, Somervell M, Nafus K, Nealey PF. Using process monitor wafers to understand directed self-assembly defects. Alternative Lithographic Technologies V, 2013, p. 86801S.
- [327] Segal-Peretz T, Ren J, Xiong S, Khaira G, Bowen A, Ocola LE, Divan R, Doxastakis M, Ferrier NJ, de Pablo J, Nealey PF. Quantitative three-dimensional characterization of block copolymer directed self-assembly on combined chemical and topographical prepatterned templates. ACS Nano 2017;11:1307–19.
- [328] Fang Q, Ye F, Yang X. Hierarchical morphology of polymer blend films induced by convection-driven solvent evaporation. Langmuir 2018;34:5551–7.
- [329] Wedershoven HMJM, Zeegers JCH, Darhuber AA. Polymer film deposition from a receding solution meniscus: The effect of laminar forced air convection. Chem Eng Sci 2018;181:92–100.
- [330] Li X, Ding Y, Shao J, Tian H, Liu H. Formation of arbitrary patterns in ultraviolet cured polymer film via electrohydrodynamic patterning. Sci World J 2014;2014:1–9.
- [331] Joo S, Park JY, Seo S, Moon S, Lee KJ, An J, Lee C-S, Bae J. Study on peculiar carbon pattern formation from polymer blend thin films under electric fields. Thin Solid Films 2018;660:846–51.
- [332] Mayer A, Ai W, Rond J, Staabs J, Steinberg C, Papenheim M, Scheer H-C, Tormen M, Cian A, Zajadacz J, Zimmer K. Electrically-assisted nanoimprint of block copolymers. J Vac Sci Technol 2018;37:011601.
- [333] Singer JP. Thermocapillary approaches to the deliberate patterning of polymers. J Polym Sci, Part B: Polym Phys 2017;55:1649–68.
- [334] Geldmeier J, Rile L, Yoon YJ, Jung J, Lin Z, Tsukruk VV. Dewetting-induced photoluminescent enhancement of poly(lauryl methacrylate)/quantum dot thin films. Langmuir 2017;33:14325–31.
- [335] Wu B-H, Chang K-C, Hsu H-H, Chiu Y-J, Chiu T-Y, Tseng H-F, Li J-W, Chen J-T. Radial linear polymer patterns driven by the marangoni instability and lateral phase separation for the formation of nanoscale perforation lines. ACS Appl Nano Mater 2019;2:3253–61.
- [336] Roy P, Mukherjee R, Bandyopadhyay D, Gooh Pattader PS. Electrodynamic-contact-line-lithography with nematic liquid crystals for template-less E-writing of mesopatterns on soft surfaces. Nanoscale 2019;11:16523–33.
- [337] Lv P, You Y, Li J, Zhang Y, Broer DJ, Chen J, Zhou G, Zhao W, Liu D. Translating 2D director profile to 3D topography in a liquid crystal polymer. Adv Sci 2021;8:2004749.

- [338] Franklin T, Streever DL, Yang R. Versatile and rapid synthesis of polymer nanodomes via template- and solvent-free condensed droplet polymerization. Chem Mater 2022;34:5960–70.
- [339] Das A, Bolleddu R, Singh AK, Bandyopadhyay D. Physicochemical defect guided dewetting of ultrathin films to fabricate nanoscale patterns. Nanotechnology 2021;32:195303.
- [340] Cheng P-T, Zhou W, Yang F, Lee S. Growth of polystyrene pillars in electric field. Langmuir 2019;35:4966–75.
- [341] Yu C, Xie Q, Bao Y, Shan G, Pan P. Crystalline and spherulitic morphology of polymers crystallized in confined systems. Crystals 2017;7:147.
- [342] Michell RM, Müller AJ. Confined crystallization of polymeric materials. Prog Polym Sci 2016;54–55:183–213.
- [343] Wei N, Zhu B, He J, Shan H, Zhou J, Huo H. Controlling the organization and stretchability of poly(3-butylthiophene) spherulites. Soft Matter 2021;17:8850–7.
- [344] Li S, Li J, Chun Y, Shrestha PK, Chang X, Pivnenko M, Chu D. Variety of ordered patterns in donor–acceptor polymer semiconductor films crystallized from solution. ACS Appl Mater Interfaces 2021;13:19055–63.
- [345] Koo J, Amoli V, Kim SY, Lee C, Kim J, Park S-M, Kim J, Ahn JM, Jung KJ, Kim DH. Low-power, deformable, dynamic multicolor electrochromic skin. Nano Energy 2020;78:105199.
- [346] Pietsch M, Rödlmeier T, Schlisske S, Zimmermann J, Romero-Nieto C, Hernandez-Sosa G. Inkjet-printed polymer-based electrochromic and electrofluorochromic dual-mode displays. J Mater Chem C 2019;7:7121–7.
- [347] Cai G, Cheng X, Layani M, Tan AWM, Li S, Eh AL-S, Gao D, Magdassi S, Lee PS. Direct inkjet-patterning of energy efficient flexible electrochromics. Nano Energy 2018;49:147–54.
- [348] Kim Y, Park C, Im S, Kim JH. Design of intrinsically stretchable and highly conductive polymers for fully stretchable electrochromic devices. Sci Rep 2020;10:16488.
- [349] Chen T, Chen Q, Liu G, Chen G. High cycling stability and well printability poly(3,4-ethylenedioxythiophene):poly(styrene sulfonate)/multi-walled carbon nanotube nanocomposites via in situ polymerization applied on electrochromic display. J Appl Polym Sci 2018;135:45943.
- [350] Hu F, Xue Y, Jian N, Qu K, Lin K, Zhu X, Wu T, Liu X, Xu J, Lu B. Pyrazine-EDOT D-A-D type hybrid polymer for patterned flexible electrochromic devices. Electrochim Acta 2020;357:136859.
- [351] Jung J-Y, Joo S, Kim D-S, Kim K-H, Shim TS, Seo S, Kim J-H. Microscale patterning of electrochromic polymer films via soft lithography. Int J Polym Sci n.d.;2018:9.
- [352] Zhang S, Chen S, Hu F, Xu R, Yan B, Jiang M, Gu Y, Yang F, Cao Y. Spray-processable, large-area, patterned and all-solid-state electrochromic device based on silica/polyaniline nanocomposites. Sol Energy Mater Sol Cells 2019;200:109951.
- [353] Zhang S, Ren J, Chen S, Luo Y, Bai X, Ye L, Yang F, Cao Y. Large area electrochromic displays with ultrafast response speed and high contrast using solution-processable and

- patternable honeycomb-like polyaniline nanostructures. J Electroanal Chem 2020;870:114248.
- [354] Yoshida T, Higuchi M. Diversity in Design of Electrochromic Devices with Metallo-Supramolecular Polymer: Multi-Patterned and Tube-Shaped Displays. J Photopol Sci Technol 2018;31:343–7.
- [355] Ji X, Liu W, Yin Y, Wang C, Torrisi F. A graphene-based electro-thermochromic textile display. J Mater Chem C 2020;8:15788–94.
- [356] Seeboth A, Lötzsch D, Ruhmann R, Muehling O. Thermochromic polymers—function by design. Chem Rev 2014;114:3037–68.
- [357] Yang J-C, Ho Y-C, Chan Y-H. Ultrabright fluorescent polymer dots with thermochromic characteristics for full-color security marking. ACS Appl Mater Interfaces 2019;11:29341–9.
- [358] Kragt AJJ, Zuurbier NCM, Broer DJ, Schenning APHJ. Temperature-responsive, multicolor-changing photonic polymers. ACS Appl Mater Interfaces 2019;11:28172–9.
- [359] Menz W, Dimov S, Fillon B, editors. Front matter. 4M 2006 Second International Conference on multi-material micro manufacture, Oxford: Elsevier; 2006, p. i–iii.
- [360] Zhan C, Yu G, Lu Y, Wang L, Wujcik E, Wei S. Conductive polymer nanocomposites: a critical review of modern advanced devices. J Mater Chem C 2017;5:1569–85.
- [361] Zou S-J, Shen Y, Xie F-M, Chen J-D, Li Y-Q, Tang J-X. Recent advances in organic light-emitting diodes: toward smart lighting and displays. Mater Chem Front 2020;4:788–820.
- [362] Stellmacher A, Liu Y, Soldera M, Rank A, Reineke S, Lasagni AF. Fast and cost effective fabrication of microlens arrays for enhancing light out-coupling of organic light-emitting diodes. Mater Lett 2019;252:268–71.
- [363] Kim A, Huseynova G, Lee J, Lee J-H. Enhancement of out-coupling efficiency of flexible organic light-emitting diodes fabricated on an MLA-patterned parylene substrate. Org Electron 2019;71:246–50.
- [364] Jürgensen N, Fritz B, Mertens A, Tisserant J-N, Kolle M, Gomard G, Hernandez-Sosa G. A single-step hot embossing process for integration of microlens arrays in biodegradable substrates for improved light extraction of light-emitting devices. Adv Mater Technol 2021;6:1900933.
- [365] Kostianovskii V, Sanyoto B, Noh Y-Y. A facile way to pattern PEDOT:PSS film as an electrode for organic devices. Org Electron 2017;44:99–105.
- [366] Kang S, Lee B-Y, Lee S-H, Lee S-D. High resolution micro-patterning of stretchable polymer electrodes through directed wetting localization. Sci Rep 2019;9:13066.
- [367] Liu M, Wang Y, Wang J, Qin Y, Liu C, Chen Y, Deng L, Li R, Zhang X, Huang W. Improving the out-coupling efficiency of polymer light-emitting diodes with soft nanoimprinted random corrugated structures. J Appl Phys 2020;127:125501.
- [368] Lin H-Y, Sher C-W, Lin C-H, Tu H-H, Chen XY, Lai Y-C, Lin C-C, Chen H-M, Yu P, Meng H-F, Chi G-C, Honjo K, Chen T-M, Kuo H-C. Fabrication of flexible white light-emitting diodes from photoluminescent polymer materials with excellent color quality. ACS Appl Mater Interfaces 2017;9:35279–86.

- [369] Han D, Khan Y, Ting J, King SM, Yaacobi-Gross N, Humphries MJ, Newsome CJ, Arias AC. Flexible blade-coated multicolor polymer light-emitting diodes for optoelectronic sensors. Adv Mater 2017;29:1606206.
- [370] Kang YJ, Bail R, Lee CW, Chin BD. Inkjet printing of mixed-host emitting layer for electrophosphorescent organic light-emitting diodes. ACS Appl Mater Interfaces 2019;11:21784–94.
- [371] Yin M, Yu Z, Pan T, Peng X, Zhang X, Zhang L, Xie W. Efficient and angle-stable white top-emitting organic light emitting devices with patterned quantum dots down-conversion films. Org Electron 2018;56:46–50.
- [372] Park J, Ha J, Seong N, Lee S, Lee C, Yang H, Hong Y. Highly efficient solution-processed inverted polymer light emitting diodes with uniformly coated poly(3,4-ethylenedioxythiophene):poly(styrene-sulfonate) layers on a hydrophobic emission layer using a dilution method. Thin Solid Films 2018;660:782–8.
- [373] Li M, Wang J, Zhang Y, Dai Y, Chen L, Zheng C, Lv W, Chen R, Huang W. Thermal imprinting and vapor annealing of interfacial layers for high-performance organic light-emitting diodes. J Mater Chem C 2019;7:10281–8.
- [374] Kim G, Lee J, Shin D-K, Park J. Roll-to-roll fabrication of PEDOT:PSS stripes using slot-die head with μ -Tips for AMOLEDs. IEEE Trans Electron Devices 2019;66:9.
- [375] Yoon DG, Kang M, Kim JB, Kang K-T. Nozzle printed-PEDOT:PSS for organic light emitting diodes with various dilution rates of ethanol. Appl Sci 2018;8:203.
- [376] Shi G, Park SH, Kim J, Kim M, Park LS. Side-chain polyimides as binder polymers for photolithographic patterning of a black pixel define layer for organic light emitting diode. Int J Polym Sci 2018;2018:e3790834.
- [377] Sim KM, Yoon S, Kim S-K, Ko H, Hassan SZ, Chung DS. Surfactant-induced solubility control to realize water-processed high-precision patterning of polymeric pemiconductors for full color organic image sensor. ACS Nano 2020;14:415–21.
- [378] Kim M, Alrowais H, Kim C, Yeon P, Ghovanloo M, Brand O. All-soft, battery-free, and wireless chemical sensing platform based on liquid metal for liquid- and gas-phase VOC detection. Lab Chip 2017;17:2323–9.
- [379] Eom J, Jaisutti R, Lee H, Lee W, Heo J-S, Lee J-Y, Park SK, Kim Y-H. Highly sensitive textile strain sensors and wireless user-interface devices using all-polymeric conducting fibers. ACS Appl Mater Interfaces 2017;9:10190–7.
- [380] Yin M, Zhang Y, Yin Z, Zheng Q, Zhang AP. Micropatterned elastic gold-nanowire/polyacrylamide composite hydrogels for wearable pressure sensors. Adv Mater Technol 2018;3:1800051.
- [381] Shen G, Chen B, Liang T, Liu Z, Zhao S, Liu J, Zhang C, Yang W, Wang Y, He X. Transparent and stretchable strain sensors with improved sensitivity and reliability based on Ag NWs and PEDOT:PSS patterned microstructures. Adv Electron Mater 2020;6:1901360.
- [382] Besar K, Dailey J, Zhao X, Katz HE. A flexible organic inverter made from printable materials for synergistic ammonia sensing. J Mater Chem C 2017;5:6506–11.
- [383] Molina-Lopez F, Gao TZ, Kraft U, Zhu C, Öhlund T, Pfattner R, Feig VR, Kim Y, Wang S,

- Yun Y, Bao Z. Inkjet-printed stretchable and low voltage synaptic transistor array. Nat Commun 2019;10:2676.
- [384] Kwon J, Takeda Y, Shiwaku R, Tokito S, Cho K, Jung S. Three-dimensional monolithic integration in flexible printed organic transistors. Nat Commun 2019;10:54.
- [385] Shields CW, Evans MA, Wang LL-W, Baugh N, Iyer S, Wu D, Zhao Z, Pusuluri A, Ukidve A, Pan DC, Mitragotri S. Cellular backpacks for macrophage immunotherapy. Sci Adv 2020;6:eaaz6579.
- [386] Fromel M, Li M, Pester CW. Surface engineering with polymer brush photolithography. Macromol Rapid Commun 2020;41:2000177.
- [387] Ng G, Judzewitsch P, Li M, Pester CW, Jung K, Boyer C. Synthesis of polymer brushes via SI-PET-RAFT for photodynamic inactivation of bacteria. Macromol Rapid Commun 2021;42:2100106.
- [388] Ng G, Li M, Yeow J, Jung K, Pester CW, Boyer C. Benchtop preparation of polymer brushes by SI-PET-RAFT: the effect of the polymer composition and structure on inhibition of a pseudomonas biofilm. ACS Appl Mater Interfaces 2020;12:55243–54.
- [389] Tan KY, Ramstedt M, Colak B, Huck WTS, Gautrot JE. Study of thiol–ene chemistry on polymer brushes and application to surface patterning and protein adsorption. Polym Chem 2016;7:979–90.
- [390] Sun X, Wang H, Wang Y, Gui T, Wang K, Gao C. Creation of antifouling microarrays by photopolymerization of zwitterionic compounds for protein assay and cell patterning. Biosens Bioelectron 2018;102:63–9.
- [391] Moeller J, Denisin AK, Sim JY, Wilson RE, Ribeiro AJS, Pruitt BL. Controlling cell shape on hydrogels using lift-off protein patterning. PloS One 2018;13:e0189901.
- [392] Kumar R, Welle A, Becker F, Kopyeva I, Lahann J. Substrate-independent micropatterning of polymer brushes based on photolytic deactivation of chemical vapor deposition based surface-initiated atom-transfer radical polymerization initiator films. ACS Appl Mater Interfaces 2018;10:31965–76.
- [393] Firkowska-Boden I, Zhang X, Jandt KD. Controlling protein adsorption through nanostructured polymeric surfaces. Adv Healthc Mater 2018;7:1700995.
- [394] Xiao Y, Wang M, Lin L, Du L, Shen M, Shi X. Integration of aligned polymer nanofibers within a microfluidic chip for efficient capture and rapid release of circulating tumor cells. Mater Chem Front 2018;2:891–900.
- [395] Jaiswal N, Hens A, Chatterjee M, Mahata N, Chanda N. Ethylenediamine assisted functionalization of self-organized poly (D,, L-lactide-co-glycolide) patterned surface to enhance cancer cell isolation. J Colloid Interface Sci 2019;534:122–30.
- [396] Zakrzewski W, Dobrzyński M, Szymonowicz M, Rybak Z. Stem cells: past, present, and future. Curr Stem Cell Res Ther 2019;10:68.
- [397] Yang Y, Wang X, Huang T-C, Hu X, Kawazoe N, Tsai W-B, Yang Y, Chen G. Regulation of mesenchymal stem cell functions by micro–nano hybrid patterned surfaces. J Mater Chem B 2018;6:5424–34.
- [398] Broderick AH, Azarin SM, Buck ME, Palecek SP, Lynn DM. Fabrication and selective

- functionalization of amine-reactive polymer multilayers on topographically patterned microwell cell culture arrays. Biomacromolecules 2011;12:1998–2007.
- [399] Lee YB, Kim S, Kim EM, Byun H, Chang H, Park J, Choi YS, Shin H. Microcontact printing of polydopamine on thermally expandable hydrogels for controlled cell adhesion and delivery of geometrically defined microtissues. Acta Biomater 2017;61:75–87.
- [400] Song Q, I. Druzhinin S, Schönherr H. Asymmetric multifunctional 3D cell microenvironments by capillary force assembly. J Mater Chem B 2019;7:3560–8.
- [401] Dou X, Li P, Schönherr H. Three-dimensional microstructured poly(vinyl alcohol) hydrogel platform for the controlled formation of multicellular cell spheroids. Biomacromolecules 2018;19:158–66.
- [402] Liu Z, Tamaddon M, Gu Y, Yu J, Xu N, Gang F, Sun X, Liu C. Cell seeding process experiment and simulation on three-dimensional polyhedron and cross-link design scaffolds. Front Bioeng Biotechnol 2020;8:104.
- [403] Théry M. Micropatterning as a tool to decipher cell morphogenesis and functions. J Cell Sci 2010;123:4201–13.
- [404] Khadpekar AJ, Khan M, Sose A, Majumder A. Low cost and lithography-free stamp fabrication for microcontact printing. Sci Rep 2019;9:1024.
- [405] Chen X, Cortez-Jugo C, Choi GH, Björnmalm M, Dai Y, Yoo PJ, Caruso F. Patterned poly(dopamine) films for enhanced cell adhesion. Bioconjugate Chem 2017;28:75–80.
- [406] Adiguzel Z, Sagnic SA, Aroguz AZ. Preparation and characterization of polymers based on PDMS and PEG-DMA as potential scaffold for cell growth. Mater Sci Eng C 2017;78:942–8.
- [407] Messner JJ, Glenn HL, Meldrum DR. Laser-fabricated cell patterning stencil for single cell analysis. BMC Biotechnol 2017;17:89.
- [408] Shrirao AB, Kung FH, Yip D, Firestein BL, Cho CH, Townes-Anderson E. A versatile method of patterning proteins and cells. JoVE 2017:55513.
- [409] Nakayama M, Toyoshima Y, Kikuchi A, Okano T. Micropatterned smart culture surfaces via multi-step physical coating of functional block copolymers for harvesting cell sheets with controlled sizes and shapes. Macromol Biosci 2021;21:2000330.
- [410] Wang P, Yin H-M, Li X, Liu W, Chu Y-X, Wang Y, Wang Y, Xu J-Z, Li Z-M, Li J-H. Simultaneously constructing nanotopographical and chemical cues in 3D-printed polylactic acid scaffolds to promote bone regeneration. Mater Sci Eng C 2021;118:111457.
- [411] SooHyun Park null, Abidian MR, Majd S. Micro-patterned films of bio-functionalized conducting polymers for cellular engineering. Annu Int Conf IEEE Eng Med Biol Soc 2017;2017:1595–8.
- [412] Luo Y, Zheng X, Yuan P, Ye X, Ma L. Light-induced dynamic RGD pattern for sequential modulation of macrophage phenotypes. Bioact Mater 2021;6:4065–72.
- [413] Tsai Y-T, Wu C-Y, Guan Z-Y, Sun H-Y, Cheng N-C, Yeh S-Y, Chen H-Y. Topologically controlled cell differentiation based on vapor-deposited polymer coatings. Langmuir 2017;33:8943–9.
- [414] Guan Z-Y, Wu C-Y, Chen H-Y. Stepwise and programmable cell differentiation pathways

- of controlled functional biointerfaces. ACS Biomater Sci Eng 2017;3:1815-21.
- [415] Fan F-R, Tian Z-Q, Lin Wang Z. Flexible triboelectric generator. Nano Energy 2012;1:328–34.
- [416] Vasandani P, Gattu B, Wu J, Mao Z-H, Jia W, Sun M. Triboelectric nanogenerator using microdome-patterned PDMS as a wearable respiratory energy harvester. Adv Mater Technol 2017;2:1700014.
- [417] Han W. Self-powered vision electronic-skin basing on piezo-photodetecting PPy/PVDF pixel-patterned matrix for mimicking vision. Nanotechnology 2018;29:255501.
- [418] Kim J, Kim JW, Kim HC, Zhai L, Ko H-U, Muthoka RM. Review of soft actuator materials. Int J Precis Eng Manuf 2019;20:2221–41.
- [419] Wang Y, Sugino T. Ionic polymer actuators: principle, fabrication and applications. In: Volosencu C, editor. Actuators, InTech; 2018.
- [420] Khaldi A, Falk D, Bengtsson K, Maziz A, Filippini D, Robinson ND, Jager EWH. Patterning highly conducting conjugated polymer electrodes for soft and flexible microelectrochemical devices. ACS Appl Mater Interfaces 2018;10:14978–85.
- [421] Ding Y, Maruf S, Aghajani M, Greenberg AR. Surface patterning of polymeric membranes and its effect on antifouling characteristics. Sep Sci Technol 2017;52:240–57.
- [422] Yang C, Tartaglino U, Persson BNJ. Influence of surface roughness on superhydrophobicity. Phys Rev Lett 2006;97:116103.
- [423] Nguyen BQH, Shanmugasundaram A, Hou T-F, Park J, Lee D-W. Realizing the flexible and transparent highly-hydrophobic film through siloxane functionalized polyurethane-acrylate micro-pattern. Chem Eng J 2019;373:68–77.
- [424] Chen Y, Meng J, Zhu Z, Zhang F, Wang L, Gu Z, Jiang L, Wang S. Controlled growth of patterned conducting polymer microsuckers on superhydrophobic micropillar-structured templates. Adv Funct Mater 2018;28:1800240.
- [425] Askar K, Phillips BM, Fang Y, Choi B, Gozubenli N, Jiang P, Jiang B. Self-assembled self-cleaning broadband anti-reflection coatings. Colloids Surf A: Physicochem Eng Asp 2013;439:84–100.
- [426] Rasappa S, Schulte L, Ndoni S, Niemi T. Directed self-assembly of a high-chi block copolymer for the fabrication of optical nanoresonators. Nanoscale 2018;10:18306–14.
- [427] Park C, Na J, Han M, Kim E. Transparent electrochemical gratings from a patterned bistable silver mirror. ACS Nano 2017;11:6977–84.
- [428] Li Y, Maynor BW, Liu J. Electrochemical AFM "dip-pen" nanolithography. J Am Chem Soc 2001;123:2105–6.
- [429] Barcelo S, Li Z. Nanoimprint lithography for nanodevice fabrication. Nano Converg 2016;3:21.
- [430] Colburn M, Suez I, Choi BJ, Meissl M, Bailey T, Sreenivasan SV, Ekerdt JG, Willson CG. Characterization and modeling of volumetric and mechanical properties for step and flash imprint lithography photopolymers. J Vac Sci Technol B 2001;19:2685.
- [431] Hagberg EC, Malkoch M, Ling Y, Hawker CJ, Carter KR. Effects of modulus and surface chemistry of thiol-ene photopolymers in nanoimprinting. Nano Lett 2007;7:233–7.

- [432] De Girolamo J, Chouiki M, Tortai J-H, Sourd C, Derrough S, Zelsmann M, Boussey J. Epoxy silsesquioxane resists for UV nanoimprint lithography. J Vac Sci TechnolB 2008;26:2271–5.
- [433] Suh KY, Langer R, Lahann J. Fabrication of elastomeric stamps with polymer-reinforced sidewalls via chemically selective vapor deposition polymerization of poly(*p* -xylylene). Appl Phys Lett 2003;83:4250–2.
- [434] Bates CM, Maher MJ, Janes DW, Ellison CJ, Willson CG. Block copolymer lithography. Macromolecules 2014;47:2–12.
- [435] Feng W, Broer DJ, Liu D. Oscillating chiral-nematic fingerprints wipe away dust. Adv Mater 2018;30:1704970.
- [436] Zhang Y, Discekici EH, Burns RL, Somervell MH, Hawker CJ, Bates CM. Single-step, spinon process for high fidelity and selective deposition. ACS Appl Polym Mater 2020;2:481– 6.
- [437] Gharbi A, Tiron R, Argoud M, Chevalier X, Belledent J, Pradelles J, Barros PP, Navarro C, Nicolet C, Hadziioannou G, Fleury G, Barnola S. Contact holes patterning by directed self-assembly of block copolymers: what would be the bossung plot? Alternative Lithographic Technologies VI, vol. 9049, SPIE; 2014, p. 325–34.
- [438] Schmidt K, Osaki H, Nishino K, Sanchez M, Liu C-C, Furukawa T, Chi C, Pitera J, Felix N, Sanders D. Strategies to enable directed self-assembly contact hole shrink for tight pitches. Alternative Lithographic Technologies VIII, 2016, p. 97771U.
- [439] Seino Y, Yonemitsu H, Sato H, Kanno M, Kato H, Kobayashi K, Kawanishi A, Azuma T, Muramatsu M, Nagahara S, Kitano T, Toshima T. Contact hole shrink process using graphoepitaxial directed self-assembly lithography. J Micro/Nanolith MEMS MOEMS 2013;12:033011.
- [440] Zhao X-M, Xia Y, Qin D, Whitesides GM. Fabrication of polymeric microstructures with high aspect ratios using shrinkable polystyrene films. Adv Mater 1997;9:251–4.
- [441] Lee AJ, Withford MJ, Dawes JM. Direct-write nanosecond laser microstructuring of heat shrinkable films. Appl Phys A 2005;80:1447–9.
- [442] Wang Z, Jiang L, Li X, Li B, Zhou S, Xu Z, Huang L. Thermally reconfigurable hologram fabricated by spatially modulated femtosecond pulses on a heat-shrinkable shape memory polymer for holographic multiplexing. ACS Appl Mater Interfaces 2021;13:51736–45.
- [443] Singh M, Wu W, Nuka V, Strzalka J, Douglas JF, Karim A. Late stage domain coarsening dynamics of lamellar block copolymers. ACS Macro Lett 2021;10:727–31.
- [444] Stegelmeier C, Exner A, Hauschild S, Filiz V, Perlich J, Roth SV, Abetz V, Förster S. Evaporation-induced block copolymer self-assembly into membranes studied by in situ synchrotron SAXS. Macromolecules 2015;48:1524–30.
- [445] Yavitt BM, Fei H, Kopanati G, Li R, Fukuto M, Winter HH, Watkins JJ. Long-range lamellar alignment in diblock bottlebrush copolymers via controlled oscillatory shear. Macromolecules 2020;53:2834–40.
- [446] Wei C, Dong J. Development and modeling of melt electrohydrodynamic-jet printing of phase-change inks for high-resolution additive manufacturing. J Manuf Sci Eng

- 2014;136:061010.
- [447] Zou W, Yu H, Zhou P, Liu L. Tip-assisted electrohydrodynamic jet printing for high-resolution microdroplet deposition. Mater Des 2019;166:107609.
- [448] Lu K. Hybrid materials a review on co-dispersion, processing, patterning, and properties. Int Mater Rev 2020;65:463–501.
- [449] Ma L, Huang H, Vargo E, Huang J, Anderson CL, Chen T, Kuzmenko I, Ilavsky J, Wang C, Liu Y, Ercius P, Alexander-Katz A, Xu T. Diversifying composition leads to hierarchical composites with design flexibility and structural fidelity. ACS Nano 2021;15:14095–104.
- [450] Pieters PF, Lainé A, Li H, Lu Y-H, Singh Y, Wang L-W, Liu Y, Xu T, Alivisatos AP, Salmeron M. Multiscale characterization of the influence of the organic–inorganic interface on the dielectric breakdown of nanocomposites. ACS Nano 2022;16:6744–54.
- [451] Qiu M, Du W, Luo X, Zhu S, Luo Y, Zhao J. Vapor-phase molecular doping in covalent organosiloxane network thin films via a lewis acid-base interaction for enhanced mechanical properties. ACS Appl Mater Interfaces 2022;14:22719–27.
- [452] Bai J, Zhang L, Hou H, Shi Z, Yin J, Jiang X. Light-written reversible 3D fluorescence and topography dual-pattern with memory and self-healing abilities. Research 2019;2019.